

**Mathematical Modelling
of the Combined Effects
of Vortex-Induced Vibration
and Galloping**

By

Robert Malcolm Corless

B.Sc., The University of British Columbia, 1980

M.Math., The University of Waterloo, 1982

A THESIS SUBMITTED IN PARTIAL FULFILLMENT OF
THE REQUIREMENTS FOR THE DEGREE OF
DOCTOR OF PHILOSOPHY

in

THE FACULTY OF GRADUATE STUDIES

Department of Mechanical Engineering

We accept this thesis as conforming
to the required standard

THE UNIVERSITY OF BRITISH COLUMBIA

November 1986

© Robert Malcolm Corless, 1986

In presenting this thesis in partial fulfilment of the requirements for an advanced degree at the University of British Columbia, I agree that the Library shall make it freely available for reference and study. I further agree that permission for extensive copying of this thesis for scholarly purposes may be granted by the head of my department or by his or her representatives. It is understood that copying or publication of this thesis for financial gain shall not be allowed without my written permission.

Department of Mechanical Engineering

The University of British Columbia
1956 Main Mall
Vancouver, Canada
V6T 1Y3

Date March 30, 1987

Abstract

In this thesis a mathematical model for the combined effects of vortex-induced oscillation and galloping of a square section cylinder in cross flow is examined. The model equations are obtained by simply combining Parkinson and Smith's Quasi-Steady Model for galloping with the Hartlen-Currie model for vortex-induced vibration, which is essentially the same model used by Bouclin in the hydrodynamic case.

The semi-empirical model is solved using three popular approximate analytical methods, and the methods of solution are evaluated. The solution of the model is compared with recent experimental data.

The methods of solution used are the Method of Van Der Pol, (also called the method of Harmonic Balance), the Method of Multiple Scales, and some results from the Hopf Bifurcation Theory. The Method of Multiple Scales provides the most useful solutions, getting good results even with just the $O(1)$ terms, although the next-order terms are necessary for the solution in the resonance regions. The phenomenon of subharmonic resonance, observed in recent experiments, is also observed in the solution of the model equations.

Contents

Abstract	ii
List of Figures	v
Nomenclature	vi
Acknowledgements	ix
1. Introduction	1
1.1 Outline of the Problem	1
1.2 Vortex-Induced Vibration	4
1.3 Galloping	6
1.4 Interaction Effects	7
2. Proposed Mathematical Model	10
2.1 General Remarks	10
2.2 Functional Form of the Parameters	16
3. Model Synthesis	20
3.1 Parameters Fixed by Static Experiments	20
3.2 Experimental Determination of a , B , and D	22
4. Methods of Solution of the Model Equations	25
4.1 Discussion of Available Methods	25
5. Solution by the Method of Van Der Pol	33
5.1 Setting up the Equations	33
5.2 Solution of the Polynomial Equations	35
5.3 Results of the Method of Van Der Pol	37
6. Hopf Bifurcations of the Model Equations	43
6.1 Introduction	43
6.2 Hopf Bifurcation Theory	44
6.1 Bifurcation Formulae	46

6.4	Bifurcation of the Quasi-Steady Model	50
6.5	Limitations of the Hopf Bifurcation Theory	54
6.6	Model Equations	55
6.7	Location of the Hopf Bifurcation Points	55
6.8	Coefficients of the Bifurcation Polynomial	58
6.9	Results of Bifurcation Formulae	61
7.	Solution by the Method of Multiple Scales	71
7.1	Overview and Choice of Time Scales	71
7.2	Case I: Resonance Case, with $\omega_0 = 1 + \mu\omega_1$	75
7.3	Solution of the $O(\mu)$ equations	79
7.4	Stability of the $O(\mu)$ solutions	81
7.5	Solution to $O(\mu^2)$	83
7.6	Case II: Nonresonance Case, with $\omega_0 \neq 1$	95
7.7	Nonresonance Solution to $O(\mu)$	108
7.8	Subharmonic Solution to $O(\mu)$: $\omega_0 = 3 + \mu\omega_3$	112
7.9	Superharmonic Solution to $O(\mu)$	120
7.10	Results of the Method of Multiple Scales	130
8.	Comparison with Experiment	146
8.1	Concordiat of Solutions	146
8.2	Behaviour in the Quasi-Steady Limit	150
8.3	Comparison of Predictions	152
9.	Conclusions	156
9.1	Conclusions	156
9.2	Suggestions for Further Work	159

List of Figures

1.3.1	Equivalent Angle of Attack	8
3.1.1	Polynomial Force Coefficients	21
5.3.1	Van Der Pol Solution Amplitude	41
5.3.2	Van Der Pol Solution Excitation	42
6.4.1	Quasi-Steady Bifurcation	53
6.9.1	Hopf Bifurcation Points	66
6.9.2	Hopf Bifurcation for larger n	67
6.9.3	Hopf Solution for Low Damping	68
6.9.4	Hopf Solution for Medium Damping	69
6.9.5	Hopf Solution for High Damping	70
7.5.1	Solution in the Resonance Region	94
7.6.1	Steady State Amplitudes $f'(0) > 0$	106
7.6.2	Steady State Amplitudes $f'(0) < 0$	107
7.6.3	Solution to $O(1)$	109
7.10.1	Low Turbulence Amplitudes	137
7.10.2	Low Turbulence Excitation	138
7.10.3	Medium Turbulence Amplitudes	139
7.10.4	Medium Turbulence Excitation	140
7.10.5	High Turbulence Amplitudes	141
7.10.6	High Turbulence Excitation	142
7.10.7	Amplitude with Subharmonic Resonance	143
7.10.8	Hydrodynamic Amplitude	144
7.10.9	Hydrodynamic Excitation	145
8.1.1	U_i versus U_0	151

Nomenclature

- A_0 — Complex amplitude of the $O(1)$ oscillation for the method of multiple scales.
 A_1 — Complex amplitude of the $O(\mu)$ oscillation for the method of multiple scales.
 A_2 — Complex amplitude of the $O(\mu^2)$ oscillation for the method of multiple scales.
 a_0 — Real amplitude of the $O(1)$ oscillation for the method of multiple scales.
 a_1 — Real amplitude of the $O(\mu)$ oscillation for the method of multiple scales.
 a_2 — Real amplitude of the $O(\mu^2)$ oscillation for the method of multiple scales.
 $a(\omega_0)$ — Van Der Pol (Rayleigh) equation coefficient.
 \mathcal{A}_k — Polynomial fit coefficients from the quasi-steady theory, $k = 1, 3, 5, \dots, N$.
 B — Acceleration coupling coefficient from the model equations.
 B_0 — Complex amplitude of the $O(1)$ excitation for the method of multiple scales.
 B_1 — Complex amplitude of the $O(\mu)$ excitation for the method of multiple scales.
 b_0 — Real amplitude of the $O(1)$ excitation for the method of multiple scales.
 b_1 — Real amplitude of the $O(\mu)$ excitation for the method of multiple scales.
 C_{F_v} — Lateral force coefficient, $= \frac{F_y}{\frac{1}{2}\rho V^2 h}$.
 C_v — Nondimensional excitation coefficient.
 C_{Y_0} — Fixed cylinder excitation amplitude.
 C_0 — $O(1)$ term of C_v used in the method of multiple scales.
 C_1 — $O(\mu)$ term of C_v used in the method of multiple scales.
 D — Velocity coupling coefficient from the model equations.
 f — vortex formation frequency from one shear layer.
 $f(a_0)$ — Polynomial in a_0 whose roots are the steady-state amplitudes to first order.
 F_y — Lateral aerodynamic force per unit cylinder span
 g — The Van Der Pol coefficient $a(\omega_0)$ in asymptotic form for the method of multiple scales: $\mu g = a(\omega_0)$.
 h — Width of cylinder cross section
 ℓ_k — Coefficient of $e^{i \cdot k T}$ in Y_2 , $k = 3, 5, 9$.
 m — Mass of cylinder per unit span.
 n — Mass ratio $\frac{\rho h^2}{2m}$.
 r_k — Quasi-steady polynomial coefficients in asymptotic form: $\mu^2 r_k = n U^2 \mathcal{A}_k / U^k$ for $k = 3, 5, 7$ and $\mu^2 r_1 = n(U - U_0) \mathcal{A}_1$.
 s — Model coupling coefficient in asymptotic form, $\mu^2 s = n U^2$.

- S — Strouhal number, $= fh/V$.
- t — Time, nondimensionalized so the natural frequency of oscillation of the cylinder is 1, $t = \omega \times \text{natural time}$.
- T — Time with detuning parameters added, $T = \Omega t$.
- U — Nondimensional wind speed, $U = \frac{V}{\omega h}$.
- U_i/U_r — Alternate notation for ω_i .
- U_0 — Critical reduced wind speed for galloping from the quasi-steady theory, $U_0 = \frac{2\beta}{nA_1}$.
- U_r — Reduced wind speed for vortex resonance, $U_r = 1/(2\pi S)$.
- V — Wind speed.
- W_0 — Ratio of U_0 to U_r , or $4\pi S\beta/nA_1$.
- Y — Nondimensional displacement of cylinder during oscillation, $Y = y/h$.
- y — Displacement of cylinder during oscillation.
- \dot{y} — Vibration velocity.
- α — Van Der Pol coefficient, in the special case $a(\omega_0) = \alpha\omega_0$.
- β — Fraction of critical viscous system damping.
- γ — Van Der Pol coefficient in asymptotic form, $\mu\gamma = \frac{4a(\omega_0)}{3C_{Y_0}^2\omega_0^2}$.
- δ — Limit cycle τ_1 -frequency.
- κ_1 — Coefficient of e^{iT} in C_1 .
- κ_3 — Coefficient of e^{i3T} in C_1 .
- $\kappa_{3\omega_0}$ — Coefficient of $e^{i(3\omega_0)T}$ in C_1 .
- $\kappa_{2\omega_0+1}$ — Coefficient of $e^{i(2\omega_0+1)T}$ in C_1 .
- $\kappa_{2\omega_0-1}$ — Coefficient of $e^{i(2\omega_0-1)T}$ in C_1 .
- κ_{ω_0+2} — Coefficient of $e^{i(\omega_0+2)T}$ in C_1 .
- κ_{ω_0-2} — Coefficient of $e^{i(\omega_0-2)T}$ in C_1 .
- λ — A convenient parameter for calculations, $\lambda = i(iD - B)A_0/(\omega_0^2 - 1)$.
- μ — An asymptotic parameter, arranged for the method of multiple scales so that $\mu^2 = n$ and $\mu \propto a(\omega_0)$.
- ν — A convenient parameter for calculations, $\nu = i\omega_0 B_0$.
- ξ_1 — Phase difference in the resonance region, $\xi_1 = \phi_1 - \psi_0$.
- ξ_2 — Phase difference in the resonance region, $\xi_2 = \phi_2 - \psi_1$.
- ρ — Fluid density.
- σ_k — Detuning parameters in Ω , $\Omega = 1 + \mu\sigma_1 + \mu^2\sigma_2 + \dots$.
- τ_k — Slow time scales, $\tau_k = \mu^k T$, $k = 1, 2, 3, 4$.

- ϕ_0 — Phase angle of $O(1)$ coefficient of e^{iT} in Y_0 , set to zero by freedom of choice of origin.
- ϕ_1 — Phase angle of $O(\mu)$ coefficient of e^{iT} in Y_1 .
- ϕ_2 — Phase angle of $O(\mu^2)$ coefficient of e^{iT} in Y_2 .
- ψ_0 — Phase angle of $O(1)$ coefficient of $e^{i\omega_0 T}$ in C_0 .
- ψ_1 — Phase angle of $O(\mu)$ coefficient of $e^{i\omega_0 T}$ in C_1 .
- ω — Natural circular frequency of oscillation of cylinder.
- ω_0 — Nondimensional wind speed (Strouhal Frequency) $\omega_0 = U/U_r$.
- ω_i — Hopf Bifurcation Point.
- Ω — Detuning, $\Omega = 1 + \sum_{k=1}^{\infty} \mu^k \sigma_k$.

Acknowledgements

I would like to thank most of all my wife Sumaya, for her truly loving support, encouragement, sympathy, and patience. Next I would like to thank my supervisor, Dr. G. V. Parkinson, for his continuing interest and useful suggestions. Also, members of my supervisory committee, in particular Dr. I. S. Gartshore and Dr. B. Seymour, raised points of interest and gave valuable suggestions. David Hare provided assistance with TeX, writing many of the macros used to produce this thesis. I also thank the Natural Science and Engineering Research Council of Canada for their generous support, and the Departments of Mechanical Engineering and Mathematics for the support offered in the form of assistantships. Lastly, I thank my parents, and my parents-in-law, for their extreme generosity and confidence; without them, this thesis would never have been possible.

Chapter 1

Introduction

*So high they stood, that they might have
been clouds in the upper air; save that
they swam not as clouds, but persisted,
and that their architecture was not cloud-
like, but steadfast, as of buildings of the
ancient earth; ... and yet all as if of no
gross substance, but rather thin spirit ...
—E. R. Eddison.*

1.1 Outline of the Problem

The problem of flow-induced vibration of two-dimensional cylinders of various cross-sections has a long history of study, arising from the discovery, in the last half century, that the aeroelastic effects of wind on structures can be as important as the effects of steady wind loads. Some of these observed aeroelastic effects are the result of coherent interaction of the wind with the structure, and should be distinguished from the response of structures to the random effects of the turbulence present in natural winds. We will consider here two of these coherent forms.

The commonest of these is that caused by the organized wake vortex system. Downstream of an aerodynamically bluff body, a separated wake forms, with breadth approximately that of the body. The separating shear layers are unstable, and roll up to form discrete vortices. Under relatively two-dimensional conditions, the vortices are swept downstream and form two parallel rows with equal vortex spacing, staggered so the vortices alternate. For a particular structure, it is observed that the vortices in each row form at a frequency f proportional to the incident wind speed V and inversely proportional to the diameter h of the body. The proportionality constant is the Strouhal number

$$S = \frac{fh}{V}.$$

This number is typically about 0.2 for cylinders of moderately symmetrical cross section.

Because of the alternating pressure loading on the structure caused by this organized wake vortex system, the structure is subject to a periodic forcing, at frequency f in the direction transverse to that of the flow, and to a weaker drag force with frequency $2f$, acting in the direction of the flow. If the natural frequency of the body is near these frequencies, one can expect the structure to develop a resonant response. The response of course depends on the natural mode corresponding to the natural frequency, but as is usual in any problem the simplest responses occur

the most often. Here we will only be considering strictly transverse oscillation of a cylinder of square cross section under two-dimensional conditions. The Strouhal number for this cylinder is 0.13.

The other important coherent form of wind-induced oscillation that we will be investigating is called galloping. Galloping is a low-frequency, high-amplitude oscillation due to a classical instability in which the body, experiencing a bump in a direction normal to the wind, receives a further aerodynamic force in the direction of the bump, tending to increase the motion. This class of oscillations occurs for the same types of structures as vortex-induced oscillations, but requires some asymmetry, so that a cylinder of circular cross-section will not undergo galloping, but a square cylinder will. The final catastrophic oscillation of the original Tacoma Narrows Suspension Bridge in 1940 was an example of torsional galloping. Transmission lines, normally too symmetrical to gallop, can become covered in ice on one side, giving enough asymmetry to gallop and ultimately break. The stall flutter of an airfoil about its stalling angle is also an example of galloping.

The interest in the interaction of the two forms of oscillation, possible under certain conditions, arises from the fact that modern tall buildings are more lightly constructed for reasons of economy than previously, and the trend in design is more toward conditions where both forms of oscillation can occur. Sullivan [24] has noted experimentally that for some reasonable parameters the observed amplitude of os-

cillation of a three dimensional model of a tower of square section in a wind tunnel simulation of the natural wind is greater than that expected from considerations of either form of oscillation alone. Further experiments by Wawzonek [26] indicated that this interaction also occurs in the case of a cylinder of square cross-section under two-dimensional flow conditions. Recent experiments by Bearman, Gartshore, Maull, and Parkinson [1] (hereafter referred to as BGMP) have confirmed this by more detailed study, including wake frequency measurements. A separate, hydrodynamic, study was earlier carried out by Bouclin [5], showing some significant interaction in the case of oscillation in water, also.

1.2 Vortex-Induced Vibration

Vortex-induced vibrations can occur for any aerodynamically bluff cylinder with an appreciable afterbody. The afterbody, downstream of the separation points, interacts with the wake system to give rise to the pressure loading on the body. Most studies of vortex-induced vibration have been carried out on the circular cylinder, which does not undergo galloping, but a square cylinder will undergo both forms of flow-induced vibration. Most of the qualitative phenomena associated with vortex-induced vibration are the same for both the square and the circular cylinder, and so the discussion which follows applies to both.

The phenomena which occur have been experimentally observed by many, in-

cluding Feng [8]. Vortex-induced vibrations characteristically are limited in amplitude to the order of magnitude of one cylinder diameter, and occur only in a discrete range of windspeeds. Nondimensionalizing time so that the natural frequency of oscillation of the body is 1, we have by the Strouhal relationship that the wake frequency of a stationary cylinder is 1 when the nondimensional wind speed $U = U_r = 1/(2\pi S)$, or equivalently when the Strouhal frequency $\omega_0 = U/U_r = 1$. One would expect that the maximum amplitude of vortex-induced oscillation would occur at this wind speed, but such is not in fact the case. Nonzero amplitudes of oscillation begin for ω_0 just less than 1, and continue for a range of ω_0 typically up to about 1.5, and the maximum amplitude occurs at about $\omega_0 = 1.3$. The frequencies measured in the wake in this wind speed range do not contain the expected Strouhal frequency, but rather just a frequency very close to the natural frequency of the body. The body is of course oscillating at this frequency. This is the phenomenon of synchronization, or lock-in. It is also possible to have a hysteresis effect, where there are two different possible stable amplitudes of oscillation at the same wind speed.

Different structures under three-dimensional conditions will have different quantitative behaviour. Most importantly, there will be several natural frequencies corresponding to different modes of oscillation, and these will correspond to different ranges of the wind speed at which vortex-induced oscillation can occur. The sys-

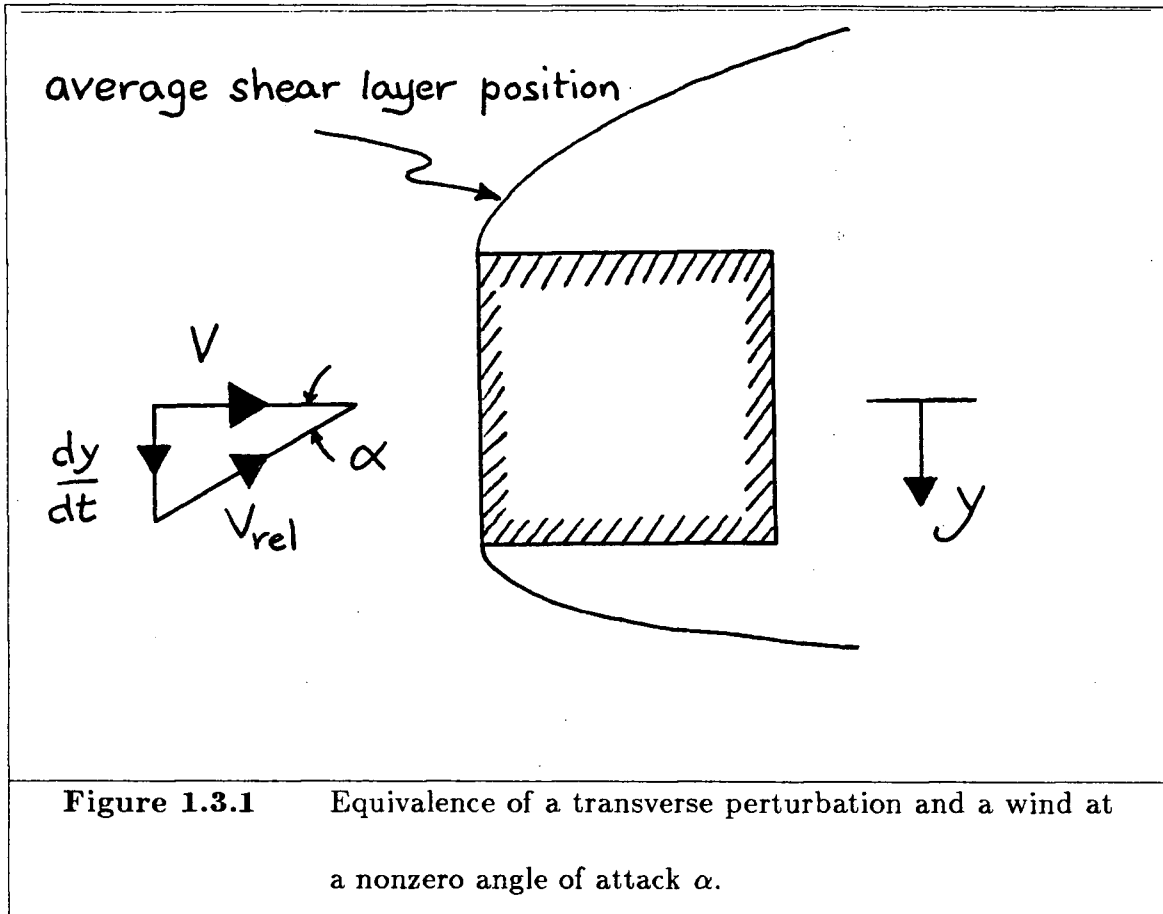
tem damping is an important parameter, and increasing the damping will naturally decrease the amplitude of oscillation. However, decreasing the system damping will only increase the amplitude of oscillation until the maximum amplitude is on the order of one diameter, as this form of flow-induced oscillation is self-limiting.

1.3 Galloping

Galloping occurs, as with vortex-induced oscillation, at the natural frequency of the body. The principal qualitative differences between vortex-induced oscillation and galloping are, first, that galloping occurs typically for all wind speeds above a critical wind speed U_0 that depends on the system damping, the mass, and the aerodynamic shape of the structure, whereas vortex-induced oscillations occur only in a discrete range, and second, that the amplitudes occurring in galloping oscillations are very much larger, having been observed to be as much as 100 times the diameter of the structure for some ice-covered transmission lines. It is important to note that the smaller size of the vortex-induced oscillations mitigates their effect somewhat, but under certain conditions can have just as deleterious an effect on a structure as a larger amplitude oscillation through fatigue of the materials involved.

For an aerodynamically bluff shape with fixed separation points, such as a square cylinder, the shear layers separating from the body can be considered symmetrical. In fact, of course, the vortex-induced fluctuations of the shear layers are also present,

but *under certain conditions* we can consider only the time-averaged placement of the shear layers. If the frequency of vortex shedding is sufficiently different from the natural frequency of oscillation of the body, then the important criterion for the force on the body is the placement of the time-averaged shear layers. This observation is what we would expect from a linear theory, but, as we have already noted in the case of vortex-induced oscillation, the linear theory is often misleading. However, this observation is justified when $U_0 \gg U_r$ by the success of the quasi-steady theory, which is based on this assumption and the assumption that the force felt on the cylinder in motion is the same as that felt on a stationary cylinder held at the equivalent angle of attack α . When the cylinder undergoes a motion in the transverse direction, the vector sum of the velocity of motion of the body and that of the wind gives rise to a wind at an apparent angle of attack α , where $\tan(\alpha) = \dot{y}/V = \dot{Y}/U$ (see Figure 1.3.1). The quasi-steady assumption is that the force on the body resulting from this apparent angle of attack is the same as that measured on a stationary cylinder mounted at that angle of attack. Thus measurements of this simpler kind give information that we can use to predict the dynamic response of the cylinder. More detailed discussion of this follows in Chapter 2.



1.4 Interaction Effects

When the vortex-shedding frequency is near the body frequency, the assumption that the time-averaged shear layer shape is the most important determining feature of the motion of the body is violated. Thus one would expect that the quasi-steady theory developed for galloping would no longer apply, as it is the periodic disturbances of these shear layers, averaged out for the quasi-steady theory, which play the largest role in the motion of the body. Here we expect the theory of vortex-induced vibration to play the largest role, and under most circumstances it does.

However, it is possible that the phenomena underlying the quasi-steady theory will play a role in this region, as well.

Significant interaction effects have in fact been observed by Sullivan [24], Wawzonek [26], and most recently by BGMP [1]. They found experimentally that when $U_0 \not\gg U_r$, that is, when $U_0 \approx U_r$ or $U_0 < U_r$, that galloping and vortex-induced vibration appeared to interact, making the theories for each individual case not as useful. In fact, the experiments indicated in the case $U_0 \approx U_r$ that the observed amplitudes were significantly higher than those predicted for either form of vibration alone. When instead $U_0 < U_r$, they found that galloping began not at U_0 as predicted by the quasi-steady theory, but rather at U_r . This appears to be a result of a quenching effect of the vortex system on the galloping instability, which holds until the vortex system itself begins to move the cylinder, at which wind speed the system begins to gallop.

Also, a small but significant apparent subharmonic resonance was detected by BGMP, strongly associated with a peak in the wake excitation at a frequency three times the natural frequency of the body. It is desired to develop a theory which will explain all of these effects, and retain the predictive capability for the case of galloping and vortex-induced vibration taken separately.

Chapter 2

Proposed Mathematical Model

*‘So we be at one as for the end,’ replied
Beroald, ‘it should be no unexampled dif-
ficulty to find out the means.’
— E. R. Eddison*

2.1 General Remarks

We are looking for a semi-empirical model of the combined effects of vortex-induced vibration and galloping. This means that we would like a mathematical model with a *few* free parameters that can be fixed by *simple* experiments; simple, that is, in comparison with the full dynamic investigations done in, e.g., [1]. Where possible, we would like the parameters to be fixed by experiments on a *static* cylinder, and thus depend only on the geometry. For simple galloping, this goal is achieved; Parkinson and Smith’s quasi-steady model [20] is very accurate, given only the polynomial fit of C_y versus $\tan(\alpha)$ data from the fixed cylinder, in the case that $U_0 \gg U_r$. For vortex-induced vibration, however, the Hartlen-Currie model

[10], requires that some forced-vibration experiments be done to fix some of the parameters, if they are not to be chosen *ad hoc*. We expect that for full agreement with the experimental data over a wide range of wind speeds that we shall have to do the same here. Note that a fully rational model would enable us to predict the dynamic behaviour when only the geometry is known; naturally, such a model would in this case be very complicated. With the present semi-empirical approach, we hope to avoid some of the complexity, while retaining the predictive characteristics: from the results of simple experiments, we hope to predict the results of complicated experiments.

Parkinson and Smith's Quasi-Steady Model [20].

The first model that we shall make use of is Parkinson and Smith's quasi-steady model of galloping. We model the displacement of the cylinder with the following equation:

$$\ddot{y} + 2\beta\dot{y} + y = \frac{\rho V^2}{2m} C_{F_y}$$

which we nondimensionalize to

$$\ddot{Y} + 2\beta\dot{Y} + Y = nU^2 C_{F_y}.$$

The forcing term on the right hand side is determined by the fluid mechanics of the system, and is modelled here by the use of the quasi-steady assumption. We saw earlier that the force on a cylinder at an angle of attack α can be measured

relatively easily; by the quasi-steady assumption, this can be taken to be the force on a cylinder moving transverse to the wind with velocity \dot{Y} , where the correspondence is given by $\tan(\alpha) = \dot{Y}/U$. We fit a polynomial in $\tan(\alpha)$ to the measured data, and use this expression as a polynomial in \dot{Y}/U in the above equation. The linear derivative term is of particular importance, and we include the system damping here by putting

$$U_0 = \frac{2\beta}{n\mathcal{A}_1}$$

which gives, redefining C_{F_y} to include this damping term,

$$\ddot{Y} + \dot{Y} = nU^2 C_{F_y}$$

where now

$$C_{F_y} = \mathcal{A}_1 \left(1 - \frac{U_0}{U}\right) \frac{\dot{Y}}{U} - \mathcal{A}_3 \left(\frac{\dot{Y}}{U}\right)^3 + \mathcal{A}_5 \left(\frac{\dot{Y}}{U}\right)^5 - \mathcal{A}_7 \left(\frac{\dot{Y}}{U}\right)^7.$$

This is a single degree of freedom nonlinear oscillator system. It can be solved analytically by many approximate methods when the mass parameter n is small enough, as it is in the case of aerodynamic oscillation, and may also be in some hydrodynamic cases. Parkinson and Smith used the method of Krylov-Bogoliubov to solve this equation, with very good results when U_0 , the above calculated critical wind speed, was much larger than U_r . In particular, all the qualitative features of galloping discussed previously were reproduced by the solution to this model, and

the quantitative accuracy of the solution is also of a high order of accuracy. Certain features of the solution are easy to see without much analysis. It is obvious that $Y \equiv 0$ is a solution of the equations, and its stability is obtained by considering the equation linearized about 0. But this is just a linear oscillator, with damping proportional to $-(1 - U_0/U)$. Thus the damping is positive if $U < U_0$, and hence the zero solution is stable. If on the other hand $U > U_0$ then the damping is negative, and the zero solution is unstable. This corresponds precisely with the observed characteristic of galloping, that galloping occurs only for winds above a certain critical wind speed. This observation is in fact independent of the size of n , which the approximate analytical solutions generally require to be small. A more complete solution, however, is required to determine the large-amplitude behaviour of this oscillator. This was done in [20], and the solution compared to experimental data. The solution included a hysteresis loop, and the mathematical solution showing this corresponded well with the experimental data.

The Hartlen-Currie Model [10].

In the case of vortex-induced vibration, no complete theory exists. However, the Hartlen-Currie model achieves a good qualitative agreement with experiment, and some reasonable quantitative accuracy. With this theory, we start with the same

equation as for the galloping theory,

$$\ddot{Y} + 2\beta\dot{Y} + Y = nU^2 C_v$$

but now the right hand side is chosen for agreement with the qualitative features of vortex-induced vibration. First, it is desired that the right-hand side reflect the periodic nature of the excitation. Next, we note that for a stationary cylinder, the excitation on the cylinder due to the wake system is *self-starting* and *self-limiting* with a limiting amplitude of C_{Y_0} , typically on the order of 1 (we have nondimensionalized so the cylinder diameter is 1). This suggests the following nonlinear oscillator equation for C_v :

$$\ddot{C}_v + \omega_0^2 C_v = \alpha\omega_0 \left(\dot{C}_v - \frac{4}{3C_{Y_0}^2 \omega_0^2} \dot{C}_v^3 \right) + D\dot{Y}.$$

This is the simplest equation giving the desired qualitative properties, and, coupled with the $D\dot{Y}$ term to the first equation, simply models the effect of the vortex system on the body. Here, α and D are essentially free parameters, to be chosen to make the solution fit the experimental data.

Proposed Mathematical Model.

Bouclin [5] took the mathematically natural approach of simply adding C_{F_y} and C_v for investigation of hydrodynamic oscillation. He also changed the functional form of $\alpha\omega_0$, making it a constant, which he called $GC_{Y_0}^2$, for unstated reasons.

We shall pursue this model further, examining some generalizations, and ultimately providing a useful approximate solution, instead of the numerical solution used by Bouclin in the hydrodynamic case. Our proposed model is only slightly generalized from his:

$$(2.1.1) \quad \tilde{Y} + Y = nU^2(C_{F_y} + C_v)$$

$$(2.1.2) \quad \tilde{C}_v + \omega_0^2 C_v = a(\omega_0) \left(\dot{C}_v - \frac{4}{3C_{Y_0}^2 \omega_0^2} \dot{C}_v^3 \right) + D(\omega_0) \dot{Y} + B(\omega_0) \tilde{Y}$$

where C_{F_y} is as in the quasi-steady model (including β) and C_v is as in the Hartlen-Currie Model. The only new term is the $B\tilde{Y}$ coupling term in the second equation, added as it is reasonable to expect some effects of the cylinder acceleration on the wake vortices. The dependence of the parameters a , B , and D on the wind speed ω_0 is also explicitly noted.

Remark Note that we take only the simplest linear combination of the two forms. Adding another parameter, λ say, making $C_{F_y} + \lambda C_v$, instead of $C_{F_y} + C_v$, can be shown to be redundant, as a scaling of the other parameters (C_{Y_0} in particular) can be used to make $\lambda = 1$.

Remark This model differs little from that used by Bouclin, aside from the new term $B(\omega_0)\tilde{Y}$. The main thrust of this thesis will be to show that there is a useful approximate analytical solution to these model equations, and to discuss the effect

of the functional dependence of the parameters on the solution. There are further natural generalizations to make; for example, adding a \dot{C}_v term to equation (2.1.1), or adding more nonlinearities to equation (2.1.2). Further nonlinearities could be added to the first equation, but these would be equivalent to changes in the second equation. We pursue the simple approach here, proceeding to complicated forms only if it proves to be necessary.

2.2 Functional Form of the Free Parameters

Of the parameters in equations (2.1.1)—(2.1.2), all are determined by experiments on a fixed cylinder, except β , $a(\omega_0)$, $B(\omega_0)$, and $D(\omega_0)$. The damping β can be determined independently of the wind speed, by still-air measurements. The parameters C_{Y_0} and A_k ($k = 1, 3, 5, 7$) are assumed constant. This assumption seems valid for the A_k , but is not strictly true for C_{Y_0} , although it is good enough for our purposes here.

The other parameters, though, are completely unspecified. Clearly by choosing the functional dependence correctly, we may fit any specified dynamic data, in an *ad hoc* fashion. However, this is contrary to the philosophy of the semi-empirical approach. We wish to have a simple functional form for the free parameters, with as few constants to be measured as necessary. In this section we explore some mathematical suggestions for the functional form of these parameters.

Hartlen and Currie [10] take $a(\omega_0) = \alpha\omega_0$, to make the logarithmic increment $\delta = \pi a(\omega_0)/2\omega_0$ independent of ω_0 , and hence constant for small changes in the Reynolds number. Bouclin [5], however, takes $a(\omega_0) = GC_{Y_0}^2$ to be constant, for unstated reasons. As he obtained quite reasonable results, except perhaps for over-predicting the amplitude near $\omega_0 = 1/3$, this may be justified, but we are interested in making a definite choice. To look at this closer, we look at the equation (2.1.2) in the simple case when $B = 0$ and $D = 0$, corresponding to a fixed cylinder. Making the change of variable $s = \omega_0 t$, $C = C_v/C_{Y_0}$, and denoting $a(\omega_0)/\omega_0$ by ϵ , we have

$$(2.2.1) \quad C'' - \epsilon(C' - \frac{4}{3}(C')^3) + C = 0$$

where $C' \equiv \frac{dC}{ds}$. Note that $\epsilon = \alpha$ in the Hartlen-Currie case, while for Bouclin $\epsilon = GC_{Y_0}^2/\omega_0$. Now (2.2.1) is a Rayleigh equation (also sometimes called a Van Der Pol equation, because they are equivalent), whose solution is well understood. For small ϵ , the solution approaches a near-circular limit cycle of radius ≈ 1 . For large ϵ , the solution approaches a nearly-discontinuous limit cycle, which has very sharp corners in it. Thus for moderately large ϵ we expect the solution to depart from a purely harmonic condition and acquire significant higher-frequency components. For this equation we do not have any even-frequency components, so the next most important frequency is 3 (corresponding to $3\omega_0$ on the t -scale). Thus if α and $GC_{Y_0}^2$ are equal at resonance ($\omega_0 = 1$), near $\omega_0 = 1/3$ we have ϵ three times larger in Bouclin's case than in the Hartlen-Currie case. The larger ϵ implies a larger

component at the higher frequency, which implies a larger superharmonic resonance in the full model. This argument is of course not meant to be rigorous, but rather to suggest that the Hartlen-Currie model is superior in this respect. Later we will see that other functional forms for $a(\omega_0)$ are useful, and do not suffer from this defect.

For $D(\omega_0)$, we look at the physical model. The original model of Hartlen-Currie used a constant, for simplicity. However, when one looks at the model, one really expects the important coupling value to be not the velocity of the cylinder, but the ratio of the velocity of the cylinder to the fluid velocity. Thus we expect that the functional form of $D(\omega_0)$ to be

$$D(\omega_0) = \frac{D}{\omega_0}.$$

We will see later that the solution of the model equations agrees better in the limit as $U_0 \gg U_r$.

Lastly, we look at the coefficient $B(\omega_0)$. It is not easy to find suggestions as to the form of this coefficient, except perhaps from the model equation itself. If we look at the quasi-steady equation, we have

$$\frac{\ddot{Y}}{U^2} + \frac{Y}{U^2} = nC_{F_y}$$

and C_{F_y} is seen to be composed of terms that depend only on the ratio \dot{Y}/U . If

the relevant parameter for the velocity coupling is \dot{Y}/ω_0 (equivalent to \dot{Y}/U), then we might try \ddot{Y}/U^2 , and thus be led to a functional form

$$B(\omega_0) = \frac{B}{\omega_0^2}.$$

We find, however, that with this form we cannot get a significant subharmonic resonant response. To exhibit a significant subharmonic response, we use the following *ad hoc* functional form for B ,

$$B(\omega_0) = B_0 + B_2\omega_0^2,$$

and choose the parameters B_0 and B_2 to give the right qualitative subharmonic response.

Chapter 3

Model Synthesis

I hope you will wisely think you beforehand, using meditations and weighings pro and contra, afore you begin...

—*E. R. Eddison*

3.1 Parameters Fixed by Static Experiments

The coefficients \mathcal{A}_1 , \mathcal{A}_3 , \mathcal{A}_5 , and \mathcal{A}_7 are fixed in the usual fashion by measuring the force on a static cylinder at different angles of attack. The main source of differences in the non-dimensional coefficients seems to be in the turbulence levels. Later, we will be comparing the approximate analytical solutions with data taken from [1], so we will use their lateral force coefficient data to find the \mathcal{A}_k . The experiments reported in [1] were done at three different turbulence intensities, and thus we must do three different polynomial fits [Fig. 3.1.1].

Remark It is of course a ‘kitchen’ problem to fit a polynomial to data, but we note here that in order to secure agreement between the \mathcal{A}_1 coefficient reported

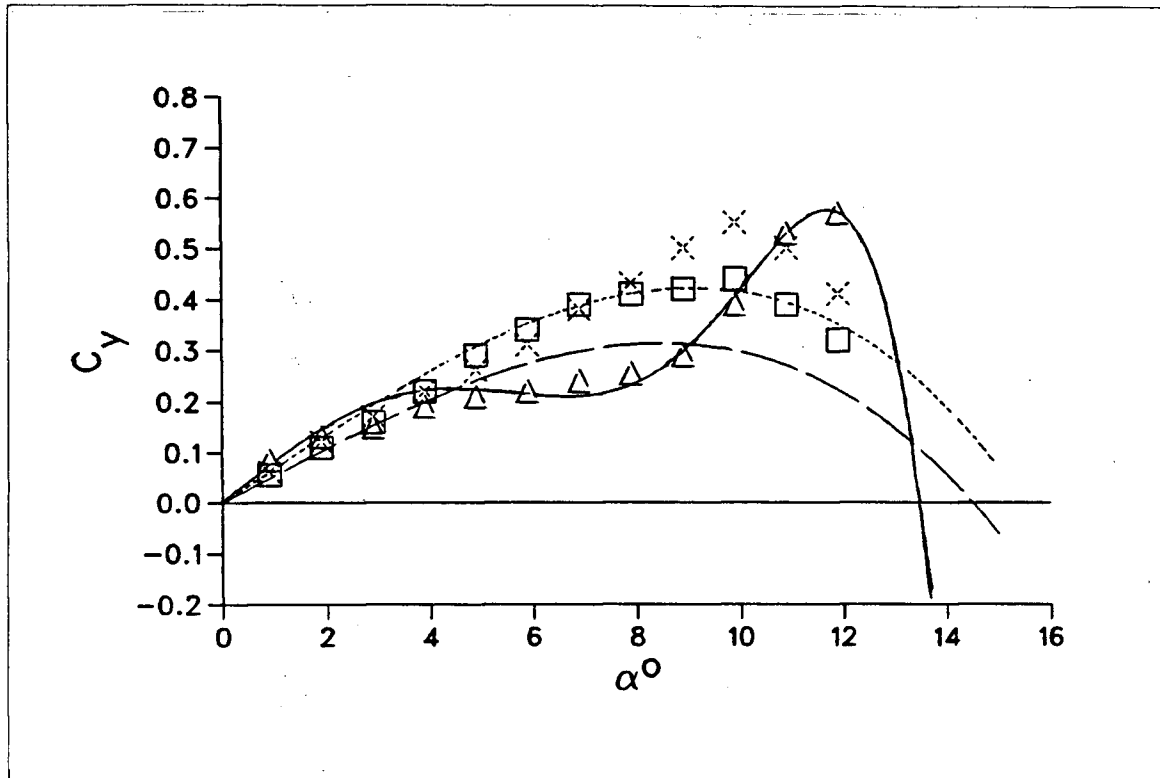


Figure 3.1.1

Lateral Force Coefficients from [1]
for varying turbulence levels

v'/V	Data	Polynomial Fit
0.0%	\triangle	— $4.87t - 421t^3 + 17000t^5 - 194000t^7$
6.5%	\times $3.95t - 51.4t^3$
10.5%	\square	-- $3.15t - 47.1t^3$

where $t = \tan(\alpha)$.

in [1] and that found with the least-squares fit, it was necessary to use a *weighted* least-squares fit. This was done because it is important to secure good values for A_1 , as the model is quite sensitive to this value. For the medium and high-turbulence case, since we were fitting a cubic rather than a 7th-degree polynomial, it was easier to do a direct fit rather than least-squares, taking the measured A_1 value from

[1] and fitting the remaining coefficient A_3 'by eye'. It was found that the most important characteristic of the data was the slope at zero, $dC_L/d\alpha|_{\alpha=0}$, and the best results were obtained when this parameter was used to fit the data. Of course, other criteria, such as the location of the maximum lateral force coefficient, could be used, with nearly as good results. The polynomials used are observed in Figure 3.1.1 to underpredict the data by as much as 30%. This is a consequence of forcing the first coefficient to be as given.

The turbulence levels measured in [1] were $v'/V = 0\%$, 6.5% , and 10.5% , the low, medium, and high levels. The data are reproduced in Fig. 3.1.1 and compared with the polynomials fitted, and the polynomial fit coefficients are given below:

k	A_k		
	Low	Medium	High
1	4.87	3.95	3.15
3	4.21×10^2	51.4	47.2
5	1.70×10^4	0.0	0.0
7	1.94×10^5	0.0	0.0

We have used a degree 7 polynomial to fit the low turbulence data in order to fit the characteristic double curvature of the data. The higher turbulence data does not have this characteristic, and qualitatively a cubic polynomial is sufficient to fit the data. Quantitatively, the polynomial fits are quite poor, but the simplicity gained by keeping only the degree three nonlinearity is worth the accuracy lost.

3.2 Experimental Determination of a , B , and D .

We will use the data reported in [2,16] to fix, for $\omega_0 = 1$, the values of the remaining free parameters. Bearman and Obasaju carried out forced-vibration experiments with a square-section cylinder in cross flow, and measured the effect on the fluctuating lift on the cylinder. Obasaju [16] reported fitting the parameters in

$$(3.2.1) \quad \ddot{C}_L - \alpha\omega_0\dot{C}_L + \frac{\gamma}{\omega_0}\dot{C}_L^3 + \omega_0^2 C_L = B\omega_0^2 \sin(\omega t)$$

to his data. He reports $C_{L_0} = 1.4$, $\alpha = 0.13$, and $B/C_{L_0} = 0.179$, for an amplitude ratio of 0.10. We compare this with the form from our model equations, with $Y = \bar{Y} \sin(\omega t)$:

$$(3.2.2) \quad \ddot{C}_v - a(\omega_0) \left(\dot{C}_v - \frac{4}{3C_{Y_0}^2 \omega_0^2} C_v^3 \right) + \omega_0^2 C_v = D\omega \bar{Y} \cos(\omega t) - B\omega^2 \bar{Y} \sin(\omega t).$$

Now, $\omega \approx 1$ in [16], and to make our form more compatible, we put $E^2 \omega_0^4 = \bar{Y}^2 (B^2 + D^2)$. Then we have $D\bar{Y} \cos(t) - B\bar{Y} \sin(t) = E\omega_0^2 \sin(t + \theta)$, where θ is defined appropriately. At resonance, (3.2.1) has the solution $C_L = \bar{C}_L \sin(t - 90^\circ)$. If $\sin(t)$ is in phase with cylinder velocity, then the angle ϕ by which the lift C_L leads the displacement is $\psi + 90^\circ = 0^\circ$. If $\sin(t)$ is in phase with the cylinder displacement, then we have $\phi = -90^\circ$. The measured ϕ , however, is more nearly -70° , than either of these. Noting that $\bar{Y} = 0.1$ in the forced-vibration experiments,

we have

$$(3.2.3) \quad E = 2.5$$

$$(3.2.4) \quad \psi - \theta = -70^\circ$$

thus

$$\theta = -20^\circ$$

so, at $\omega_0 = 1$,

$$B(1) = -2.5 \cos(20^\circ) = -2.35$$

$$D(1) = 2.5 \sin(20^\circ) = 0.855.$$

Note also that $a(1) = 0.13$.

Remark It is possible to determine more than just one value from this data. However, all the data in [16] is from the resonance region, and I believe that it is necessary to gather data outside the resonance region, and in particular in the subharmonic and superharmonic resonance regions, before this practice becomes useful. These values give a good fit with the \overline{C}_L observed in the resonance region (as Obasaju's already did), and a slightly better fit for the phase angle data.

Chapter 4

Methods of Solution of the Model Equations

*I myself have since, by divers ways, as
many lines as meet in a dial's centre,
come nearer the truth.*
—E. R. Eddison

4.1 Discussion of Available Methods

There are several methods in our 'kitchen' for finding an approximate solution of the model equations, each with their advantages and disadvantages. We shall consider four different approaches here: the method of Van Der Pol, the method of multiple scales, a bifurcation solution, and a direct numerical approach. This last method is the simplest in concept as well as the simplest in execution, but we shall see that in many ways it is the least satisfactory. All of the other methods reduce ultimately to numerical computation of one sort or another, but as is usual a computer is no substitute for thought. It is useful to note at this point that we use

the symbolic manipulation language REDUCE [11] for many of the computations that occur. REDUCE makes the manipulation of polynomials and asymptotic series easy, and in this context represents a proper use of a computer.

The first method we consider is a natural one, the method of Van Der Pol [14,27,10]. We expect to see oscillation at or near the natural frequency, so we look for a solution of the form

$$(4.1.1) \quad \begin{aligned} Y &= \bar{Y} \cos(\Omega t) \\ C_v &= \bar{C}_v \cos(\Omega t + \psi) \end{aligned}$$

On substitution into the model equations, we get two inconsistent equations, in that the coefficients of the terms $\cos(3\Omega t)$, $\sin(3\Omega t)$, and higher frequencies, are not equal on both sides of the equations. However, we can insist that the coefficients of $\cos(\Omega t)$ and $\sin(\Omega t)$ are equal, and this gives us four equations for the four unknowns \bar{Y} , \bar{C}_v , ψ , and Ω . Due to the polynomial character of our model equations, we will get four coupled polynomial algebraic equations. Theoretically, this is a step forward. Surprisingly, in spite of the dubiousness of ignoring the effect of the higher-frequency terms, this method is quite accurate (when we can solve the resulting polynomial equations). There are three main theoretical difficulties, however: No error estimate is available, so we do not know how accurate our solution is; there is no obvious way of computing the stability of the computed solution; and there is no provision for the sometimes-important higher-frequency terms. All of these combine to make

the method of Van Der Pol useful only as a first approximation. There is a further practical difficulty, more important if a more complicated form than (4.1.1) is taken, and that is the difficulty of solving systems of polynomial equations. There are many efficient methods for solving such systems: for example, the homotopy methods, which develop a system of differential equations with complex initial conditions whose limiting solutions are the roots of the original polynomial system, and use a numerical ODE solver to find these roots. It is amusing to note that this is the precise reverse of the classical technique for solving differential equations! In this case, this could still be justified by the fact that the resulting ODE's would be nonstiff, and much easier to solve numerically than the original system. We consider next a direct numerical solution of the model equations. There are many efficient methods for the solution of such initial value problems, and many existing packages which we can take advantage of. There are three problems here: expense; the fact that a numerical solution obscures the effect of the various parameters, and gives relatively little insight into the solution; and the fact that we must vary our initial conditions to obtain all the stable solutions, while the unstable solutions remain inherently undetectable. First, we consider the cost of solving the system. We add the following (variable) initial conditions to the model equations, variable because

we do not know precisely what the physical initial conditions are:

$$(4.1.2) \quad \begin{aligned} Y(0) &= F_1 & C_v(0) &= F_2 \\ \dot{Y}(0) &= F_3 & \dot{C}_v(0) &= F_4 \end{aligned}$$

where the F_i are unspecified at present. Now, we need at least 10 values of the solution in each cycle, and we know from the experience of the Quasi-Steady model that the time taken to reach the limiting amplitude is $O(1/n)$ as $n \rightarrow 0$. For $n \simeq 10^{-3}$ this means about 10^4 values need to be calculated; now, for a reasonable response curve we need ~ 100 values of the limiting amplitude; this is already $\sim 10^6$ operations, and this is for a single set of initial conditions. We must also vary the other parameters of the model equations. If we have the computing resources available (and they have nothing better to be used for), then this approach is reasonable. We can improve the efficiency a great deal if we risk omitting any disconnected solutions by using the method of continuation. That is, we use the limiting amplitude of the previous wind speed solution as an initial condition for the current wind speed. This is a closer model of what actually happens in a wind tunnel (the wind speed is increased or decreased gradually, and the oscillations are allowed to reach a steady amplitude from there). This avoids the great deal of time involved in reaching the limit cycle.

However, we can do much better, at least for the case of small n , by using an asymptotic approach. As n increases, the cost of the direct numerical approach

decreases, while the asymptotic solution becomes less accurate. In this sense, the two methods complement each other, and this suggests that the numerical method is more appropriate for the case of oscillation in water, while the asymptotic approach is more appropriate for the case of oscillation in air. Of course, we would like the asymptotic approach to be useful for water as well.

We consider two essentially different asymptotic approaches: the method of multiple scales [3,13,15,25], and a bifurcation approach [6,12,21,22]. The method of multiple scales uses the physical parameters present in the problem, n and $a(\omega_0)$, and produces a solution that is asymptotic to the exact solution as $n \rightarrow 0$ and $a \rightarrow 0$. As a device to aid in the solution of the resulting equations, we will assume that $a \propto \sqrt{n}$ as $n \rightarrow 0$. This is reasonable, as the physical values of the parameters that we use are approximately of these orders, and in fact is crucial to the ease of solution; assuming that the two parameters are of the same order leads to a much more difficult set of algebraic equations. The idea for using this order of expansion came from an analysis of the solution of the model equations by the method of Van Der Pol near the resonance region, where the Van Der Pol solution was not precisely as expected.

We note that the resulting equations are still quite complicated, and although the solution to first order is possible by hand with some degree of certainty, the next term is harder, and the use of the symbolic manipulation language REDUCE

is justified. The third terms, obtained as a check on the consistency of the solution and as an error estimate, would not have been obtainable by hand without heroic effort.

For a solution, we get an asymptotic expansion in powers of $\mu = \sqrt{n}$, and we hope that the physical value of n is small enough to give reasonable answers from the asymptotic solution, with only a few terms needed. We will find three time scales useful in our solution: T , characteristic of the time for one oscillation, $\tau_1 = \mu T \sim \alpha T$, the time scale on which the vortex excitation grows, and $\tau_2 = \mu^2 T \sim nT$, the time scale of the amplitude growth as in the quasi-steady theory. We should note at this point the different meanings of the $O(n)$ symbol to the mathematician and the engineer: to a mathematician, the phrase $X = O(n)$ as $n \rightarrow 0$ means precisely that the quantity X satisfies

$$\lim_{n \rightarrow 0} \frac{X}{n} = K < \infty$$

where K is any constant. To an engineer, the phrase $X = O(n)$ when $n = 10^{-3}$ simply means that X is about 10^{-3} . It is one of the more useful features of asymptotic series that the constants K that come up are often of moderate size, so that the two meanings of $O(n)$ then approximately coincide; in fact, we often find that the constants are such that our asymptotic series give results far better than we have a right to expect. Here the method of multiple scales will give a solution of

the form

$$(4.1.3) \quad \begin{aligned} Y &= Y_0 + \mu Y_1 + \mu^2 Y_2 + \cdots \\ C_v &= C_0 + \mu C_1 + \mu^2 C_2 + \cdots \end{aligned}$$

and we shall find that we get good accuracy with only two terms for Y and one term for C_v . Further, the stability of the solutions is immediately available, as well as an asymptotic error estimate, although, as noted above, this is not the same thing as a practical error estimate, unless we are lucky. Thus, we still need some sort of assurance that our constants are not too large, and an estimate of the error made by taking so few terms. Thus we consider another asymptotic method, that used for bifurcation theory.

As in the Hopf Bifurcation Theory, we introduce the new parameter $\epsilon = \omega_0 - \omega_i$, where ω_i is an easily-found value of the non-dimensional wind speed at which some pair of eigenvalues of the system linearized about 0 crosses the imaginary axis. As this parameter actually goes to zero physically, we know that this parameter will be small enough (at least in some region of the response curve) to provide an arbitrarily accurate solution. Some formulae for these calculations were worked out for the Hartlen-Currie model by Poore and Al-Rawi [21,22], and an adaptation of their work provides us with a solution which is very accurate near these Hopf Bifurcation Points and near the zero solution. This last restriction limits the utility of the approach, as all of the solutions found by this method are *unstable*, but these

are the only completely accurate solutions we have any information about, so they are useful in checking the other methods. It is also interesting and informative to investigate how these periodic solutions bifurcating from the zero solution affect the ‘nearby-in- Y ’ solutions predicted by, for example, the method of Van Der Pol.

We find in conclusion that all four methods have their uses, and complement each other somewhat. The method of multiple scales is the method of choice for small n , but it needs checking; near zero by the bifurcation solution, and away from zero by the method of Van Der Pol. The numerical method is most useful for larger n , although we hope that the method of multiple scales will be useful even for quite large n , due to our experience with the surprising power of asymptotic methods.

Chapter 5

Solution of the Model Equations by the Method of Van Der Pol

*And now,—thinking on't in cold blood—
go, 'tis a thing not believable!*
—E. R. Eddison

5.1 Setting up the Equations

We look for a solution of the model equations (2.1.1)—(2.1.2) of the form

$$Y = \bar{Y} \cos(\Omega t)$$

$$C_v = \bar{C}_v \cos(\Omega t + \psi).$$

On putting these into the model equations, and ignoring the higher frequency terms, we have

$$(1 - \Omega^2) \bar{Y} \cos(\Omega t) = nU^2(-f(\bar{Y}) \sin(\Omega t) + \bar{C}_v \cos(\Omega t + \psi))$$

$$(\omega_0^2 - \Omega^2) \bar{C}_v \cos(\Omega t + \psi) = -a(\omega_0)g(\bar{C}_v) \sin(\Omega t + \psi) - D\Omega \bar{Y} \sin(\Omega t) - B\Omega^2 \bar{Y} \cos(\Omega t)$$

where

$$f(\bar{Y}) = p_1(\Omega\bar{Y}) - p_3(\Omega\bar{Y})^3 + p_5(\Omega\bar{Y})^5 - p_7(\Omega\bar{Y})^7$$

$$g(\bar{C}_v) = \Omega\bar{C}_v \left(1 - \frac{\Omega^2 \bar{C}_v^2}{C_{Y_0}^2 \omega_0^2} \right)$$

and

$$p_1 = \mathcal{A}_1 \left(1 - \frac{U_0}{U} \right) \cdot \frac{1}{U}$$

$$p_3 = \frac{3\mathcal{A}_3}{4U^3}$$

$$p_5 = \frac{5\mathcal{A}_5}{8U^5}$$

$$p_7 = \frac{35\mathcal{A}_7}{64U^7}$$

so, equating coefficients of $\sin(\Omega t)$, $\cos(\Omega t)$, we have

$$(5.1.1) \quad (1 - \Omega^2)\bar{Y} = nU^2\bar{C}_v \cos(\psi)$$

$$(5.1.2) \quad 0 = nU^2(f(\bar{Y}) + \bar{C}_v \sin(\psi))$$

$$(5.1.3) \quad (\omega_0^2 - \Omega^2)\bar{C}_v = D\Omega\bar{Y} \sin(\psi) - B\Omega^2\bar{Y} \cos(\psi)$$

$$(5.1.4) \quad 0 = a(\omega_0)g(\bar{C}_v) + D\Omega\bar{Y} \cos(\psi) + B\Omega^2\bar{Y} \sin(\psi).$$

This gives us four equations in the four unknowns Ω , ψ , \bar{C}_v , and \bar{Y} . We can eliminate ψ from the (5.1.1) and (5.1.2) by using (5.1.3) and (5.1.4) as linear equations in $\sin(\psi)$ and $\cos(\psi)$, and then squaring and adding appropriately (5.1.3) and (5.1.4) we get three polynomial equations in the unknowns Ω , \bar{C}_v , and \bar{Y} . With

$E^2 \equiv \Omega^2 D^2 + \Omega^4 B^2$, we have then

$$(5.1.5) \quad E^2 \bar{Y}^2 = (\omega_0^2 - \Omega^2) \bar{C}_v^2 + a^2 g^2(\bar{C}_v)$$

$$(5.1.6) \quad f(\bar{Y}) E^2 \bar{Y} = -\Omega^2 B a g(\bar{C}_v) \bar{C}_v + \Omega D(\omega_0^2 - \Omega^2) \bar{C}_v^2$$

$$(5.1.7) \quad (1 - \Omega^2) E^2 \bar{Y}^2 = n U^2 \left(-\Omega^2 B(\omega_0^2 - \Omega^2) \bar{C}_v^2 - \Omega D a g(\bar{C}_v) \bar{C}_v \right)$$

Remark This is an approximate solution of the differential equations (2.1.1)—(2.1.2) in the classical sense; that is, we have “reduced” the problem of finding the solution of a system of differential equations to that of finding a solution of a system of algebraic equations. As stated previously, this is in fact a difficult numerical problem, in general, especially when we have no initial guesses for the roots of the polynomial system. For this system, however, we do not need sophisticated general polynomial system solver routines, as with a simple further approximation we can reduce the system (5.1.5)—(5.1.7) to a single polynomial in a single variable. If we had started with a more complicated form for the solution of the model equations, however, this *ad hoc* approach would not work, and we would need a good polynomial system solver.

5.2 Solution of the Polynomial Equations

If we ignore solutions that have \bar{Y} small, then we are led by (5.1.7) to the conclusion that $\Omega^2 = 1 + O(n)$. This simplifies the solution considerably. We have

in this case

$$(5.2.1) \quad E^2 \bar{Y}^2 = (\omega_0^2 - 1)^2 \bar{C}_v^2 + a^2 g^2(\bar{C}_v)$$

$$(5.2.2) \quad E^2 \bar{Y} f(\bar{Y}) = \bar{C}_v^2 D(\omega_0^2 - 1) - a B \bar{C}_v g(\bar{C}_v)$$

and further,

$$(5.2.3) \quad \Omega^2 = 1 + \frac{n U^2 \bar{C}_v^2}{E^2 \bar{Y}^2} \left(B(\omega_0^2 - 1) + a D \left(1 - \frac{\bar{C}_v^2}{C_{Y_0}^2 \omega_0^2} \right) \right).$$

We may substitute (5.2.1) into (5.2.2) to get a single polynomial equation in \bar{C}_v^2 , which is solvable by standard numerical methods.

Remark Even single polynomial equations are sometimes difficult numerically, if there are roots that are close together. Here we do not have this problem, at least most of the time. This polynomial is degree 11 in \bar{C}_v^2 , and the coefficients were obtained by REDUCE for the FORTRAN program used to find the roots. The library routine RPOLY1 was used, as it is efficient and reliable.

Remark Now that we have provided an answer to the question of what the amplitudes are of the solution to the model equations, we would like also to answer the following questions:

1. How accurate is the solution?
2. Where is the solution stable, and where is it unstable?

3. Are there regions where the higher frequencies become important?

The first question is really unanswerable by this method. In ignoring the higher frequency terms, we seem to have made an error of $O(a)$ or $O(n)$, but the details are not clear. The second question can be answered, but it is not simple. In [27], Wood carries out a stability analysis for a similar series of models of vortex-induced vibration. He does not, however, allow for a sufficiently general variation. Thus when he claims a root is unstable, his results are correct, but when he claims a root is stable, his results are unconvincing. We will find that the stability analysis is much easier, in fact automatic, when the method of multiple scales is used instead. The third question can be addressed by using a more complicated form for the solution, instead of $\bar{Y} \cos(\Omega t)$ and $\bar{C}_v \cos(\Omega t + \psi)$. If we include higher-frequency terms (although it is difficult *a priori* to decide which frequencies to include), we should get more accuracy, and be able to tell when the higher-frequency terms are important. However, the polynomial systems that arise become unwieldy rather quickly, with each new term added, and as the method of solution in this case was rather *ad hoc*, this is not practical.

5.3 Results of the Method of Van Der Pol

The following figures, Figure 5.3.1 and Figure 5.3.2, show the results of the

method of Van Der Pol compared with data taken from [1]. We compare with the low turbulence data only, as illustration. We see that the agreement is quite good, except in the medium damping case near the upper range of values. We see some of the features of the quasi-steady model present in the solutions of this model, notably in the medium damping case, where we see three branches of the solution. There is a qualitative difference from the quasi-steady solution, however, in that a new branch of the solution is present, continuing the lower branch of the solution past $\omega_0 \approx 5$. When we compare this solution with that from the method of multiple scales, we see that this new branch is unstable. Comparison of this solution with experimental data is problematical in this case. The lower branch of the curve agrees quite well with the data, but one would have expected the experiments to show the upper curve as well, as for $\omega_0 < 5$ they appear to be within the range of measurement. However, past $\omega_0 \approx 5$ for the medium turbulence case, this model predicts that the upper branch would be outside the allowable deflections of the physical model. Since the upper branch can be detected only by decreasing the wind speed from a speed at which the upper branch is established, it may have been that the upper branch was in fact not detectable with the physical model. This could be verified by repeating the experiments, and giving the model a “bump” in the indicated wind speed range, to see if the upper branch could be detected. However, the lack of an upward curve in the data near the end of the predicted range of the lower stable

branch indicates to the contrary that the upper branch is not located correctly by the model equations.

Another curious feature is the “V”-shaped curve at the beginning of the high-damping case. Again, the later solution by the method of multiple scales shows that the left branch of the “V” is in fact unstable, leaving a more usual-looking curve. The solution in the resonance region is not clear from the graph, but other investigations not reported here have shown that the solution in the resonance region consists, for the high-damping case, of a “double humped response”. The solution in this region rises from zero before exact resonance to a peak, and then returns to zero precisely at resonance. This is followed by a second rise to a peak and then back again to zero. The method of multiple scales predicts similar solutions, but as we shall see in Chapter 7, different in detail. It is worth noting that the unexpected return to zero at exact resonance is an artifact of the method used to solve the polynomial equations, and that a more exact solution does not have this feature. It is consideration of this that led to the proper asymptotic form of the solution used in the method of multiple scales.

The low damping solution appears to be overpredicted just after the resonance region, perhaps by as much as 40%. Also, the kink near $\omega_0 \approx 3$ is not reflected in the solution. If in fact this is a subharmonic resonance, this is to be expected. The method of Van Der Pol is, in this simple form, incapable of describing the effects of

the higher frequencies.

One good feature of the solution of the model equations for the low damping case is that the nonzero solution begins near $\omega_0 \approx 1$, and not at the value predicted by the quasi-steady theory. This is a major qualitative feature of interest. The quasi-steady model was incapable of reflecting this feature, observed experimentally.

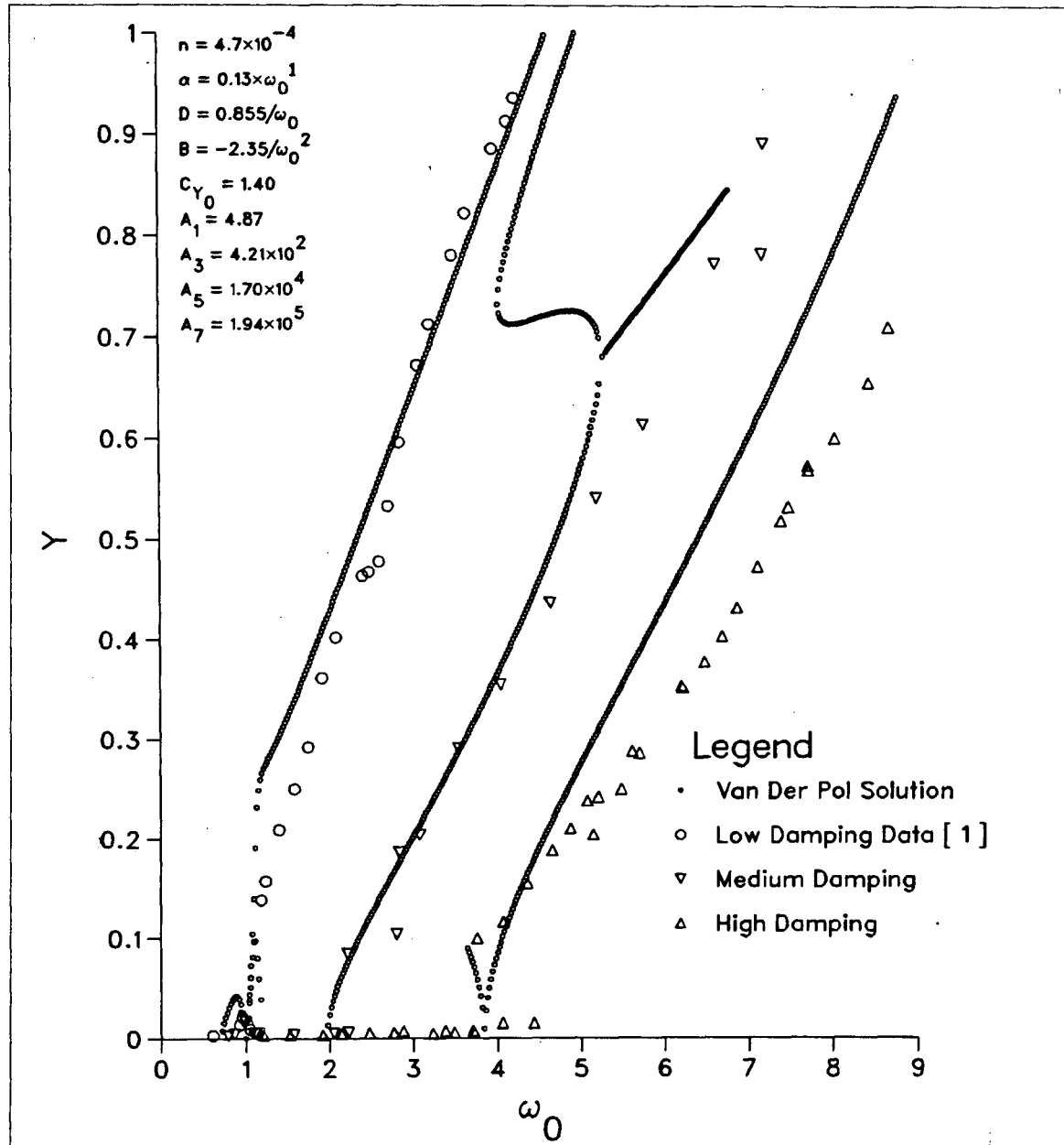


Figure 5.3.1 Van Der Pol Solution in the Low Turbulence Case.

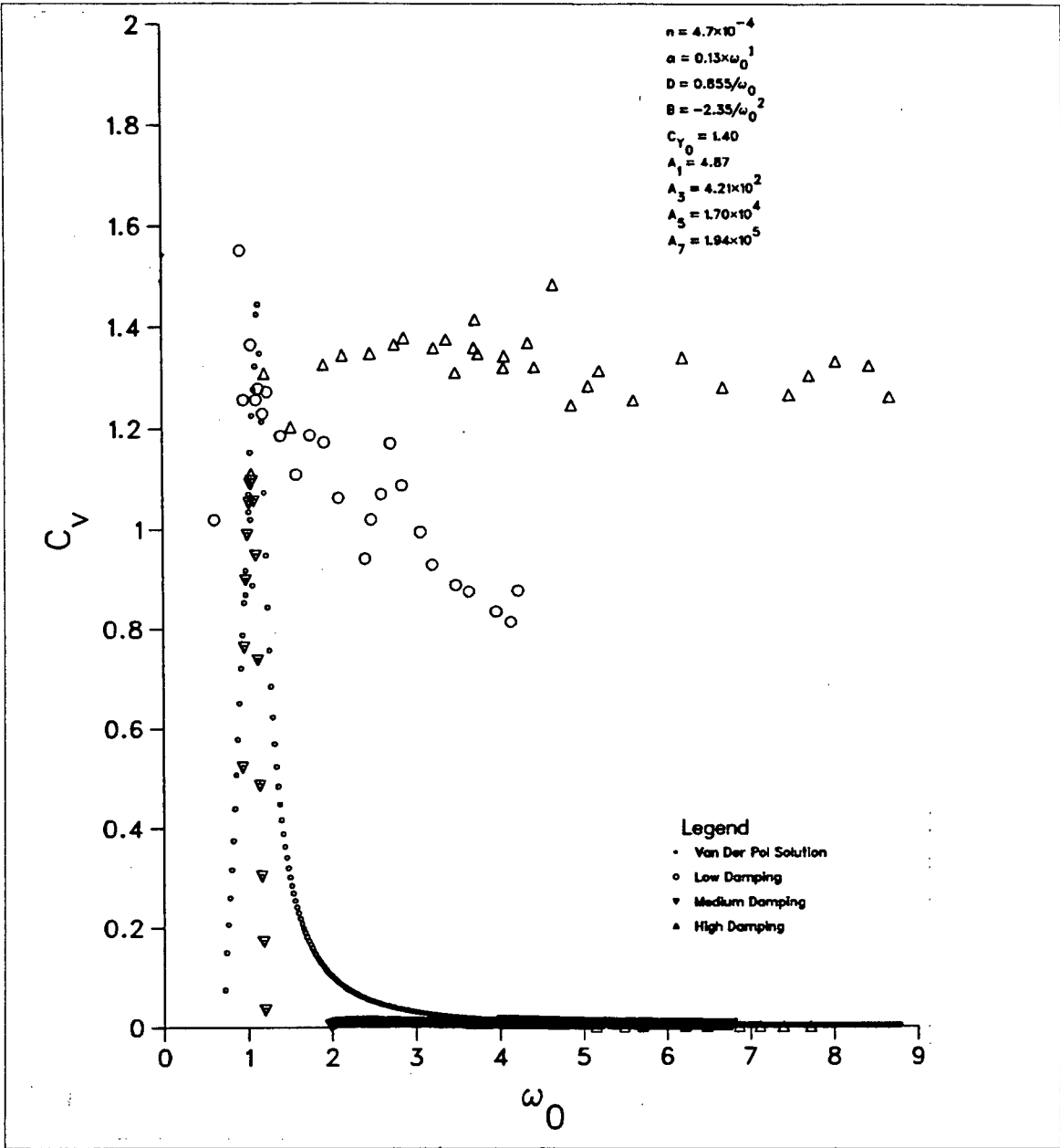


Figure 5.3.2 Excitation by the VDP solution in the Low Turbulence Case.

Chapter 6

Hopf Bifurcations of the Model Equations

*But first I would have you, as a politic
prince who will not lay your foundations
in the dirt but on archæan crust, refer
the whole estate to your highness' delib-
erate overviewing again.*

—E. R. Eddison

6.1 Introduction

In view of the fact that the model synthesis is semi-empirical, we must be somewhat more cautious in applying traditional methods of approximate solution. For example, we have no *a priori* assurance that the solutions to the model equations are sensible periodic solutions, or indeed exist at all. Also, we have seen that if we wish to apply the Method of Van Der Pol to solve the equations, it is helpful to have some idea of the form of the solution, and we will see that for the Method of Multiple Scales, it is helpful to try to estimate the effect of the size of the ‘small’ mass parameter n . This ideally would permit investigation of the model

for both the aerodynamic and the hydrodynamic cases. Thus we must try to find as much information about the exact solutions to the model equations as possible before putting any faith in the results of our approximate solutions. Of course, we cannot hope to solve these nonlinear equations exactly, but there are certain parameter values near which we can say a great deal about the solution, by the use of the mathematical tool, Hopf Bifurcation Theory.

Hopf Bifurcation Theory provides much useful information about the exact solutions of certain kinds of nonlinear equations, and also provides a method of calculating an approximate solution, guaranteed to be accurate in some (possibly small) neighbourhood of the zero solution. This will give us information about the model equations that will be valid for all values of the mass parameter n , and thus will include both the aerodynamic and the hydrodynamic cases. Of course, the theory has its limitations, which will be discussed after the basic ideas have been explained. An elementary, if somewhat terse, introduction to Hopf Bifurcation Theory can be found in [12].

6.2 Hopf Bifurcation Theory

This theory predicts the bifurcation of periodic solutions from steady-state solutions (in our case the zero solution) of nonlinear differential equations. Let the

equation be written as

$$\dot{x} = A(\omega_0)x + f(x, \omega_0)$$

where $x = (x, \dots, x_n)^T$, $A(\omega_0)$ is $n \times n$, f is the strictly nonlinear part of the equations, and ω_0 is a scalar parameter. The theory locates values of the parameter ω_0 , denoted ω_i , at which a periodic solution is initiated, and gives a method for finding the direction of bifurcation, the frequency of oscillation, and the amplitude and stability of this periodic solution, *all in a neighbourhood of the critical value of ω_0 and the zero solution*.

The basic idea of the theory is to first find the critical values of ω_0 , called Hopf Bifurcation Points (HBP's), and then use a local coordinate transformation to change the possibly strongly nonlinear equations to a set of weakly nonlinear equations, with a new parameter μ which is proportional to $\omega_0 - \omega_i$. These weakly nonlinear equations can then be solved in an asymptotic sense, and this asymptotic solution gives information about the exact solution in a neighbourhood of $\mu = 0$. This analysis does not depend on the possibly small mass parameter n , but rather on an artificially introduced new parameter which is guaranteed to be small enough, at least in a neighbourhood of the Hopf Bifurcation Point. The first task is to locate these Hopf Bifurcation Points. This is easily done, as they are the values of ω_0 for which some pair of eigenvalues of $A(\omega_0)$ cross simply the imaginary axis. When the equation is linearized at this point, the resulting linear equations have a purely

periodic solution. This is the basis of the theory, and of the asymptotic solution of the new weakly nonlinear equations. Thus if the eigenvalues of $A(\omega_0)$ are $\zeta_i(\omega_0)$ the HBP's are the roots of

$$\operatorname{Re}(\zeta_i(\omega_0)) = 0$$

subject to

$$\begin{aligned}\operatorname{Im}(\zeta_i(\omega_0)) &\neq 0 \\ \frac{\partial \operatorname{Re}(\zeta_i(\omega_0))}{\partial \omega_0} &\neq 0.\end{aligned}$$

If all the other eigenvalues of $A(\omega_0)$ have negative real parts, the HBP is also associated with the loss or gain of stability of the zero solution, as the parameter ω_0 is varied through the HBP.

In our model, the bifurcation parameter is the dimensionless wind speed ω_0 (or equivalently $U = U_r \omega_0$). Before proceeding with the analysis, we note that Poore and Al-Rawi [21,22] have developed formulae for the direction, stability, and amplitude of the periodic solutions for general ODE systems. They applied their formulae to the Hartlen-Currie model of vortex-induced vibration, and a similar application to this model is desired.

6.3 Bifurcation Formulae [21,22]

With some notational changes, the following theorems and formulae are taken

from [21,22]:

Let

$$x = \mu y$$

$$(1 + \mu\gamma)s = t$$

$$\varepsilon = \mu\delta = \omega_0 - \omega_i \quad (\mu > 0)$$

$$A^\varepsilon = A(\omega_0) = A(\omega_i + \varepsilon)$$

$$\varepsilon B^\varepsilon = A^\varepsilon - A^0$$

$$B^0 = \left. \frac{dA^\varepsilon}{d\varepsilon} \right|_{\varepsilon=0} = A'(\omega_i)$$

$$\mu^2 Q(y, \mu, \varepsilon) = f(\mu y, \omega_i + \varepsilon)$$

This transforms the differential equation (5.1) to

$$\frac{dy}{ds} = A^0 y + \mu G(y, \mu, \delta, \gamma)$$

where

$$G = \delta B^{\mu\delta} y + \gamma A^{\mu\delta} y + (1 + \mu\gamma)Q$$

Notice that the equation for y is a weakly nonlinear equation, in that as $\omega_0 \rightarrow \omega_i$, $\mu \rightarrow 0$. The theorems and formulae reproduced below are a consequence of the fact that this weakly nonlinear system of equations may be solved much more easily than the original system, and as the artificially introduced parameter μ does go to zero in a region of interest, we are guaranteed that the formulae given below will apply, at least in some possibly small region around the HBP. For details of this process, see [12]. The parameter $\delta(\mu) = \delta(0) + \mu\delta'(0) + \dots$ can be shown to have $\delta(0) = 0$; thus

$\mu^2 \delta'(0) \approx \omega_0 - \omega_i$ and then the sign of $\delta'(0)$ gives the direction of bifurcation. The parameter γ represents a detuning of the frequency of the oscillation, and it can be shown [12] that the amplitude of the bifurcating periodic solution is proportional to $\sqrt{\mu}$.

We know that at the Hopf Bifurcation Point, some pair of the eigenvalues of $A(\omega_0)$ are purely imaginary. Let $r(\varepsilon) \pm if_0(\varepsilon)$ be the continuous extension of these purely imaginary eigenvalues. We are now in a position to reproduce three theorems [21,22] which reduce the bifurcation problem to an explicit algebraic computation.

Theorem 1 [21] *Let $F(x, \varepsilon) \in C^k [D \times (-\varepsilon_0, \varepsilon_0)]$ for some $\varepsilon_0 \geq 0$, $k \geq 3$, and D a domain in \mathbf{R}^4 containing 0. We assume that A^0 has a pair of complex conjugate purely imaginary eigenvalues $\pm if_0$ with $f_0 > 0$, and if λ is any other eigenvalue of A^0 then $\lambda \neq 0$ and $\lambda \neq \pm imf_0$ for any integer m . Let $r(\varepsilon) + if_0(\varepsilon)$ denote the eigenvalue of A^ε which is a continuous extension of $+if_0$ and let $T = 2\pi/f_0$.*

If $r'(0) \neq 0$, then for some sufficiently small $\mu_1 > 0$ there exist real valued functions $\delta(\mu)$ and $\gamma(\mu) \in C^{(k-2)}[-\mu_1, \mu_1]$ and a T -periodic function $y(s, \mu)$ such that $\delta(0) = \gamma(0) = 0$ and

$$x(t, \mu) = \mu y\left(\frac{t}{1 + \mu\gamma(\mu)}, \mu\right)$$

is a $(1 + \mu\gamma(\mu)) \cdot T$ -periodic solution of

$$\frac{dx}{dt} = A^\varepsilon x + F(x, \varepsilon(\mu))$$

for $\varepsilon(\mu) = \mu\delta(\mu)$. If $\delta = \delta(\mu)$ and $\gamma = \gamma(\mu)$ in the transformed equation

$$\frac{dy}{ds} = A^0 y + \mu G(y, \mu, \delta, \gamma)$$

then $y(s, \mu)$ is a T -periodic solution of this transformed equation.

Theorem 2 [21] (stability result) If $k \geq 4$, $r'(0)\delta'(0) > 0$, and $\text{Re}(\lambda_1^0) < 0$ for the other eigenvalues, then the bifurcated periodic solution will be asymptotically orbitally stable.

Theorem 3 [21] (algebraic expressions) If u and v are the left and right eigenvectors of A^0 corresponding to the eigenvalue $+if_0$, normalized so that $u \cdot v = 1$, and B is any nonzero real two-dimensional vector, then

$$r'(0) + if_0'(0) = uB^0v$$

and

$$\begin{aligned} & 8r'(0)\delta'(0) + i8(f_0'(0)\delta'(0) + f_0\gamma'(0)) \\ &= B \cdot B \left(-u_l \frac{\partial^3 F^l}{\partial x_j \partial x_k \partial x_p} v_j v_k \bar{v}_p + 2u_l \frac{\partial^2 F^l}{\partial x_j \partial x_k} v_j (A^0)^{-1}_{kr} \frac{\partial^2 F^r}{\partial x_p \partial x_q} v_p \bar{v}_q \right. \\ & \quad \left. + u_l \frac{\partial^2 F^l}{\partial x_j \partial x_k} \bar{v}_j [(A^0 - 2if_0 I)^{-1}]_{kr} \frac{\partial^2 F^r}{\partial x_p \partial x_q} v_p v_q \right) \end{aligned}$$

Poore and Al-Rawi remark that as $\varepsilon = \mu\delta = \mu^2\delta'(0) + O(\mu^4)$, the periodic orbit bifurcates to $\varepsilon > 0$ when $\delta'(0) > 0$ and to $\varepsilon < 0$ when $\delta'(0) < 0$. They further note that the initial conditions on the periodic orbit may be approximated by

$$x(0, \varepsilon) \sim \sqrt{\frac{\varepsilon}{\delta'(0)}} \left(B_1 \frac{(\bar{v} - v)}{2i} + B_2 \frac{(\bar{v} + v)}{2} \right) + O(\varepsilon) \text{ as } \varepsilon \rightarrow 0$$

where $B = (B_1, B_2)$ is any real nonzero vector, essentially representing the choice of initial conditions, and v is the same as in Theorem 3. Poore and Al-Rawi used this last observation as initial conditions for numerical solution of the equations in the neighbourhood of the Hopf Bifurcation Point — we will use it for an analytical approximation to the amplitude of the periodic orbit near the HBP.

6.4 Bifurcation of the Quasi-Steady Model

In this section we will illustrate the ideas of Hopf Bifurcation Theory by using the results of the previous sections to analyze the simpler quasi-steady model of galloping due to Parkinson [17]. The model equations are

$$\ddot{Y} + Y = nU^2 \left(\mathcal{A}_1 \left(1 - \frac{U_0}{U} \right) \frac{\dot{Y}}{U} - \mathcal{A}_3 \left(\frac{\dot{Y}}{U} \right)^3 + \mathcal{A}_5 \left(\frac{\dot{Y}}{U} \right)^5 - \mathcal{A}_7 \left(\frac{\dot{Y}}{U} \right)^7 \right)$$

where n , \mathcal{A}_1 , \mathcal{A}_3 , ... and U_0 are empirical constants. This is a two-dimensional

system, and written in first-order form, with $x_1 = Y$ and $x_2 = \dot{Y}$, we have

$$\begin{bmatrix} \dot{x}_1 \\ \dot{x}_2 \end{bmatrix} = \begin{bmatrix} 0 & 1 \\ -1 & n\mathcal{A}_1(U - U_0) \end{bmatrix} \begin{bmatrix} x_1 \\ x_2 \end{bmatrix} + \begin{bmatrix} 0 \\ -\frac{n\mathcal{A}_3}{U}x_2^3 + \dots \end{bmatrix}$$

The eigenvalues of the linear part of the equation are easily calculated explicitly:

$$\zeta = \frac{n\mathcal{A}_1(U - U_0) \pm i\sqrt{1 - (n\mathcal{A}_1(U - U_0))^2}}{2}$$

and for $|n\mathcal{A}_1(U - U_0)| < 1$ we see that $\text{Re}(\zeta) = n\mathcal{A}_1(U - U_0)/2$, which is zero if and only if $U = U_0$, while $\frac{\partial \text{Re}\zeta}{\partial U} = n\mathcal{A}_1/2 \neq 0$. Thus the only Hopf Bifurcation Point of the Quasi-Steady Model is at the point $U = U_0$. This is in accord with the approximate analytical solution. There remains the calculation of the direction and amplitude of the bifurcated periodic orbit. By straightforward calculation using the formulae of Poore and Al-Rawi, we have

$$u = \begin{bmatrix} \frac{1}{\sqrt{2}} & \frac{-i}{\sqrt{2}} \end{bmatrix}$$

and

$$v = \begin{bmatrix} \frac{1}{\sqrt{2}} & \frac{i}{\sqrt{2}} \end{bmatrix}^T$$

so, choosing $B = [1, 1]$, we get

$$8r'(0)\delta'(0) + i \cdot (8\gamma'(0)) = \frac{3n\mathcal{A}_3}{U}$$

which gives $\gamma'(0) = 0$ and

$$\delta'(0) = \frac{3\mathcal{A}_3}{4\mathcal{A}_1 U} > 0$$

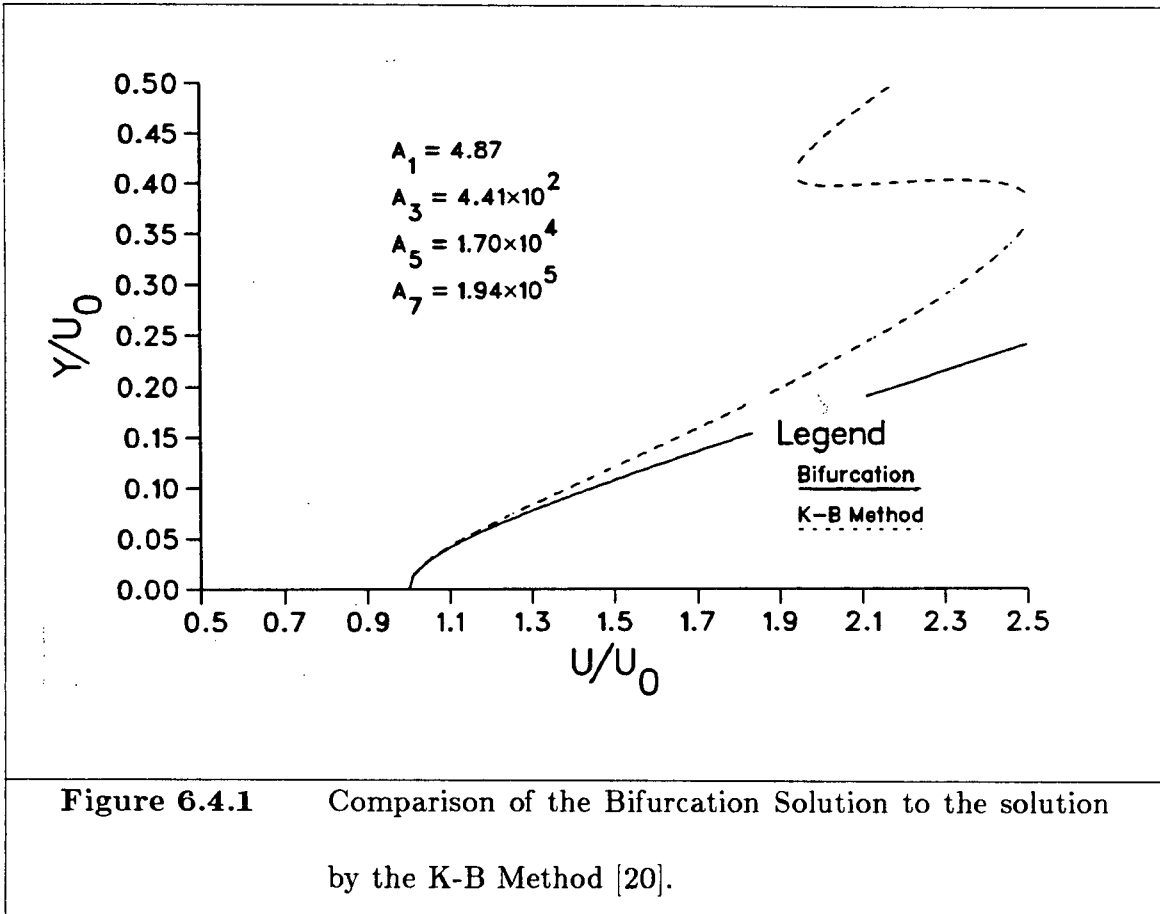
so we see that the periodic orbit bifurcates for $U > U_0$, and in fact is stable. By straightforward use of the formula for the initial conditions on the periodic orbit, we deduce that the amplitude of the stable bifurcated periodic orbit is

$$\bar{Y} = \sqrt{\frac{4\mathcal{A}_1 U (U - U_0)}{3\mathcal{A}_3}}$$

which is precisely that obtained by the approximate solution in the small n case when $\mathcal{A}_5 = \mathcal{A}_7 = 0$ by the method of Krylov-Bogoliubov, used by Parkinson and Smith [20]. For a comparison of the two solutions, see Figure 6.4.1. This result is somewhat surprising, as it is independent of n (one expected some terms of order n , n^2 , etc cropping up). Note that this solution is valid even if $\mathcal{A}_5, \mathcal{A}_7 \neq 0$, but we are only guaranteed accuracy when U is near U_0 .

Also, no form of the solution was assumed *a priori*, and the oscillatory nature of the solution was derived directly from the differential equations, and we are guaranteed that the actual solution of the differential equations does in fact look like this, in a neighbourhood of U_0 . This enables us to draw a *local response diagram* which we can compare in this simple case with the well-known approximate solution.

When we examine Figure 6.4.1, we see that the two solutions given agree best near $U = U_0$, as predicted by the theory. The agreement remains quite good for a



reasonable range of wind speed values, but eventually diverges, as the assumption that $U \approx U_0$ is violated. Also, the global features of the approximate solution presented in [20], notably the two branches of the solution, are not predicted by the bifurcation theory. It is interesting to note that if $A_5 = A_7 = 0$ these curves would coincide precisely, so we would have in that case obtained a globally valid solution by local considerations only. This must be regarded as a coincidence, and it is not expected to occur in the more complicated model we are interested in next. To summarize, the Hopf Bifurcation Theory gives us formulae that predict the loca-

tion(s) in parameter space at which periodic solutions to the differential equations are initiated, and allows us to calculate the local behaviour of such solutions. This is of interest physically, as the wind speeds at which nonzero amplitude vibrations are initiated are important design parameters. It is also important for the theoretical investigation of models for such vibrations as unrealistic behaviour is detected at an early stage.

6.5 Limitations of the Hopf Bifurcation Theory

The theory is essentially local: it cannot provide information about the solution of the equations away from the Hopf Bifurcation Points, or away from the steady state solution (the zero solution) that the periodic solutions bifurcate from. Thus isolated branches of periodic solutions are not predicted (as in the experimentally observed closed loops of Wawzonek), and secondary bifurcation from the periodic solution is not detectable with this simple analysis. It is the latter bifurcation that we are more interested in, as the zero solution of our model equations is always *unstable*, and hence any physically observed bifurcations are in fact bifurcations from a limit cycle solution, and not from the zero steady state. It is important to note that by zero solution we mean the solution $Y \equiv 0$, $C_v \equiv 0$, which is the only steady-state solution of the model equations. The fact that this solution is unstable follows from the fact that the damping in the second equation is negative,

at least for small values of C_v . However, we will find that these solutions will be useful as error checks for the other methods of solution, and as a quick indicator of the behaviour of the solution. The interaction between the steady-state bifurcation analysed here and the secondary bifurcations that are observed are interesting of themselves, and worth further study.

6.6 Model Equations

The model equations that we shall be analysing are reproduced here for convenience:

$$\ddot{Y} + Y = nU^2 \left(\mathcal{A}_1 \left(1 - \frac{U_0}{U} \right) \frac{\dot{Y}}{U} - \mathcal{A}_3 \left(\frac{\dot{Y}}{U} \right)^3 + \mathcal{A}_5 \left(\frac{\dot{Y}}{U} \right)^5 - \mathcal{A}_7 \left(\frac{\dot{Y}}{U} \right)^7 + C_v \right)$$

$$\ddot{C}_v + \omega_0^2 C_v = a(\omega_0) \left(\dot{C}_v - \frac{4}{3C_{Y_0}^2 \omega_0^2} \dot{C}_v^3 \right) + D\dot{Y} + B\ddot{Y}$$

Naturally, the details of the location of the Hopf Bifurcation Points will depend on the exact nature of the functions $a(\omega_0)$, $B(\omega_0)$, $D(\omega_0)$, and C_{Y_0} . The analysis itself, however, is not so sensitive. Once we get down to details, the models we will actually investigate are the Hartlen-Currie model, with $a(\omega_0) = \alpha\omega_0$, and Bouclin's hydrodynamic model, with $a(\omega_0) = GC_{Y_0}^2$, where α , G , C_{Y_0} (and all the other parameters) are constants.

6.7 Location of the Hopf Bifurcation Points

To locate the Hopf Bifurcation Points, we use only the linear part of the equations. We change the notation slightly, putting $x_1 = Y$, $x_2 = \dot{Y}$, $x_3 = C_v$, and $x_4 = \dot{C}_v$, and writing the matrix as:

$$(6.7.1) \quad A = \begin{bmatrix} 0 & 1 & 0 & 0 \\ -1 & \epsilon(\omega_0 - W_0) & \epsilon\eta\omega_0^2 & 0 \\ 0 & 0 & 0 & 1 \\ -B & D + \epsilon(\omega_0 - W_0)B & -\omega_0^2 + \epsilon\eta\omega_0^2 B & a \end{bmatrix}$$

where $\epsilon = nA_1U_r$, $\eta = \frac{U_r}{A_1}$, and $W_0 = \frac{U_0}{U_r}$.

This matrix has the characteristic polynomial

$$P(\zeta) = a_0 + a_1\zeta + a_2\zeta^2 + a_3\zeta^3 + \zeta^4$$

where

$$(6.7.2) \quad \begin{aligned} a_0 &= \omega_0^2 \\ a_1 &= -(a(\omega_0) + \epsilon\eta D\omega_0^2 + \epsilon\omega_0^2(\omega_0 - W_0)) \\ a_2 &= 1 + \omega_0^2 + a(\omega_0)\epsilon(\omega_0 - W_0) - B\epsilon\eta\omega_0^2 \\ a_3 &= -(a(\omega_0) + \epsilon(\omega_0 - W_0)) \end{aligned}$$

Notice that the effect of the additional $B\ddot{Y}$ coupling term is confined to the coefficient of ζ^2 .

Now, when are some pair of roots of $P(\zeta)$ purely imaginary? One way to find

out would be to use the analytic solution of a quartic equation to try to find smooth expressions for the roots of $P(\zeta)$, and then try to find the parameter values for which some of these roots had zero real parts. This is tedious, except in the limit as $n \rightarrow 0$, when reasonable expressions can be obtained for the roots of $P(\zeta)$. It is easily seen that

$$\begin{aligned}\zeta_1(\omega_0) &= i + n \cdot \sigma_1(\omega_0) + O(n^2) \\ \zeta_3(\omega_0) &= \frac{a + \sqrt{a^2 - 4\omega_0^2}}{2} + n \cdot \sigma_2 + O(n^2)\end{aligned}$$

and if $n \ll a$ then the Hopf Bifurcation Points are the zeros of $\sigma_1(\omega_0)$. Note also that for small n , $\text{Re}(\zeta_3) = a/2 + O(n) > 0$, so any bifurcating periodic orbit is initially *unstable*.

However, there is a simpler method that works for all values of n , and not just those which are small compared to a . When the roots of $P(\zeta)$ cross the imaginary axis, they do so in pairs. Thus the polynomial $\zeta^2 + f^2$, say, is a divisor of $P(\zeta)$ at this point. By long division,

$$P(\zeta) = (\zeta^2 + f^2)Q(\zeta) + (a_1 - a_3f^2)\zeta + a_0 - (a_2 - f^2)f^2$$

So at a Hopf Bifurcation Point, the remainder must be the zero polynomial. We thus get two equations in the two unknowns f^2 and ω_0 , as follows:

$$(6.7.3) \quad a_1 - a_3f^2 = 0$$

$$(6.7.4) \quad a_0 - a_2f^2 + f^4 = 0$$

This system of equations applies for all n , and we can reduce it to a single equation quite easily. If $a_3 \neq 0$, then $f^2 = a_1/a_3$, which is required to be > 0 . Substituting in the second equation gives a single equation in ω_0 :

$$P_B(\omega_0) \equiv a_3^2 a_0 - a_1 a_2 a_3 + a_1^2 = 0 \quad (6.7.5)$$

Any root of this equation is a candidate for a Hopf Bifurcation Point.

If, however, $a_3 = 0$, we are led to the possibility of a *double bifurcation*, $P(\zeta) = (\zeta^2 + f_1^2)(\zeta^2 + f_2^2)$. If $a_3 = 0$, the system (6.7.3)—(6.7.4) becomes

$$(6.7.6) \quad a_1 = 0$$

$$(6.7.7) \quad a_0 - a_2 f^2 + f^4 = 0$$

If equation (6.7.7) has positive roots for some selection of the parameters, then this is a double bifurcation point and must be handled specially. The bifurcation theory for this case has been worked out [21,22], but we shall see that the actual occurrence of this in our model is too rare to warrant special consideration, as any special features can be derived by taking limits.

6.8 Coefficients of the Bifurcation Polynomial

For Bouclin's model, we take $B(\omega_0) = 0$, $a(\omega_0) = GC_{Y_0}^2$ constant, and $D(\omega_0) =$

H , also constant. If $\hat{\eta} = \frac{HU_r}{A_1}$ and $g = GC_{Y_0}^2$, we find by REDUCE that

$$P_B(\omega_0) = c_5\omega_0^5 + c_4\omega_0^4 + c_3\omega_0^3 + c_2\omega_0^2 + c_1\omega_0 + c_0$$

where

$$c_0 = W_0g(1 + g^2 - \epsilon W_0g)$$

$$c_1 = -g(1 + g^2 - 2\epsilon W_0g)$$

$$c_2 = \hat{\eta}g - 2W_0g + \epsilon(\hat{\eta}W_0g^2 + \hat{\eta}W_0 - g^2(1 + W_0^2)) + \epsilon^2gW_0^2(W_0 - \hat{\eta})$$

$$c_3 = 2g + \epsilon(2W_0g^2 - \hat{\eta}(1 + g^2)) + \epsilon^2W_0g(2\hat{\eta} - 3W_0)$$

$$c_4 = (W_0 - \hat{\eta})g + \epsilon(\hat{\eta}^2 - \hat{\eta}W_0 - g^2) + \epsilon^2(-\hat{\eta}g + 3W_0g)$$

$$c_5 = -g + \epsilon\hat{\eta} - \epsilon^2g$$

Notice that the only dependence on β is through $W_0 = U_0/U_r = 2\beta/nA_1U_r$, but that ϵ depends on n also, so the roots of $P_B(\omega_0)$ depend on β and n independently, unless n is so small that terms of $O(\epsilon)$ may be neglected. Thus a graph of U_i versus β/n is insufficient, except in the case of small n .

For the original Hartlen-Currie model, we take $B(\omega_0) = 0$ and $D(\omega_0) = H$ as before, but $a(\omega_0) = \alpha\omega_0$ where α is a constant. This changes the character of $P_B(\omega_0)$ markedly. We find again by REDUCE that

$$P_B(\omega_0) = c_6\omega_0^6 + \cdots + c_1\omega_0 + 0$$

so in this case $\omega_0 = 0$ is always a root of the bifurcation polynomial. However, by

inspection we see that for $\omega_0 = 0$, $f_0 = 0$ also, so this is *not* a Hopf bifurcation point. The coefficients c_i are given by:

$$c_0 = 0$$

$$c_1 = W_0 \alpha$$

$$c_2 = -\alpha + \epsilon(\hat{\eta}W_0 - \alpha^2W_0^2)$$

$$c_3 = \alpha(\hat{\eta} + W_0(\alpha^2 - 2)) + \epsilon(2W_0\alpha^2 - \hat{\eta}) + \epsilon^2W_0^2\alpha(W_0 - \hat{\eta})$$

$$c_4 = \alpha(2 - \alpha^2) + \epsilon(\hat{\eta}(\hat{\eta} + W_0\alpha^2 - W_0) - \alpha^2(1 + W_0^2)) + \epsilon^2W_0\alpha(2\hat{\eta} - 3W_0)$$

$$c_5 = \alpha(W_0 - \hat{\eta}) + \epsilon(2W_0\alpha^2 + \hat{\eta}(1 - \alpha^2)) + \epsilon^2(-\hat{\eta}\alpha + 3W_0\alpha)$$

$$c_6 = -\alpha(1 + \epsilon\alpha + \epsilon^2)$$

Remark

Both polynomials have roots which approach W_0 as $W_0 \rightarrow \infty$, which is realistic.

The asymptotic form for these roots is the same for each polynomial:

$$\omega_i = W_0 - \hat{\eta} + O\left(\frac{1}{W_0}\right) \text{ as } W_0 \rightarrow \infty$$

As $\epsilon \rightarrow 1^-$, one root of Bouclin's model goes to ∞ as the leading coefficient goes to 0. This may be unrealistic, and the Hartlen-Currie model does not have this problem.

As $\epsilon \rightarrow 0$, both polynomials approach the corresponding initiation polynomials derived from the approximate analytical solutions obtained by the Methods of Van

Der Pol and Multiple Scales. This is to be contrasted with the quasi-steady case, where the bifurcation polynomial was exactly the initiation polynomial, and the dependence on n dropped out completely.

Remark Note that for each functional dependence of $B(\omega_0)$, $D(\omega_0)$, and $a(\omega_0)$ that the polynomial $P_B(\omega_0)$ has a different form. Strictly speaking, it is a polynomial only for certain forms. However, we are concerned only with at most rational forms for the parameters, so we will always have a polynomial in ω_0 to deal with.

6.9 Results of Bifurcation Formulae

Using the formulae from Poore and Al-Rawi's Theorem 3, we have the following results, tabulated here for convenience. If ζ is an eigenvalue of A , then the left and right eigenvectors associated with ζ are

$$u = [-(\zeta(\zeta - a) + \omega_0^2(1 - \epsilon\eta b) + b)/\zeta \quad \zeta(\zeta - a) + \omega_0^2(1 - \epsilon\eta b) \quad \zeta - a \quad 1]$$

$$v = \left[1 \quad \zeta \quad \frac{\zeta^2 + 1 - \epsilon(\omega_0 - W_0)\zeta}{\epsilon\eta\omega_0^2} \quad \frac{\zeta(\zeta^2 + 1 - \epsilon(\omega_0 - W_0)\zeta)}{\epsilon\eta\omega_0^2} \right]^T$$

except for the normalization, $u \cdot v = 1$. To satisfy this criterion, we divide each of u and v by $\pm\sqrt{|u \cdot v|}$. Now, with $B^0 = \frac{\partial A}{\partial \omega_0}$, and $B = [1, 1]$, we have

$$r'(\omega_i) + if'(\omega_i) = uB^0v$$

and

$$8r'(\omega_i)\delta'(\omega_i) + i \cdot 8 [f'(\omega_i)\delta'(\omega_i) + f(\omega_i)\gamma(\omega_i)] \\ = 2 \left(-u_2 \frac{\partial^3 F^2}{\partial x_2^3} v_2^2 \bar{v}_2 - u_4 \frac{\partial^3 F^4}{\partial x_4^3} v_4^2 \bar{v}_4 \right)$$

where

$$\frac{\partial^3 F^2}{\partial x_2^3} = \frac{-6A_3 n}{U} \\ \frac{\partial^3 F^4}{\partial x_4^3} = \frac{-8a(\omega_0)}{C_{Y_0}^2 \omega_0^2}$$

These formulae allow us to calculate, for any given set of parameters, the location, direction, stability, and amplitude of any bifurcating periodic solutions of the differential equations. A FORTRAN program has been written to do this for a range of W_0 , given the other parameters. This allows us to plot the location of the Hopf bifurcation points versus the critical wind speed W_0 . From experimental evidence, we expect that the bifurcation points will approach 1 and W_0 as $W_0 \rightarrow \infty$, if the model is realistic.

From Figures 6.9.1—6.9.2, we see that this is not in fact the case. Figure 6.9.1 shows the location of the HBP's obtained using the functional form $a(\omega_0) = \alpha\omega_0$, for a constant value of $n = 4.7 \times 10^{-4}$ and for varying β , so $W_0 = 2\beta/(nA_1U_r)$ varies also. There is an HBP that approaches W_0 as $W_0 \rightarrow \infty$, but the HBP's near 1 disappear for $W_0 > 3.6$. As W_0 goes to 0, the HBP's coalesce and go to 1, except for $W_0 < 0.5$, when we have two new HBP's appearing. These appear to be unrealistic, but they occur for values of β too small to compare with experiment, at least in the aerodynamic case.

Figure 6.9.2 shows the location of the HBP's obtained with a larger value of n , $n = 7.32 \times 10^{-2}$ but with the same functional form, compared with the location of the HBP's obtained with $a(\omega_0) = GC_{Y_0}^2$, constant. This figure shows the difference in predictions for the two types of models, and by comparison with 6.9.1 shows the effect of a small change in the value of n . We see that the predictions of the two models are quite different, and quite sensitive to the value of n . In Figure 6.9.2, the graph of the location of the HBP's for $a(\omega_0) = \alpha\omega_0$ has at least one HBP for all values of the critical wind speed W_0 , while the model with $a = \text{constant}$ has a range of W_0 for which there are no HBP's. The asymptotic behaviour of one branch of the solution is apparently the same as the asymptotic behaviour of one branch of the solution for the other model. This branch apparently has $\omega_i \sim W_0$ as $W_0 \rightarrow \infty$, which agrees in the limit with the quasi-steady model. Thus both models seem to agree in the quasi-steady limit.

The location of the HBP's does depend strongly on n , however, as we see comparing Figures 6.9.1 and 6.9.2. There is still the branch approaching W_0 as $W_0 \rightarrow \infty$ in both cases, but the locations of the HBP's for small W_0 are quantitatively and qualitatively different. In the larger n case we see that the HBP which was near 1 in the smaller n case has moved to a value above 2. This suggests that graphs of U_i versus β/n as presented in [19] may be insufficient to capture the full functional dependence of U_i on β and n .

We present in Figs 6.9.3—6.9.5 the bifurcation solutions compared with the low turbulence data of [1]. The data are compared with the solutions obtained with the functional form $a(\omega_0) = \alpha\omega_0$. Again the agreement for the medium and high damping seems reasonable, except for the resonance region. The medium damping case has at least the correct qualitative features predicted in the resonance region, but the amplitude is vastly overpredicted. The fact that the predicted amplitudes in the resonance region cross is of no physical significance, as the curves are valid only in a neighborhood of the zero solution. Thus very little information about the resonance region can be deduced from the Hopf Bifurcation analysis.

The bifurcation point for the onset of galloping is much better, and in fact gives good quantitative results. Because of the local character of the bifurcation solution, only a few points were generated by the computer program. In the medium damping case, it was of interest to extend the curve to compare the global behaviour. This extension shows that in the medium damping case the global agreement with the data of [1] is quite good, up until $\omega_0 \approx 3.0$. Note that the bifurcation point is at $\omega_0 = 2.00$, so the supposedly small parameter $\omega_0 - \omega_i$ is about 1.0 at this point. Thus we see that even though the assumption that the parameter is small is violated, we can still get good results. This is similar to the coincidence noted in the bifurcation solution of the Quasi-Steady model equation.

The resonance solution in the high damping case is not even correct qualitatively,

with the bifurcating amplitudes apparently going in the wrong direction. However, at least they indicate that something of interest is occurring in that region. For the low damping case, even this much is not true. If we compare this solution to the complete resonance region solution by the method of multiple scales, or the solution in the resonance region by the method of Van Der Pol, we see that this bifurcation is the beginning of an unstable solution that occurs before the actual resonance region, and that the occurrence of a stable nonzero solution for Y must in fact be a secondary bifurcation, bifurcating from the periodic solution near $C_v = C_{Y_0} \cos(T + \psi)$, Y small. These observations support the assertion that the bifurcation method is useful as a preliminary and supplementary solution but does not give the complete solution.

Considering that the onset of the galloping amplitudes is also in fact a secondary bifurcation, it is remarkable that the bifurcation theory gives anything useful at all in this situation. Yet we see apparently good agreement for the values presented.

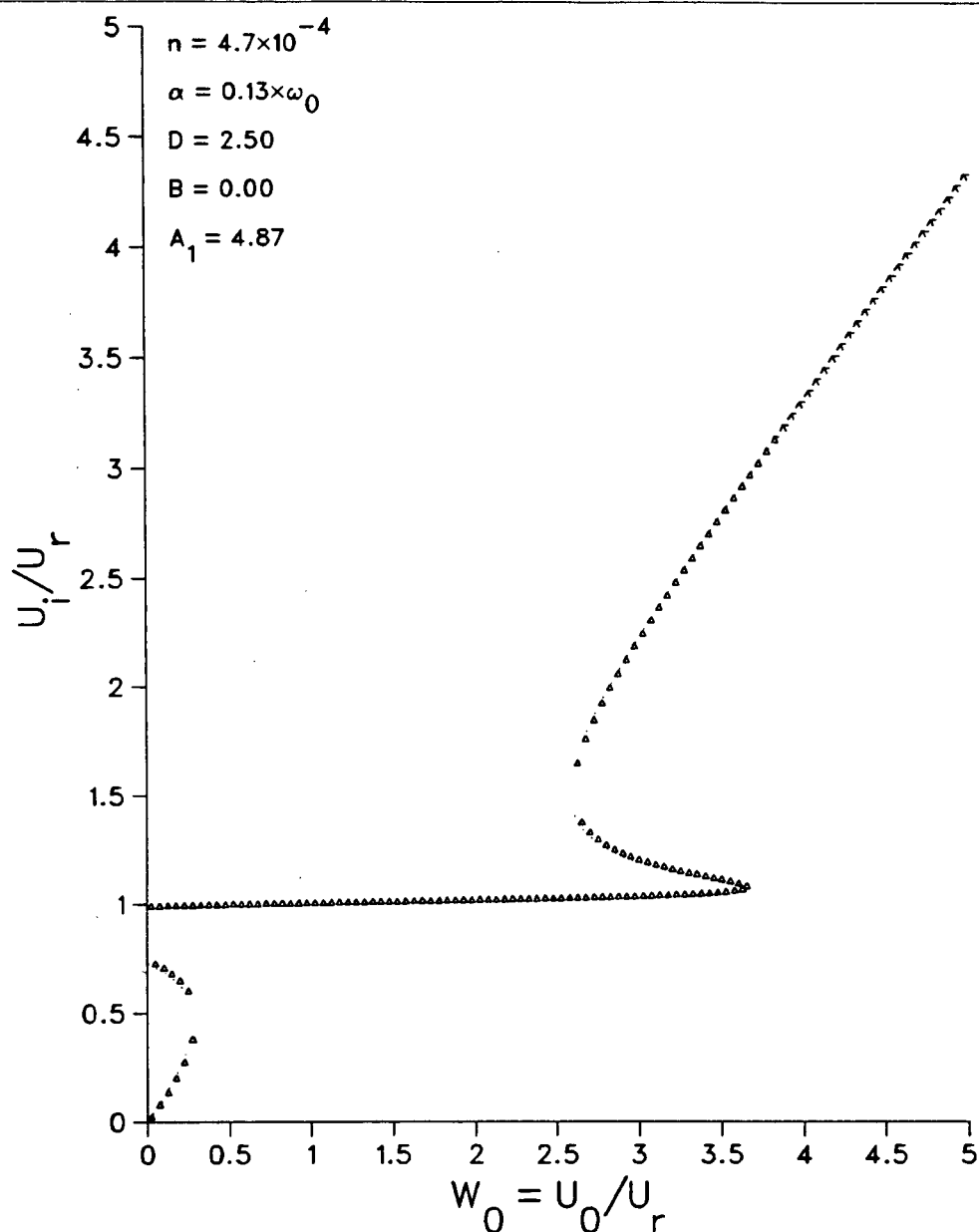


Figure 6.9.1 Location of HBP's compared with the Quasi-Steady Critical Parameter $U_0/U_r = W_0$.

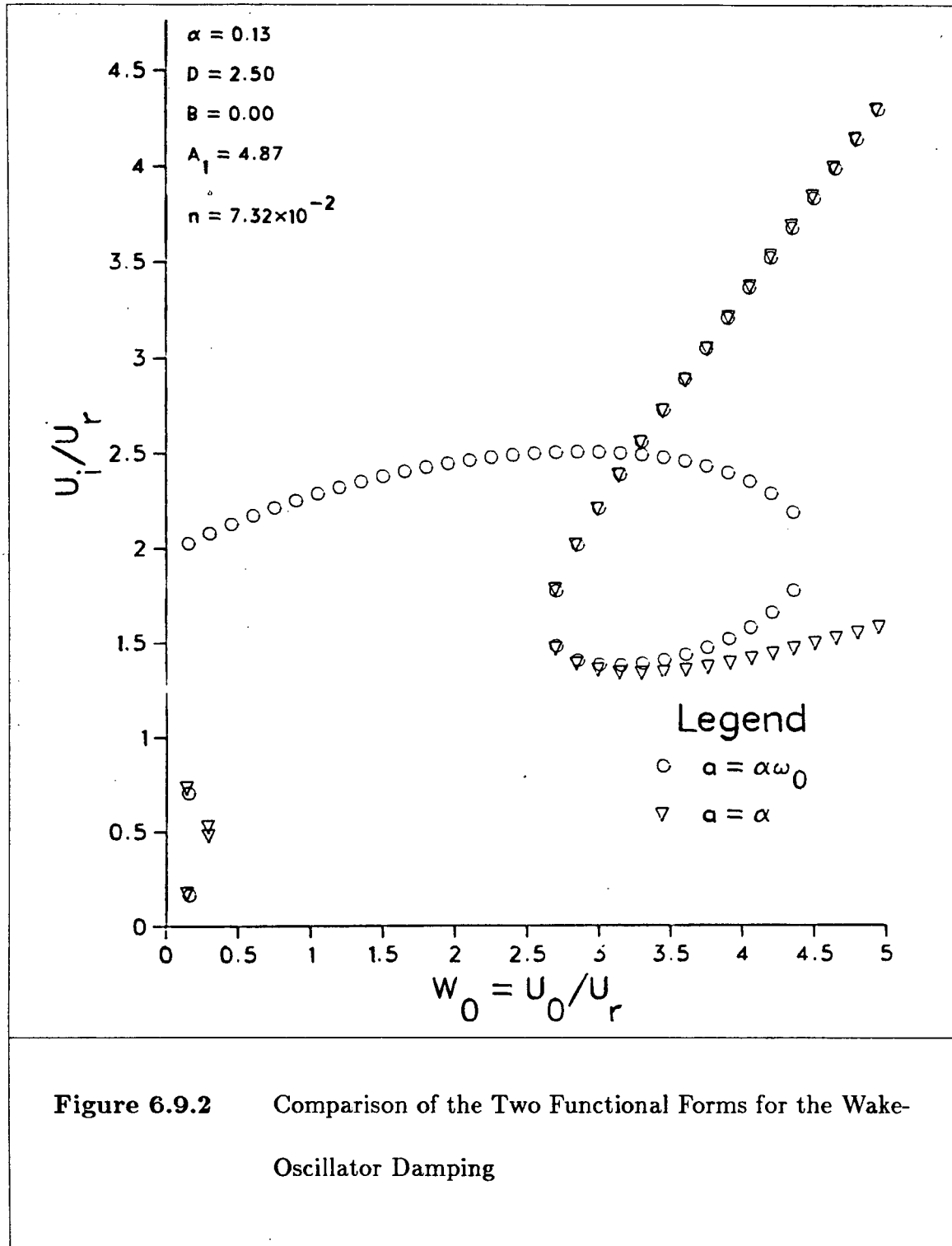


Figure 6.9.2 Comparison of the Two Functional Forms for the Wake-Oscillator Damping

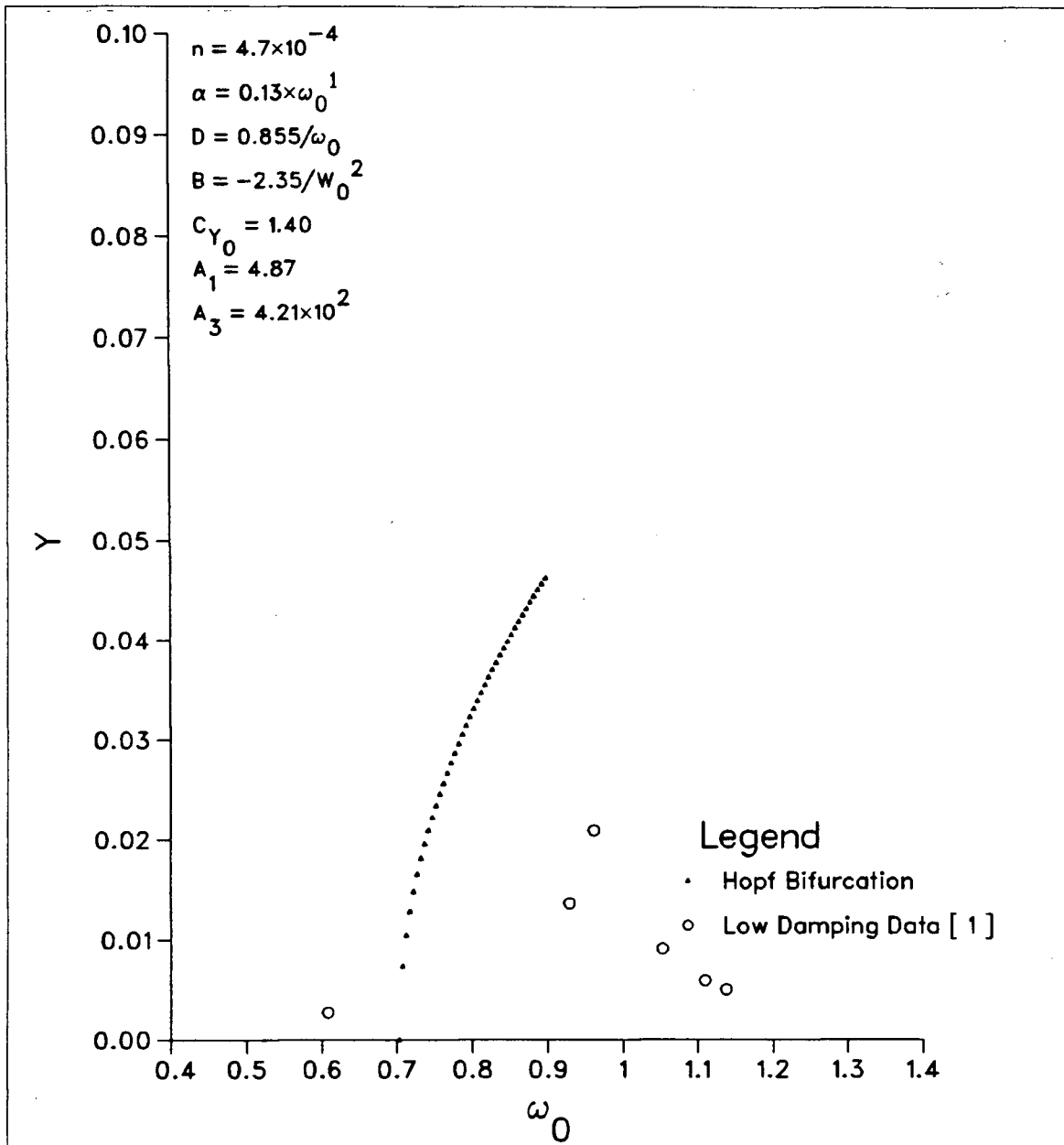


Figure 6.9.3 Bifurcation Solution in the Low Turbulence, Low Damping case.

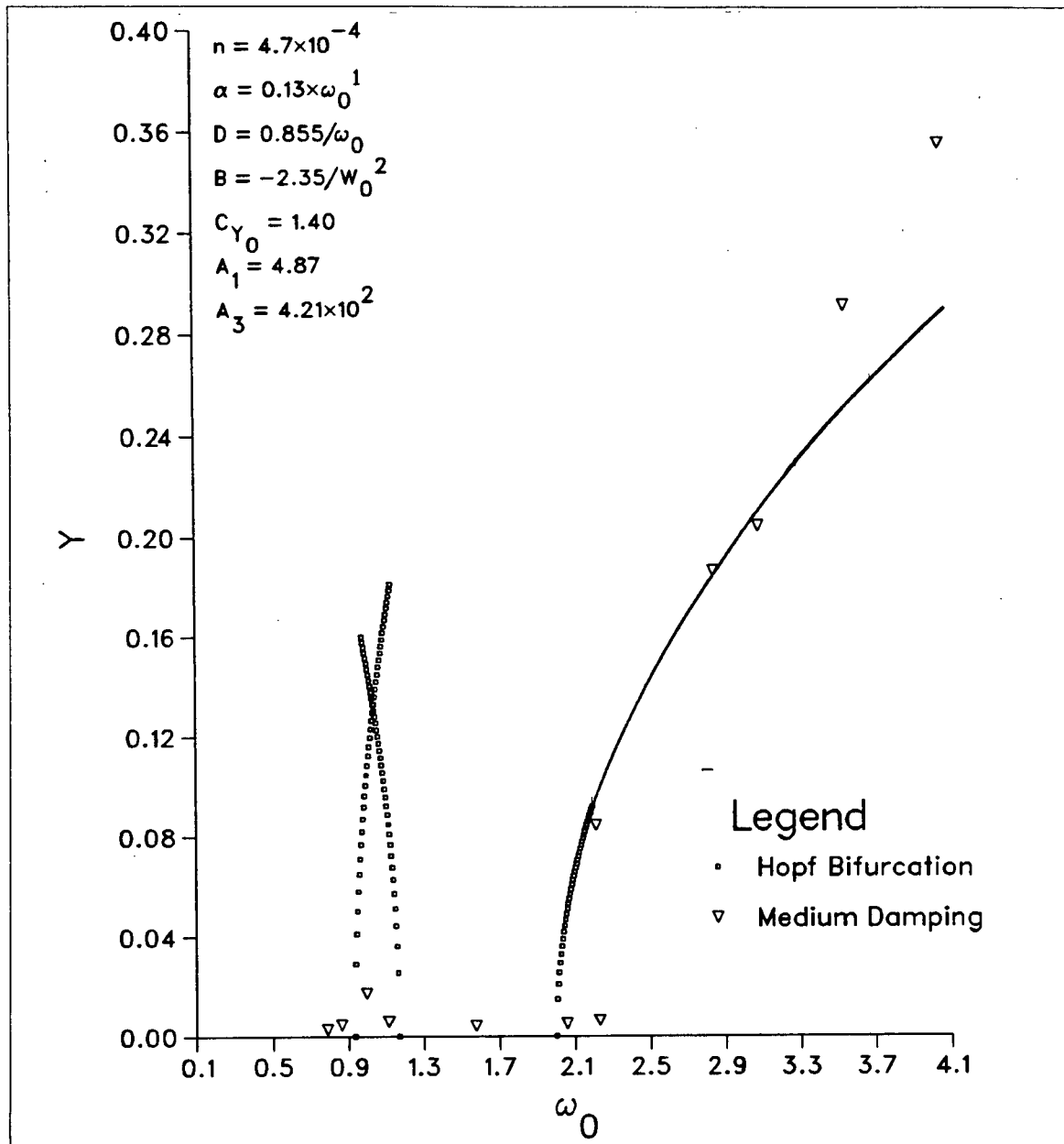


Figure 6.9.4 Bifurcation Solution in the Low Turbulence, Medium Damping case.

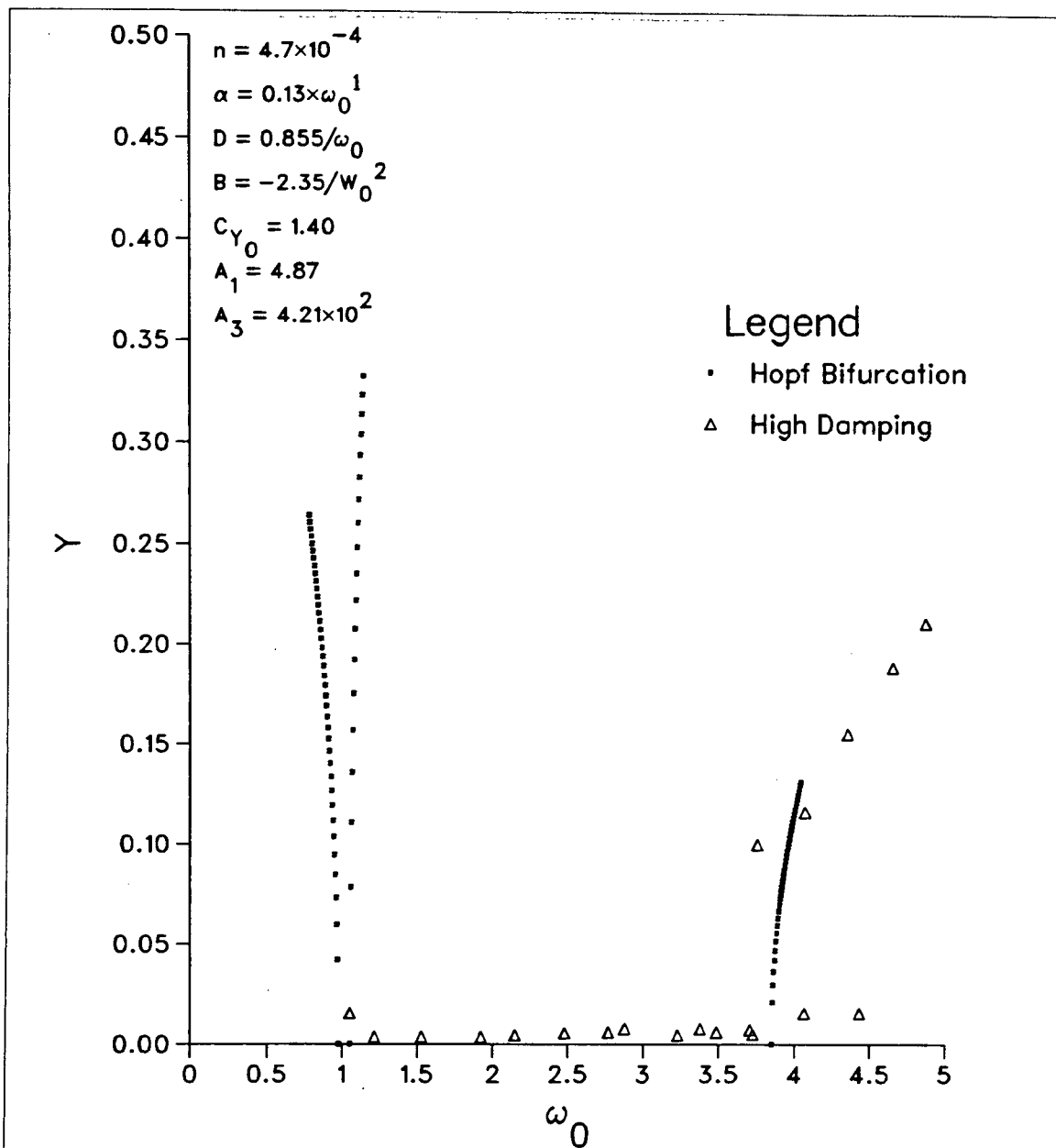


Figure 6.9.5 Bifurcation Solution in the Low Turbulence, High Damping case.

Chapter 7

Solution of the Model Equations by the Method of Multiple Scales

*'Tis a first point of wisdom, to affirm
nought upon hearsay.
—E. R. Eddison*

7.1 Overview and Choice of Time Scales

The choice of time scales is the key to a successful solution of the model equations. After a certain amount of preliminary investigation, we are led to choose the following:

$$T = \Omega t$$

$$\tau_k = \mu^k T \quad k = 1, 2, 3, 4$$

where

$$\Omega = 1 + \mu\sigma_1 + \mu^2\sigma_2 + \mu^3\sigma_3 + \cdots$$

and the σ_i remain to be chosen. We wish to associate μ with $a(\omega_0)$ (the parameter characteristic of the damping of the second oscillator), while μ^2 is to be associated with n , the mass parameter of the first oscillator. This approach is reasonable

for the values of the parameters that we are interested in, and mathematically convenient in that it decouples the resulting equations. Associating μ with n leads to coupled equations, while associating μ^3 with n increases the amount of work necessary without substantially improving the results (although in our case, since we have $a(\omega_0) = O(10^{-1})$ and $n = O(10^{-3})$ we would expect better results from letting $n \approx a(\omega_0)^3$). To be more precise, we let $\mu = \sqrt{n}$ and define $g = a(\omega_0)/\mu$. This presumes that we will find the numerical value of g to be not too far from 1, and in practice this is the case.

Remark We will find that only the first three scales, T , τ_1 , and τ_2 , are necessary for consistent results. In [13], it is noted that for the calculation of terms to $O(\mu^2)$ for a general system of this type, we should need the additional time scales $\mu^3 T$ and $\mu^4 T$, but due to the fact that we will be looking for steady state solutions only, we will see that the first three time scales will suffice. The higher-order time scales are included for completeness.

Our equations become

$$(7.1.1) \quad \bar{Y} + Y = \mu^2 \left(r_1 \dot{Y} - r_3 \dot{Y}^3 + r_5 \dot{Y}^5 - r_7 \dot{Y}^7 + s C_v \right)$$

$$(7.1.2) \quad \bar{C}_v + \omega_0^2 C_v = \mu g \dot{C}_v - \mu \gamma \dot{C}_v^3 + D \dot{Y} + B \bar{Y}$$

where $\mu g = a(\omega_0)$, $\mu \gamma = 4a(\omega_0)/(3C_{Y_0}^2 \omega_0^2)$, $\mu^2 r_1 = n A_1(U - U_0)$, $\mu^2 s = n U^2$, and $\mu^2 r_i = n U^2 A_i / U^i$ for $i = 3, 5, 7$.

Remark Note that most authors solving systems of this type assume that B and D are small; that is, $O(\mu)$. When the numerical values are inserted, they are usually not small at all. This inconsistency does no harm to the solutions as they are after all coefficients of linear terms, which never present any difficulties. Here the inconsistency is avoided, by explicitly allowing B and D to be $O(1)$, as they are experimentally [2, 16].

The derivative operators are then, to $O(\mu^4)$,

$$\begin{aligned} \frac{d}{dt} = & \frac{\partial}{\partial T} + \mu \left(\sigma_1 \frac{\partial}{\partial T} + \frac{\partial}{\partial \tau_1} \right) + \mu^2 \left(\sigma_2 \frac{\partial}{\partial T} + \sigma_1 \frac{\partial}{\partial \tau_1} + \frac{\partial}{\partial \tau_2} \right) \\ & + \mu^3 \left(\sigma_3 \frac{\partial}{\partial T} + \sigma_2 \frac{\partial}{\partial \tau_1} + \sigma_1 \frac{\partial}{\partial \tau_2} + \frac{\partial}{\partial \tau_3} \right) \\ & + \mu^4 \left(\sigma_4 \frac{\partial}{\partial T} + \sigma_3 \frac{\partial}{\partial \tau_1} + \sigma_2 \frac{\partial}{\partial \tau_2} + \sigma_1 \frac{\partial}{\partial \tau_3} + \frac{\partial}{\partial \tau_4} \right) + \dots \end{aligned} \quad (7.1.3)$$

$$\begin{aligned} \frac{d^2}{dt^2} = & \frac{\partial^2}{\partial T^2} + \mu \left(2 \frac{\partial^2}{\partial T \partial \tau_1} + 2 \sigma_1 \frac{\partial^2}{\partial T^2} \right) \\ & + \mu^2 \left[(\sigma_1^2 + 2\sigma_2) \frac{\partial^2}{\partial T^2} + 4\sigma_1 \frac{\partial^2}{\partial T \partial \tau_1} + \frac{\partial^2}{\partial \tau_1^2} + 2 \frac{\partial^2}{\partial T \partial \tau_2} \right] \\ & + \mu^3 \left[(2\sigma_3 + 2\sigma_1\sigma_2) \frac{\partial^2}{\partial T^2} + 2(\sigma_1^2 + 2\sigma_2) \frac{\partial^2}{\partial T \partial \tau_1} \right. \\ & \quad \left. + 2 \frac{\partial^2}{\partial T \partial \tau_3} + 2\sigma_1 \frac{\partial^2}{\partial \tau_1^2} + 4\sigma_1 \frac{\partial^2}{\partial T \partial \tau_2} + 2 \frac{\partial^2}{\partial \tau_1 \partial \tau_2} \right] \\ & + \dots \end{aligned} \quad (7.1.4)$$

and finally, our solution will take the form

$$(7.1.5) \quad Y = Y_0(T, \tau_1, \tau_2, \tau_3, \tau_4) + \mu Y_1(T, \tau_1, \tau_2, \tau_3) + \mu^2 Y_2(T, \tau_1, \tau_2) + \dots$$

$$(7.1.6) \quad C_v = C_0(T, \tau_1, \tau_2, \tau_3, \tau_4) + \mu C_1(T, \tau_1, \tau_2, \tau_3) + \dots$$

Before proceeding with the solution of the model equations, we give a brief overview of the organisation of the solution. The equations (7.1.1) and (7.1.2) are replaced by a sequence of simpler equations at each order. Equation (7.1.1) will give rise to the First $O(1)$ equation, the First $O(\mu)$ equation, the First $O(\mu^2)$ equation, and all the higher orders. Equation (7.1.2) will give rise to the Second $O(1)$ equation, the Second $O(\mu)$ equation, and so on. We will solve the $O(1)$ equations first, and then proceed sequentially to the higher orders. Of any given order, the First equation will be solved before the Second, as we will find that the second equation depends on the solution of the first, but not vice versa, so they are effectively uncoupled. Each equation after the $O(1)$ equations will give rise to an anti-secularity equation for determining the dependence of the previous terms on the higher-order time scales.

When the $O(1)$ equations are solved, we will find the solution divided into two cases by the Second $O(1)$ equation and the requirement that the solution be bounded. We will see that the solution to the Second $O(1)$ equation will be different depending on whether the wind speed is in the resonance region or not. This affects all subsequent equations.

When the $O(\mu)$ equations are solved in the nonresonance case, the Second $O(\mu)$ equation will give rise to two new subcases, the subharmonic resonance case when $\omega_0 \approx 3$, and the superharmonic resonance case when $\omega_0 \approx 1/3$. These will *not* affect

the amplitude of the Y_0 term, though through anti-secularity, they will affect the excitation C_0 . Of course, they will affect the $O(\mu)$ terms, and we will see that this will be a noticeable feature of the solution for practical values of the parameters.

When the $O(\mu^2)$ equations are solved (mostly as a check on the validity of the solution to $O(\mu)$ and to provide an error estimate) we will find several new resonances at $\omega_0 \approx 1/5, 1/2, 2, 5$, and 7 — but interestingly, not at $1/7$. These will not be investigated, as the effects are confined to the $O(\mu^2)$ term, and only in small regions.

We thus will provide a complete solution to $O(\mu)$ for Y , and a solution to $O(1)$ for C_v , with a nearly complete solution to one more term in each as a validity check and error estimate.

7.2 Case I: Resonance Case, with $\omega_0 = 1 + \mu\omega_1$

The equation (7.1.2) becomes

$$\begin{aligned}\ddot{C}_v + C_v &= -2\mu\omega_1 C_v - \mu^2\omega_1^2 C_v \\ &\quad + \mu g \dot{C}_v - \mu\gamma \dot{C}_v^3 + D\dot{Y} + B\ddot{Y}\end{aligned}$$

so, substituting (7.1.5) and (7.1.6) in and looking only at the $O(1)$ terms, we have

$$(7.2.1) \quad \frac{\partial^2 Y_0}{\partial T^2} + Y_0 = 0$$

$$(7.2.2) \quad \frac{\partial^2 C_0}{\partial T^2} + C_0 = D \frac{\partial Y_0}{\partial T} + B \frac{\partial^2 Y_0}{\partial T^2}$$

These linear equations are solved very easily, as they are effectively uncoupled.

Equation (7.2.1) gives

$$Y_0 = A_0(\tau_1, \tau_2, \tau_3, \tau_4)e^{iT} + \text{complex conjugate}$$

as the most general *real* solution, where A_0 is an unknown (complex) quantity. This form is adopted for computational convenience, as in [15]. Meanwhile, equation (7.2.2) becomes

$$\frac{\partial^2 C_0}{\partial T^2} + C_0 = (iD - B)A_0e^{iT} + \text{c.c.}$$

Thus, to avoid secular terms in C_0 we must have $A_0 \equiv 0$. Thus the $O(1)$ solution is

$$(7.2.3) \quad Y_0 = 0$$

$$(7.2.4) \quad C_0 = B_0(\tau_1, \tau_2, \tau_3, \tau_4)e^{iT} + \text{c.c.}$$

where B_0 is as yet undetermined. The $O(\mu)$ equations are now

$$\frac{\partial^2 Y_1}{\partial T^2} + Y_1 = -2\frac{\partial^2 Y_0}{\partial T \partial \tau_1} - 2\sigma_1 \frac{\partial^2 Y_0}{\partial T^2} \equiv 0 \quad \text{by (7.2.3)}$$

and

$$(7.2.5) \quad \begin{aligned} \frac{\partial^2 C_1}{\partial T^2} + C_1 = & -2\frac{\partial^2 C_0}{\partial T \partial \tau_1} - 2\sigma_1 \frac{\partial^2 C_0}{\partial T^2} - 2\omega_1 C_0 \\ & + g \frac{\partial C_0}{\partial T} - \gamma \left(\frac{\partial C_0}{\partial T} \right)^3 + D \frac{\partial Y_1}{\partial T} + B \frac{\partial^2 Y_1}{\partial T^2} \end{aligned}$$

so

$$(7.2.6) \quad Y_1 = A_1(\tau_1, \tau_2, \tau_3)e^{iT} + \text{c.c.}$$

We thus substitute (7.2.4) and (7.2.6) into the right hand side of (7.2.5). This gives a simple linear oscillator equation for C_1 . For this equation to have a bounded solution, we must have the coefficient of $e^{iT} = 0$. The coefficients of e^{iT} are easily obtained, as only one term contains higher frequencies, the cubic term. Substituting (7.2.4) into this term we get

$$\left(\frac{\partial C_0}{\partial T}\right)^3 = -iB_0^3 e^{i \cdot 3T} + 3iB_0^2 \bar{B}_0 e^{iT} + \text{c.c.}$$

so, when we set the coefficient of $e^{iT} = 0$ this gives us as our anti-secularity equation

$$(7.2.7) \quad -2\omega_1 B_0 + 2\sigma_1 B_0 - 2i \frac{\partial B_0}{\partial \tau_1} + i\gamma B_0 - i \cdot 3\gamma B_0^2 \bar{B}_0 + (iD - B)A_1 = 0$$

and equation (7.2.5) becomes a simple oscillator equation with a single term of frequency 3 on the right hand side, which is easily solved, giving

$$(7.2.8) \quad C_1 = B_1(\tau_1, \tau_2, \tau_3) e^{iT} - \frac{1}{8} i\gamma B_0^3 e^{i \cdot 3T} + \text{c.c.}$$

Equation (7.2.7) connects B_0 and A_1 , but we need one more equation. We look at the $O(\mu^2)$ equations, and the first of these will provide our required second equation. The first $O(\mu^2)$ equation is

$$\frac{\partial^2 Y_2}{\partial T^2} + Y_2 = -2\sigma_1 \frac{\partial^2 Y_1}{\partial T^2} - 2 \frac{\partial^2 Y_1}{\partial T \partial \tau_1} + sC_0$$

so the anti-secularity equation is

$$(7.2.9) \quad -2i \frac{\partial A_1}{\partial \tau_1} + 2\sigma_1 A_1 + sB_0 = 0$$

which leaves $Y_2 = A_2(\tau_1, \tau_2)e^{iT} + \text{c.c.}$ as in the $O(\mu)$ case.

Remark The quasi-steady term plays no part as yet. We will see that the $O(\mu)$ terms are determined in the resonance region completely independently of the quasi-steady excitation. This makes physical sense as we would expect the vortex effects to dominate in the resonance region.

If we put equations (7.2.8) and (7.2.9) in real form, with $A_1 = \frac{1}{2}a_1 e^{i\phi_1}$ and $B_0 = \frac{1}{2}b_0 e^{i\psi_0}$ where $a_1 = a_1(\tau_1, \tau_2, \tau_3)$, $b_0 = b_0(\tau_1, \tau_2, \tau_3, \tau_4)$, $\phi_1 = \phi_1(\tau_1, \tau_2, \tau_3)$, and $\psi_0 = \psi_0(\tau_1, \tau_2, \tau_3, \tau_4)$, we get

$$(7.2.10) \quad b_0 \frac{\partial \psi_0}{\partial \tau_1} + (\sigma_1 - \omega_1)b_0 - \frac{a_1 D}{2} \sin(\xi_1) - \frac{a_1 B}{2} \cos(\xi_1) = 0$$

$$(7.2.11) \quad -\frac{\partial b_0}{\partial \tau_1} + \frac{gb_0}{2} \left[1 - \frac{b_0^2}{C_{Y_0}^2} \right] + \frac{a_1 D}{2} \cos(\xi_1) - \frac{a_1 B}{2} \sin(\xi_1) = 0$$

$$(7.2.12) \quad a_1 \frac{\partial \phi_1}{\partial \tau_1} + \sigma_1 a_1 + \frac{1}{2}sb_0 \cos(\xi_1) = 0$$

$$(7.2.13) \quad -\frac{\partial a_1}{\partial \tau_1} - \frac{1}{2}sb_0 \sin(\xi_1) = 0$$

where $\xi_1 = \phi_1 - \psi_0$.

Remark These equations are singular when $a_1 b_0 = 0$, due to the transfor-

mation to real form. This necessitates special handling for the stability of the zero solution.

7.3 Solution of the $O(\mu)$ equations

We wish to solve equations (7.2.10)–(7.2.13) explicitly; unfortunately, this is not possible. However, we can find special solutions of these equations, which will be enough for our purposes. We look for limit cycle or steady-state solutions. We remark that a steady-state solution of equations (7.2.10)–(7.2.13) is not in general possible, as only the phase difference ξ_1 appears in the steady equations. This means that when the τ_1 derivatives are zero, we get a system of four equations in three unknowns, which is in general inconsistent. Instead of requiring each of ϕ_1 and ψ_0 to be steady, we can require that their difference ξ_1 be steady. This can also be viewed as looking for a limit cycle solution where the frequency of ϕ_1 and ψ_0 is the same on the τ_1 -scale. This leads to a consistent set of four equations in four unknowns. By putting $\phi_1 = \delta\tau_1 + \phi(\tau_2, \tau_3)$, $\psi_0 = \delta\tau_1 + \psi_0(\tau_2, \tau_3, \tau_4)$, the phase difference $\xi_1 = \phi_1 - \psi_0$ is independent of τ_1 . If further $\frac{\partial a_1}{\partial \tau_1} = \frac{\partial b_0}{\partial \tau_1} = 0$ our equations become

$$(7.3.1) \quad b_0(\sigma_1 + \delta - \omega_1) - \frac{a_1 D}{2} \sin(\xi_1) - \frac{a_1 B}{2} \cos(\xi_1) = 0$$

$$(7.3.2) \quad \frac{gb_0}{2} \left[1 - \frac{b_0^2}{C_{Y_0}^2} \right] + \frac{a_1 D}{2} \cos(\xi_1) - \frac{a_1 B}{2} \sin(\xi_1) = 0$$

$$(7.3.3) \quad a_1(\sigma_1 + \delta) + \frac{1}{2}sb_0 \cos(\xi_1) = 0$$

$$(7.3.4) \quad -\frac{1}{2}sb_0 \sin(\xi_1) = 0$$

These equations are easily solved. Note that $A_1 = B_0 = 0$ is a solution of the original equations (7.2.7) and (7.2.9), so we may restrict ourselves here to looking for solutions with at least one of a_1 or b_0 nonzero. Note however that if $a_1 = 0$, then (7.3.3) and (7.3.4) together imply that $b_0 = 0$ also; likewise, if $b_0 = 0$, then (7.3.1) and (7.3.2) together imply $a_1 = 0$, if $B^2 + D^2 \neq 0$. Thus we may assume henceforth that neither a_1 nor b_0 is zero. Thus (7.3.4) gives $\xi_1 = 0$ or $\xi_1 = \pi$, and (7.3.3) then gives

$$(7.3.5) \quad \sigma_1 + \delta = \frac{-sb_0}{2a_1} \cos(\xi_1) = \mp \frac{sb_0}{2a_1}$$

and we are left with the two polynomial equations (7.3.1) and (7.3.2) for the two remaining unknowns a_1 and b_0 . To keep track of the signs, we leave $\cos(\xi_1)$ in the equations. With (7.3.4), (7.3.1) becomes a quadratic equation for b_0/a_1 , with solutions

$$(7.3.6) \quad \frac{b_0}{a_1} = \frac{-\omega_1}{s \cos(\xi_1)} \pm \frac{1}{s} \sqrt{\omega_1^2 - Bs}$$

whenever this is *strictly* positive. Thus for each ξ_1 , we have two possible solutions

for b_0/a_1 . Lastly, (7.3.2) now becomes

$$(7.3.7) \quad a_1^2 = \frac{C_{Y_0}^2}{(b_0/a_1)^2} \left[1 + \frac{D \cos(\xi_1)}{g(b_0/a_1)} \right]$$

whenever this is strictly positive. Note that if $B < 0$, this ratio b_0/a_1 is never zero throughout the range for ω_1 . If, however, B is zero, one can show that when $\omega_1 = O(\mu)$ that there is *no* steady-state or simple limit-cycle solution to the equations (7.2.10) — (7.2.13). We ignore this exceptional case.

Thus we have at most four different limit cycle solutions, for any given set of parameters, and one free parameter (either σ_1 or δ , so long as (7.3.4) is satisfied).

Remark We must investigate the τ_2 -scale to see if this is a consistent solution. The fact that we have found a solution only at a limit cycle means that we must take care that the higher-order time scales do not disturb this limit cycle. Thus we must investigate the effect of the next terms on the solution found at this stage.

Also, we are concerned with the stability of the limit-cycle solution found in this section. The previous remarks noted that we would like to see the effect of the higher-order time scales and smaller terms on the solution, but with the stability question we are more concerned with the effects on the limit-cycle solutions of perturbations of the first terms, perhaps caused by the effects of the higher order terms. Thus we first look at the linear stability of the limit-cycle solutions.

7.4 Stability of the $O(\mu)$ solutions

Noticing that we can combine equations (7.2.10) and (7.2.12) to get

$$(7.4.1) \quad \frac{\partial \xi_1}{\partial \tau_1} + \omega_1 + \left(\frac{sb_0^2}{2a_1b_0} + \frac{a_1^2B}{2a_1b_0} \right) \cos(\xi_1) + \frac{a_1^2D}{2a_1b_0} \sin(\xi_1) = 0$$

and that $\frac{\partial \xi_1}{\partial \tau_1} = \delta - \delta = 0$ at the limit cycle, we can investigate the stability of the limit cycle by linearizing the equations (7.2.11), (7.2.13), and (7.4.1) about the steady state of this compressed system. The signs of the eigenvalues of the 3×3 Jacobian determine the linear stability of the system in the usual fashion. The Jacobian is

$$(7.4.2) \quad J_f(a_1, b_0, \xi_1) = \begin{pmatrix} 0 & 0 & -\frac{1}{2}sb_0 \cos(\xi_1) \\ \frac{1}{2}D \cos(\xi_1) & \frac{1}{2}g \left[1 - 3\frac{b_0^2}{C_{Y_0}^2} \right] & -\frac{1}{2}a_1B \cos(\xi_1) \\ \left(\frac{b_0}{2a_1^2}s - \frac{B}{2b_0} \right) \cos(\xi_1) & \left(-\frac{1}{2a_1}s + \frac{Ba_1}{2b_0^2} \right) \cos(\xi_1) & -\frac{1}{2b_0}a_1D \cos(\xi_1) \end{pmatrix}$$

and then, with the usual linearization about the steady state (a_1^*, b_0^*, ξ_1^*) ,

$$\frac{\partial}{\partial \tau_1} \begin{bmatrix} \Delta a_1 \\ \Delta b_0 \\ \Delta \xi_1 \end{bmatrix} = J_f(a_1^*, b_0^*, \xi_1^*) \begin{bmatrix} \Delta a_1 \\ \Delta b_0 \\ \Delta \xi_1 \end{bmatrix} + \text{higher order terms.}$$

This analysis *fails* if $a_1b_0 = 0$, due to the singularity in the transformation to real form. To analyze the stability of the zero solution, we must go back to the original (complex) form, equations (7.2.7) and (7.2.9). Linearizing about $(Y, C_v) = (0, 0)$

we get

$$\frac{\partial}{\partial \tau_1} \begin{bmatrix} A_1 \\ B_0 \end{bmatrix} = \begin{bmatrix} -i\sigma_1 & -i \cdot \frac{1}{2}s \\ \frac{1}{2}(D + iB) & \frac{g}{2} + i(\omega_1 - \sigma_1) \end{bmatrix} \begin{bmatrix} A_1 \\ B_0 \end{bmatrix} + \text{h. o. t.}$$

and the real part of the trace of this matrix is $g/2 > 0$, so at least one eigenvalue must have positive real part; and thus the zero solution is *unstable* throughout the resonance region.

Remark This result is consistent with the experimental phenomena we are attempting to model. Notice that the simple quasi-steady model, for example, does not predict the instability of the zero solution in the resonance region. Of course, as to this order our model is indistinguishable from the (generalized) Hartlen-Currie model, the Hartlen-Currie model does predict this instability.

Remark The solution to $O(1)$ for Y_0 is zero, and we cannot establish the stability of this solution in the normal fashion. Looking at nearby solutions and investigating their relationship with the zero solution is not a valid procedure in this case, because there *are* no other solutions, nearby or otherwise. This is the mathematical phenomenon of rigidity, and in one sense it means that the $O(1)$ solution is stable, in that there is no other. However, this is less satisfactory than, say, asymptotic stability, because it is not clear what happens physically when the $O(\mu)$ solution becomes large. Thus we are concerned with the stability of the $O(\mu)$ solution, including the zero $O(\mu)$ solution, on the assumption that this is the physically relevant quantity.

7.5 Solution to $O(\mu^2)$

We wish to determine A_2 and B_1 , and to ensure that the τ_2 -scale does not affect the first term solution A_1 and B_0 . The second terms may be important in the case of larger n (i.e. oscillation in water), and should also help to smoothly join the resonance and non-resonance regions. We look first at the second $O(\mu^2)$ equation:

$$\begin{aligned}
\frac{\partial^2 C_2}{\partial T^2} + C_2 = & -2\omega_1 C_1 - \omega_1^2 C_0 - 2\sigma_1 \frac{\partial^2 C_1}{\partial T^2} - 2 \frac{\partial^2 C_1}{\partial T \partial \tau_1} \\
& - (\sigma_1 + 2\sigma_2) \frac{\partial^2 C_0}{\partial T^2} - 4\sigma_1 \frac{\partial^2 C_0}{\partial T \partial \tau_1} - \frac{\partial^2 C_0}{\partial \tau_1^2} - 2 \frac{\partial^2 C_0}{\partial T \partial \tau_2} \\
& + g \left[\frac{\partial C_1}{\partial T} + \sigma_1 \frac{\partial C_0}{\partial T} + \frac{\partial C_0}{\partial \tau_1} \right] \\
& - 3\gamma \left(\frac{\partial C_0}{\partial T} \right)^2 \left[\frac{\partial C_1}{\partial T} + \sigma_1 \frac{\partial C_0}{\partial T} + \frac{\partial C_0}{\partial \tau_1} \right] \\
& + D \left[\frac{\partial Y_2}{\partial T} + \frac{\partial Y_1}{\partial \tau_1} + \sigma_1 \frac{\partial Y_1}{\partial T} \right] \\
& + B \left[\frac{\partial^2 Y_2}{\partial T^2} + 2 \frac{\partial^2 Y_1}{\partial T \partial \tau_1} + 2\sigma_1 \frac{\partial^2 Y_1}{\partial T^2} \right]
\end{aligned}$$

and as

$$\begin{aligned}
\left(\frac{\partial C_0}{\partial T} \right)^2 \frac{\partial C_1}{\partial T} = & \left(iB_0 e^{iT} + \text{c.c.} \right) \left(iB_1 e^{iT} + \frac{3}{8} \gamma B_0^3 e^{i \cdot 3T} + \text{c.c.} \right) \\
= & \left(i \cdot 2B_0 \overline{B_0} B_1 + iB_0^2 \overline{B_1} + \frac{3}{8} \gamma B_0^3 \overline{B_0}^2 \right) e^{iT} + \text{other frequencies}
\end{aligned}$$

our anti-secularity equation becomes

$$(7.5.1) \quad \left[-2i \frac{\partial B_1}{\partial \tau_1} + (2\sigma_1 - 2\omega_1) B_1 + ig B_1 \right]$$

$$\begin{aligned}
& -3\gamma i(2B_0\bar{B}_0B_1 + B_0^2\bar{B}_1) - \frac{9}{8}\gamma^2 B_0^3\bar{B}_0^2 \\
& + (iD - B)A_2 - \omega_1^2 B_0 \\
& + (\sigma_1 + \delta)(igB_0 - 9i\gamma B_0^2\bar{B}_0 + (iD - 2B)A_1) \Big] \\
& + \left[-2i\frac{\partial B_0}{\partial \tau_2} + (\sigma_1^2 + 2\sigma_2 + 4\sigma_1\delta + \delta^2)B_0 \right] = 0
\end{aligned}$$

where we have used $\frac{\partial B_1}{\partial \tau_1} = \delta B_0$ and $\frac{\partial A_1}{\partial \tau_1} = \delta A_1$, which is true *at the limit cycle*.

Remark This equation is a nonlinear partial differential equation, in the variables τ_1 and τ_2 , which again we cannot solve in general. However, we will show that we can satisfy these equations by separately setting the quantities in square brackets to zero. Note that this equation can be split up in several ways in a search for special solutions.

We will also need the first $O(\mu^3)$ equation:

$$\begin{aligned}
\frac{\partial^2 Y_3}{\partial T^2} + Y_3 = & -2\sigma_1 \frac{\partial^2 Y_2}{\partial T^2} - 2 \frac{\partial^2 Y_2}{\partial T \partial \tau_1} \\
& - 2 \frac{\partial^2 Y_1}{\partial T \partial \tau_2} - \frac{\partial^2 Y_1}{\partial \tau_1^2} - 4\sigma_1 \frac{\partial^2 Y_1}{\partial T \partial \tau_1} \\
& - (\sigma_1^2 + 2\sigma_2) \frac{\partial^2 Y_1}{\partial T^2} - 2 \frac{\partial^2 Y_0}{\partial T \partial \tau_3} \\
& + r_1 \frac{\partial Y_1}{\partial T} + sC_1
\end{aligned}$$

which gives as our anti-secularity equation

$$(7.5.2) \quad \left[-2i \frac{\partial A_0}{\partial \tau_3} \right] + \left[-2i \frac{\partial A_1}{\partial \tau_2} + (\sigma_1^2 + 2\sigma_2 + 4\sigma_1\delta + \delta^2) A_1 \right] + \left[-2i \frac{\partial A_2}{\partial \tau_1} + 2\sigma_1 A_2 + sB_1 + ir_1 A_1 \right] = 0$$

Again, we split this equation up into the equations in square brackets and require that they be zero separately. We note first that the two τ_2 -scale equations

$$(7.5.3) \quad -2i \frac{\partial A_1}{\partial \tau_2} + \left(\sigma_1^2 - \omega_1^2 + 2\sigma_2 + 4\sigma_1\delta + \delta^2 \right) A_1 = 0$$

$$(7.5.4) \quad -2i \frac{\partial B_0}{\partial \tau_2} + \left(\sigma_1^2 - \omega_1^2 + 2\sigma_2 + 4\sigma_1\delta + \delta^2 \right) B_0 = 0$$

are easily solved, and imply that $\frac{\partial \xi_1}{\partial \tau_2} = \frac{\partial}{\partial \tau_2}(\phi_1(\tau_2) - \psi_0(\tau_2)) = 0$ and that $\frac{\partial a_1}{\partial \tau_2} = \frac{\partial b_0}{\partial \tau_2} = 0$, so the τ_2 -scale has no effect on the first terms, regardless of the choice of σ_1 , δ , or σ_2 . Thus we can get a consistent solution from this separation, which justifies *ex post facto* the separation used. Notice that the τ_3 -scale does not affect the solution at all in this separation, as $A_0 \equiv 0$. Now we look at the system formed from the third set of brackets from (7.5.2) together with the first set of brackets from (7.5.1). We try to solve this system for B_1 and A_2 . We look for special limit-cycle solutions as before, and in fact insist that the new terms have the same

τ_1 -frequency. Thus we set

$$\begin{aligned} A_2 &= \frac{1}{2} a_2(\tau_1, \tau_2) e^{i(\phi_2(\tau_1, \tau_2) + \delta \tau_1)} \\ B_1 &= \frac{1}{2} b_1(\tau_1, \tau_2, \tau_3) e^{i(\psi_1(\tau_1, \tau_2, \tau_3) + \delta \tau_1)} \end{aligned}$$

where the δ is the same as in the first terms obtained. For notational convenience, we define $\xi_2 = \phi_2 - \psi_1$, $\psi_d = \psi_0 - \psi_1$, and use the shorthand notation $s_1 = \sin(\xi_1)$, $c_1 = \cos(\xi_1)$, $s_d = \sin(\psi_d)$, $s_{2d} = \sin(2\psi_d)$, and similarly for $\sin(\xi_2)$ and the other phase angles. Then, what is left of (7.5.2) becomes in real form

$$(7.5.6) \quad \begin{aligned} s_2 \frac{\partial a_2}{\partial \tau_1} + c_2 a_2 \frac{\partial \phi_2}{\partial \tau_1} + (\sigma_1 + \delta) c_2 a_2 \\ + \frac{1}{2} s b_1 - \frac{1}{2} r_1 a_1 c_1 s_d = 0 \end{aligned}$$

$$(7.5.7) \quad \begin{aligned} -c_2 \frac{\partial a_2}{\partial \tau_1} + s_2 a_2 \frac{\partial \phi_2}{\partial \tau_1} + (\sigma_1 + \delta) s_2 a_2 \\ - \frac{1}{2} r_1 a_1 c_1 c_d = 0 \end{aligned}$$

where we have used the fact that $\xi_1 = 0$ or π . Thus, at a τ_1 -steady state,

$$(7.5.8) \quad (\sigma_1 + \delta) c_2 a_2 + \frac{1}{2} s b_1 - \frac{1}{2} r_1 a_1 c_1 s_d = 0$$

$$(7.5.9) \quad (\sigma_1 + \delta) s_2 a_2 - \frac{1}{2} r_1 a_1 c_1 c_d = 0$$

This allows us to eliminate ξ_2 , and when $\sigma_1 + \delta \neq 0$ we have

$$(7.5.10) \quad a_2^2 = \frac{1}{4(\sigma_1 + \delta)^2} \left((r_1 a_1 c_1 s_d - s b_1)^2 + (r_1 a_1 c_1 c_d)^2 \right).$$

Now we examine the first bracket in (7.5.1). We use the symbolic computation lan-

guage REDUCE [11] now as the equations are getting tedious for hand computation.

By REDUCE, the equations in real form are

$$\begin{aligned}
 (7.5.11) \quad & b_1 \frac{\partial \psi_1}{\partial \tau_1} + (\sigma_1 + \delta - \omega_1) b_1 + \frac{3}{8} \gamma b_0^2 s_{2d} b_1 \\
 & + c_d \left(-\frac{1}{2} \omega_1^2 b_0 + \frac{9}{256} \gamma^2 b_0^5 - B(\sigma_1 + \delta) c_1 a_1 \right) \\
 & + s_d \left(\frac{9}{8} \gamma b_0^3 - \frac{1}{2} g b_0 - \frac{1}{2} D c_1 a_1 \right) (\sigma_1 + \delta) \\
 & - \frac{1}{2} B a_2 c_2 - \frac{1}{2} D a_2 s_2 = 0
 \end{aligned}$$

and

$$\begin{aligned}
 (7.5.12) \quad & -\frac{\partial b_1}{\partial \tau_1} + \left(\frac{1}{2} g - \frac{3}{4} \gamma b_0^2 - \frac{3}{8} \gamma b_0^2 c_{2d} \right) b_1 \\
 & - c_d \left(\frac{9}{8} \gamma b_0^3 - \frac{1}{2} g b_0 - \frac{1}{2} D c_1 a_1 \right) (\sigma_1 + \delta) \\
 & + s_d \left(-\frac{1}{2} \omega_1^2 b_0 + \frac{9}{256} \gamma^2 b_0^5 - B(\sigma_1 + \delta) c_1 a_1 \right) \\
 & + \frac{1}{2} D a_2 c_2 - \frac{1}{2} B a_2 s_2 = 0.
 \end{aligned}$$

We can use (7.5.8) and (7.5.9) to eliminate both ξ_2 and a_2 from these equations, at

a τ_1 -steady state. Putting for notational convenience

$$\begin{aligned}
 q_1 &= \frac{1}{2}g - \frac{3}{4}\gamma b_0^2 \\
 q_2 &= \frac{1}{2(\sigma_1 + \delta)} \\
 p_1 &= \sigma_1 + \delta - \omega_1 \\
 p_2 &= \frac{3}{8}\gamma b_0^2 \\
 p_3 &= -\frac{1}{2}\omega_1^2 b_0 + \frac{9}{256}\gamma^2 b_0^5 - B(\sigma_1 + \delta)c_1 a_1 \\
 p_4 &= \left(\frac{9}{8}\gamma b_0^3 - \frac{1}{2}g b_0 - \frac{1}{2}D c_1 a_1 \right) (\sigma_1 + \delta) \\
 p_5 &= -\frac{1}{2}B \\
 p_6 &= -\frac{1}{2}D,
 \end{aligned}
 \tag{7.5.13}$$

then (7.5.11) and (7.5.12) become, at steady τ_1 -state,

$$\begin{aligned}
 (7.5.14) \quad & p_1 \cdot b_1 + p_2 \cdot s_{2d} \cdot b_1 + (p_3 - q_2 p_6 r_1 a_1 c) c_d \\
 & + (p_4 + q_2 p_5 r_1 a_1 c) s_d - q_2 p_5 s b_1 = 0
 \end{aligned}$$

$$\begin{aligned}
 (7.5.15) \quad & q_1 \cdot b_1 - p_2 \cdot c_{2d} \cdot b_1 - (p_4 + q_2 p_5 r_1 a_1 c) c_d \\
 & + (p_3 - q_2 p_6 r_1 a_1 c) s_d + q_2 p_6 s b_1 = 0.
 \end{aligned}$$

These equations are nonlinear in ψ_d , but we may solve them by forming the combinations $c_d \times (7.5.14) + s_d \times (7.5.15)$ and $s_d \times (7.5.14) - c_d \times (7.5.15)$, which because of the identities $c_d s_{2d} - s_d c_{2d} = s_d$ and $s_d s_{2d} + c_d c_{2d} = c_d$ are linear in c_d and s_d .

From here we proceed to a complete solution. Making these combinations gives

$$(7.5.16) \quad (p_1 b_1 - q_2 p_5 s b_1) c_d + (q_1 b_1 + p_2 + q_2 p_6 s b_1) s_d \\ = -p_3 + q_2 p_6 r_1 a_1 c_1$$

$$(7.5.17) \quad (-q_1 b_1 + p_2 - q_2 p_6 s b_1) c_d + (p_1 b_1 - q_2 p_5 s b_1) s_d \\ = -p_4 - q_2 p_5 r_1 a_1 c_1.$$

Remark The solution of these linear equations for c_d and s_d in terms of b_1 and the first-term solutions allows us to set up a single equation in the single remaining unknown b_1 by noting $c_d^2 + s_d^2 = 1$. On solution of this equation for b_1 , we then use the linear equations to determine c_d and s_d and hence ψ_d , and then we can use (7.5.8)–(7.5.10) to determine a_2 and ξ_2 .

Putting

$$A_{11} = p_1 - q_2 p_5 s$$

$$A_{12} = q_1 + q_2 p_6 s$$

$$A_{21} = -A_{12}$$

$$A_{22} = A_{11}$$

$$B_{11} = -p_3 + q_2 p_6 r_1 a_1 c_1$$

$$B_{22} = -p_4 - q_2 p_5 r_1 a_1 c_1$$

then the solution of the system (7.5.16)—(7.5.17) can be obtained by e.g. Cramer's rule:

$$c_d = \frac{\begin{vmatrix} B_{11} & A_{12}b_1 + p_2 \\ B_{22} & A_{11}b_1 \end{vmatrix}}{\begin{vmatrix} A_{11}b_1 & A_{12}b_1 + p_2 \\ -A_{12}b_1 + p_2 & A_{11}b_1 \end{vmatrix}}$$

$$s_d = \frac{\begin{vmatrix} A_{11}b_1 & B_{11} \\ -A_{12}b_1 + p_2 & B_{22} \end{vmatrix}}{\begin{vmatrix} A_{11}b_1 & A_{12}b_1 + p_2 \\ -A_{12}b_1 + p_2 & A_{11}b_1 \end{vmatrix}}$$

and our last equation, for b_1 , is $c_d^2 + s_d^2 = 1$. By inspection, we see that this single equation for b_1 is a quartic equation, so an analytical solution is available if desired. It makes better numerical sense, however, to use a more general numerical method to find the real positive roots, as the analytical formula can be unstable numerically.

Remark Strictly speaking, we should calculate the stability of the $O(\mu^2)$ terms in a manner similar to the process used for the $O(\mu)$ terms. However, we shall see in the later section on the solution in the nonresonance region that the stability of the higher-order terms is effectively determined by the stability of the first terms calculated. We shall *assume* that the same situation holds in the resonance region. This is reasonable, as the solution to this order will only be used for error-checking, and if the solution to this order does not differ too much from the solution to the previous order, then we can think of the second-order terms as a perturbation of the first-order solution, and rely on the first-order stability analysis. If on the other

hand the difference between the solution to the two orders is large, then we can no longer rely on the previous stability analysis. However, if this is the case, then the *validity* of the solution to the previous order is then in doubt as well, and a stability analysis of the second-order terms would tell us nothing useful. In Figure 7.5.1, we see a demonstration of this effect. For $\omega_0 < 1.04$, we have good agreement between the solution to one term and the solution to two terms. Since the stability analysis for the first term solution shows that this branch of the solution is stable, we can conclude that the solution in this region is accurate. However, we see at or near $\omega_0 = 1.04$ the beginning of large oscillations in the two-term solution. This is not physically significant, but merely signals the possible end of the region of good accuracy for the one-term solution. Recall that here the method of multiple scales is expected to give an *asymptotic* series as the solution of the model equations. In an asymptotic series, taking more terms does not always increase the accuracy obtained: in fact, the usual case is that there is an optimal number of terms to which to take the series to for minimal error, and if more terms than this are taken, the error begins to grow. Thus when we see good agreement between the solution to one term and the solution to two terms we feel confident that the true solution is represented well by the solutions presented. However, when the solutions do *not* agree, we have less confidence in the *two term* solution; the one term solution may still be adequately accurate.

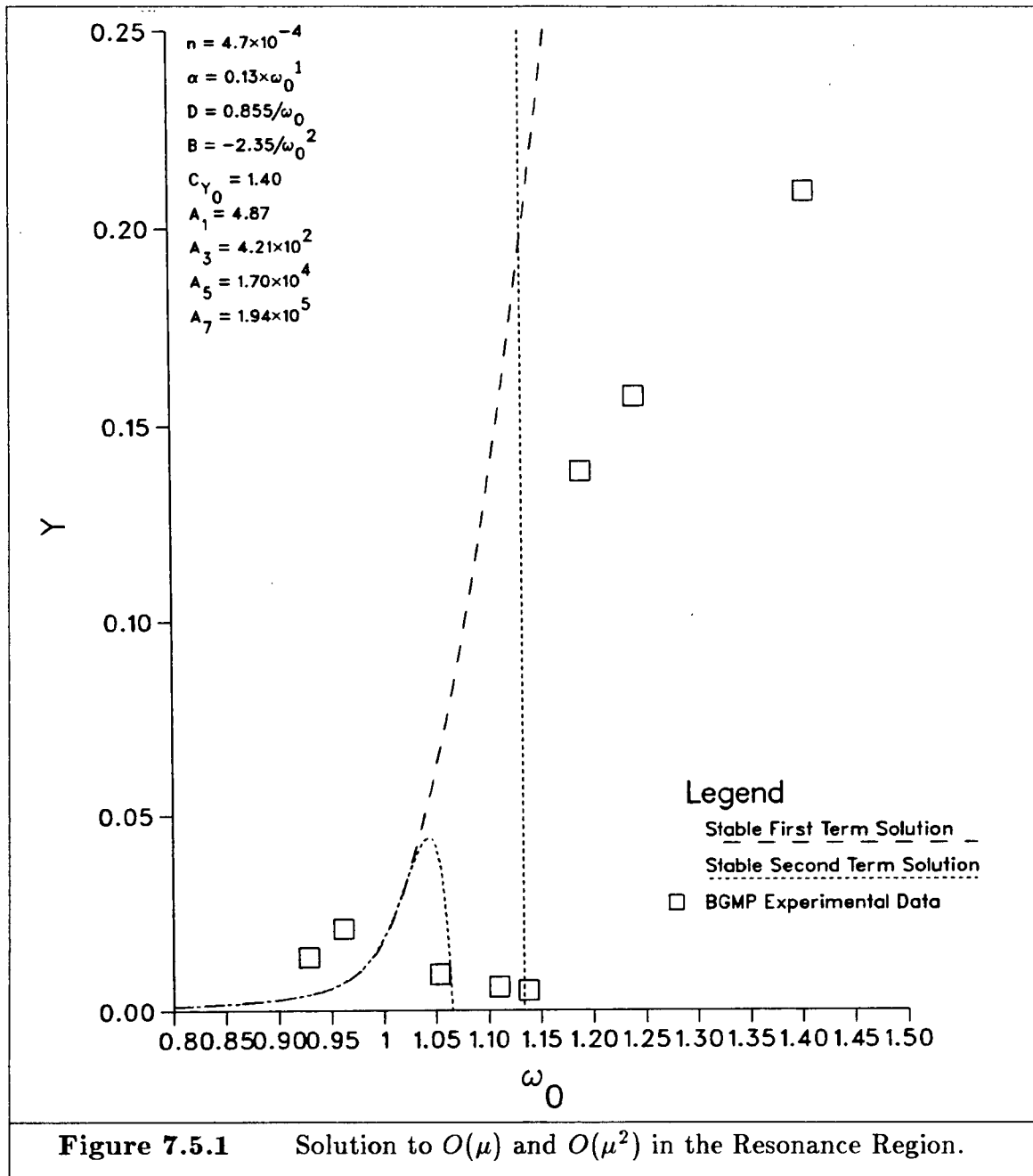
Here, we can see that the solution to the first term is sufficient up until $\omega_0 = 1.04$, as the true solution should be between the solution to one term and the solution to two terms. After the solution to two terms starts to oscillate, however, we have no guarantees of the accuracy of the solution, and the true solution of the model equations may follow the one term solution (as it can be expected to for some range after $\omega_0 = 1.04$) but cannot be trusted. Eventually, the one-term solution becomes very large, and this is a further indication of the loss of accuracy. This loss of accuracy arises out of the breaking down of the assumptions about the size of Y_1 , which is becoming $O(1)$ rather than $O(\mu)$.

There are some experimental values from [1] also plotted in Figure 7.5.1 for comparison purposes. The solution agrees with the general upward trend of the data, though it overpredicts the size of the amplitudes.

Recapitulation In terms of the original (nondimensional) variables, the solution obtained so far may be written as

$$\begin{aligned}
 Y &= \mu a_1 \cos \left[(1 + \mu(\sigma_1 + \delta) + \mu^2 \sigma_2 + \cdots) t + \phi_1 \right] \\
 &\quad + \mu^2 a_2 \cos \left[(1 + \mu(\sigma_1 + \delta) + \mu^2 \sigma_2 + \cdots) t + \phi_2 \right] + O(\mu^3) \\
 C_v &= b_0 \cos \left[(1 + \mu(\sigma_1 + \delta) + \mu^2 \sigma_2 + \cdots) t + \psi_0 \right] \\
 &\quad + \mu b_1 \cos \left[(1 + \mu(\sigma_1 + \delta) + \mu^2 \sigma_2 + \cdots) t + \psi_1 \right] + O(\mu^2)
 \end{aligned}$$

where we may take $\phi_1 = 0$ because of the autonomous nature of the model equations,



and all the other parameters (except σ_2 , which we are free to choose) have been determined in the previous sections. Note that the parameter δ appears throughout only in the combination $\sigma_1 + \delta$, and thus could profitably have been omitted. This

was not evident *a priori* however, so δ was left in the analysis. At this point we may set it to 0, however. Notice also that the effect of σ_2 is not felt on the τ_2 -scale, as $\sigma_2\tau_2$ occurs in the solution for $\psi_0(\tau_2, \tau_3, \tau_4)$ and cancels with the occurrence of $\sigma_2\mu^2t$ in the argument to $b_0\cos(\cdot)$. Any effects of the choice of σ_2 are thus confined to higher order terms, so we may as well take $\sigma_2 = 0$. The nature of the solution is that of a limit cycle in four dimensional phase space. We can easily determine the stability of this limit cycle, through the stability analysis of the first order solution.

7.6 Case II: Nonresonance Case, with $\omega_0 \neq 1$

This section will complete the solution to $O(\mu)$ in Y and to $O(1)$ in C_v in the nonresonance case, and show where the superharmonic and subharmonic cases arise from. We will investigate the latter cases in the sections following.

Here the $O(1)$ equations are, almost as before,

$$(7.6.1) \quad \frac{\partial^2 Y_0}{\partial T^2} + Y_0 = 0$$

$$(7.6.2) \quad \frac{\partial^2 C_0}{\partial T^2} + \omega_0^2 C_0 = D \frac{\partial Y_0}{\partial T} + B \frac{\partial^2 Y_0}{\partial T^2}$$

which have solutions

$$(7.6.3) \quad Y_0 = A_0(\tau_1, \tau_2, \tau_3, \tau_4)e^{iT} + \text{c.c.}$$

$$(7.6.4) \quad C_0 = B_0(\tau_1, \tau_2, \tau_3, \tau_4)e^{i\omega_0 T} + \frac{(iD - B)}{\omega_0^2 - 1}A_0e^{iT} + \text{c.c.}$$

The $O(\mu)$ equations are then

$$(7.6.5) \quad \frac{\partial^2 Y_1}{\partial T^2} + Y_1 = -2\sigma_1 \frac{\partial^2 Y_0}{\partial T^2} - 2 \frac{\partial^2 Y_0}{\partial T \partial \tau_1}$$

and

$$(7.6.6) \quad \begin{aligned} \frac{\partial^2 C_1}{\partial T^2} + \omega_0^2 C_1 = & -2\sigma_1 \frac{\partial^2 C_0}{\partial T^2} - 2 \frac{\partial^2 C_0}{\partial T \partial \tau_1} \\ & + g \frac{\partial C_0}{\partial T} - \gamma \left(\frac{\partial C_0}{\partial T} \right)^3 \\ & + D \left[\frac{\partial Y_1}{\partial T} + \sigma_1 \frac{\partial Y_0}{\partial T} + \frac{\partial Y_0}{\partial \tau_1} \right] \\ & + B \left[\frac{\partial^2 Y_1}{\partial T^2} + 2\sigma_1 \frac{\partial^2 Y_0}{\partial T^2} + 2 \frac{\partial^2 Y_0}{\partial T \partial \tau_1} \right] \end{aligned}$$

and our first anti-secularity equation is

$$(7.6.7) \quad 2\sigma_1 A_0 - 2i \frac{\partial A_0}{\partial \tau_1} = 0$$

giving

$$(7.6.8) \quad A_0 = A_0(\tau_2, \tau_3, \tau_4) e^{-i\sigma_1 \tau_1}$$

after which (7.6.5) gives

$$(7.6.9) \quad Y_1 = A_1(\tau_1, \tau_2, \tau_3) e^{iT} + \text{c.c.}$$

To get the anti-secularity equation for (7.6.6), we must set the coefficient of $e^{i\omega_0 T}$ to zero. For notational convenience, put $\nu = i\omega_0 B_0$ and $\lambda = -(D + iB)A_0/(\omega_0^2 - 1)$.

Then, using (7.6.4),

$$\begin{aligned}
 (7.6.10) \quad \left(\frac{\partial C_0}{\partial T} \right)^3 &= \nu^3 e^{i3\omega_0 T} + 3\nu^2 \bar{\nu} e^{i\omega_0 T} \\
 &\quad + 3 \left[\nu^2 \lambda e^{i(2\omega_0+1)T} + 2\nu \bar{\nu} \lambda e^{iT} + \nu^2 \bar{\lambda} e^{i(2\omega_0-1)T} \right] \\
 &\quad + 3 \left[\nu \lambda^2 e^{i(\omega_0+2)T} + 2\nu \lambda \bar{\lambda} e^{i\omega_0 T} + \bar{\lambda}^2 \nu e^{i(\omega_0-2)T} \right] \\
 &\quad + \lambda^3 e^{i3T} + 3\lambda^2 \bar{\lambda} e^{iT} + \text{c.c.}
 \end{aligned}$$

We wish to investigate which values of ω_0 give rise to resonance. Thus, we look at the frequencies present in the equation (7.6.6) after (7.6.10) has been substituted in, and ask which terms have frequencies that resonate with ω_0 . For different values of ω_0 , there may be different terms entering in to this process. For example, if $\omega_0 = 1 + O(\mu)$, then $2\omega_0 - 1 = \omega_0 + O(\mu)$ and this causes a resonance. By inspection of the equation, there are four different cases: $\omega_0 \approx 1$, which has already been handled in the previous sections, $\omega_0 \approx 1/3$, $\omega_0 \approx 3$, and lastly, $\omega_0 \not\approx 1, 1/3, \text{ or } 3$, the nonresonance case. If $\omega_0 = 1/3 + O(\mu)$, this is the phenomenon of superharmonic resonance, and the $-(2\omega_0 - 1)$ term in (7.6.10) goes into the anti-secularity equation here, resonating with ω_0 , and the $3\omega_0$ term will later resonate with 1. If $\omega_0 = 3 + O(\mu)$, then the term at frequency 3 will resonate with ω_0 , while later the $\omega_0 - 2$ term will resonate with 1. We will see later that the subharmonic resonance is the more important of the two for our models. In this section, we assume henceforth that $\omega_0 \not\approx 1/3$ and that $\omega_0 \not\approx 3$. Under this last assumption, the

anti-secularity equation for (7.6.6) becomes

$$(7.6.11) \quad -2i\omega_0 \frac{\partial B_0}{\partial \tau_1} + (2\sigma_1\omega_0^2 + i\omega_0 g)B_0 - \gamma(3\nu^2\bar{\nu} + 6\nu\lambda\bar{\lambda}) = 0$$

which leaves in (7.6.6)

$$(7.6.12) \quad \frac{\partial^2 C_1}{\partial T^2} + \omega_0^2 C_1 = \left((iD - B)A_1 + g\lambda - \gamma(6\nu\bar{\nu}\lambda + 3\lambda^2\bar{\lambda}) \right) e^{iT} - \gamma \left[\nu^3 e^{i \cdot 3\omega_0 T} + 3\nu^2 \lambda e^{i(2\omega_0+1)T} + 3\nu^2 \bar{\lambda} e^{i(2\omega_0-1)T} + 3\nu \lambda^2 e^{i(\omega_0+2)T} + 3\nu \bar{\lambda}^2 e^{i(\omega_0-2)T} + \lambda^3 e^{i \cdot 3T} \right] + \text{c.c.}$$

which is easily solved, giving

$$(7.6.13) \quad C_1 = B_1(\tau_1, \tau_2) e^{i\omega_0 T} + \kappa_1 e^{iT} + \kappa_{3\omega_0} e^{i(3\omega_0)T} + \kappa_{2\omega_0+1} e^{i(2\omega_0+1)T} + \kappa_{2\omega_0-1} e^{i(2\omega_0-1)T} + \kappa_{\omega_0+2} e^{i(\omega_0+2)T} + \kappa_{\omega_0-2} e^{i(\omega_0-2)T} + \kappa_3 e^{i \cdot 3T} + \text{c.c.}$$

where $\kappa_s = c_s/(\omega_0^2 - s^2)$, with c_s equal to the coefficient of e^{isT} in (7.6.12), for

$s = 1, 3\omega_0, 2\omega_0 + 1, 2\omega_0 - 1, \omega_0 + 2, \omega_0 - 2$, and 3.

Remark The nonresonance case is more complicated than the resonance case, in that there are more frequencies present in the $O(1)$ and $O(\mu)$ terms. However, this presents no real difficulty, just a little more work.

We solve the anti-secularity equation (7.6.11) by splitting it into real and imaginary parts: putting $B_0 = \frac{1}{2}b_0e^{i\psi_0}$, we have

$$(7.6.14) \quad \omega_0 b_0 \frac{\partial \psi_0}{\partial \tau_1} + \sigma_1 \omega_0^2 b_0 = 0$$

$$(7.6.15) \quad -\frac{\partial b_0}{\partial \tau_1} + \omega_0 g b_0 / 2 - \gamma \left[\frac{3}{8} \omega_0^3 b_0^3 + \frac{3\omega_0(D^2 + B^2)a_0^2 b_0}{4(\omega_0^2 - 1)^2} \right] = 0$$

which has solution $b_0 = 0$ or

$$(7.6.16) \quad \psi_0 = -\sigma_1 \omega_0 \tau_1 + \psi_0(\tau_2, \tau_3, \tau_4)$$

$$(7.6.17) \quad b_0 = \frac{C_{Y_0} \sqrt{h}}{\sqrt{1 - K(\tau_2, \tau_3, \tau_4)e^{-hg\tau_1}}} \quad \text{if } h \geq 0$$

where

$$(7.6.18) \quad h = h(\tau_2, \tau_3, \tau_4) = 1 - \frac{2(D^2 + B^2)}{C_{Y_0}^2 \omega_0^2 (\omega_0^2 - 1)^2} a_0^2(\tau_2, \tau_3, \tau_4).$$

and $K(\tau_2, \tau_3, \tau_4)$ is an arbitrary constant of integration on the τ_1 -scale.

Remark If $h < 0$, then it is easily verified that all solutions of equation (7.6.15) decay exponentially to 0. This shows that if a_0 is too large, then the only stable solution for b_0 , the $O(1)$ amplitude of the Strouhal frequency component in the wake, is zero. This occurs only in the resonance region, when $\omega_0 \sim 1$. This corresponds to the entrainment or lock-in of the wake frequency to that of the body.

Remark We see that equation (7.6.18) implies that for any fixed τ_2, τ_3, τ_4 , $b_0 \rightarrow C_{Y_0} \sqrt{h}$, if $h > 0$. This tells us that the excitation, to first order, is determined wholly by the τ_1 -scale. We must check that the higher-order equations are consistent with this solution.

We must yet determine $a_0(\tau_2, \tau_3, \tau_4)$, $\phi_0(\tau_2, \tau_3, \tau_4)$, and $\psi_0(\tau_2, \tau_3, \tau_4)$ to complete the solution to first order. To do this, we look at the first $O(\mu^2)$ equation:

$$\begin{aligned}
 (7.6.19) \quad \frac{\partial^2 Y_2}{\partial T^2} + Y_2 = & -2\sigma_1 \frac{\partial^2 Y_1}{\partial T^2} - 2 \frac{\partial^2 Y_1}{\partial T \partial \tau_1} \\
 & - (\sigma_1^2 + 2\sigma_2) \frac{\partial^2 Y_0}{\partial T^2} - 4\sigma_1 \frac{\partial^2 Y_0}{\partial T \partial \tau_1} \\
 & - \frac{\partial^2 Y_0}{\partial \tau_1^2} - 2 \frac{\partial^2 Y_0}{\partial T \partial \tau_2} \\
 & + r_1 \frac{\partial Y_0}{\partial T} - r_3 \left(\frac{\partial Y_0}{\partial T} \right)^3 + r_5 \left(\frac{\partial Y_0}{\partial T} \right)^5 - r_7 \left(\frac{\partial Y_0}{\partial T} \right)^7 \\
 & + sC_0
 \end{aligned}$$

so to avoid secularity we must have

$$\begin{aligned}
 (7.6.20) \quad & -2i \frac{\partial A_1}{\partial \tau_1} + 2\sigma_1 A_1 \\
 & + \left[(\sigma_1^2 + 2\sigma_2) A_0 - 4\sigma_1^2 A_0 \right. \\
 & + \sigma_1^2 A_0 - 2i \frac{\partial A_0}{\partial \tau_2} \\
 & + i[r_1 A_0 - 3r_3 A_0^2 \bar{A}_0 \\
 & \quad \left. + 10r_5 A_0^3 \bar{A}_0^2 - 35r_7 A_0^4 \bar{A}_0^3] \right. \\
 & \left. + s \frac{(iD - B)}{\omega_0^2 - 1} A_0 \right] e^{-i\sigma_1 \tau_1} = 0
 \end{aligned}$$

and to avoid secularity on the τ_1 -scale in *this* equation, we must have the coefficient of $e^{-i\sigma_1 \tau_1}$ equal to zero.

Remark Contrast this with the resonance case solution, where we had to choose how to split up the higher-order resonance equations. Here we automatically have two different equations on the two different time scales, which gives much greater confidence in the solution.

Thus we have the following equations:

$$(7.6.21) \quad -2i \frac{\partial A_1}{\partial \tau_1} + 2\sigma_1 A_1 = 0$$

which has solution

$$(7.6.22) \quad A_1(\tau_1, \tau_2, \tau_3) = A_1(\tau_2, \tau_3) e^{-i\sigma_1 \tau_1}$$

and the other equation is

$$(7.6.23) \quad \begin{aligned} & -2i \frac{\partial A_0}{\partial \tau_2} + 2(\sigma_2 - \sigma_1^2) A_0 - \frac{sB}{\omega_0^2 - 1} A_0 \\ & + i[r_1 A_0 - 3r_3 A_0^2 \bar{A}_0 + 10r_5 A_0^3 \bar{A}_0 - 35r_7 A_0^4 \bar{A}_0^3] \\ & + i \frac{sD}{\omega_0^2 - 1} = 0 \end{aligned}$$

or, in real form, with $A_0 = \frac{1}{2} a_0 e^{i\phi_0}$,

$$(7.6.24) \quad a_0 \frac{\partial \phi_0}{\partial \tau_2} + (\sigma_2 - \sigma_1^2 - \frac{sB}{2(\omega_0^2 - 1)}) a_0 = 0$$

$$(7.6.25) \quad \frac{\partial a_0}{\partial \tau_2} = f(a_0)$$

where

$$(7.6.26) \quad \begin{aligned} f(a_0) = \frac{a_0}{2} \left[r_1 + \frac{sD}{\omega_0^2 - 1} - \frac{3}{4} r_3 a_0^2 \right. \\ \left. + \frac{5}{8} r_5 a_0^4 - \frac{35}{64} r_7 a_0^6 \right]. \end{aligned}$$

Remark We can solve these equations completely, though in the general case our solution for a_0 is in an implicit form. In the special case $r_5 = r_7 = 0$, we can provide an explicit solution for a_0 also. It is interesting to compare these equations with the corresponding equations we get from the simple quasi-steady model due

to Parkinson and Smith [20]:

$$(7.6.27) \quad \frac{\partial a_0}{\partial \tau_2} = \frac{a_0}{2} \left[r_1 - \frac{3}{4} r_3 a_0^2 + \frac{5}{8} r_5 a_0^4 - \frac{35}{64} r_7 a_0^6 \right]$$

which differs only in the linear term. This means this model is precisely as easy to solve as the quasi-steady model is, although the higher-dimensionality of the problem complicates the geometric picture of the limit cycles. We will also see later that equation (7.6.25) is unaffected by the subharmonic and superharmonic cases, thus confining their effects to the higher-order terms.

Before we proceed to solve the anti-secularity equation, we exhibit the form of the solution for Y_2 from what is left of (7.6.19):

$$(7.6.28) \quad \begin{aligned} Y_2 = & A_2(\tau_1, \tau_2) e^{iT} + \ell_3 e^{i \cdot 3T} \\ & + \ell_5 e^{i \cdot 5T} + \ell_7 e^{i \cdot 7T} \\ & + \ell_{\omega_0} e^{i \cdot \omega_0 T} + \text{c.c.} \end{aligned}$$

where

$$\begin{aligned} \ell_3 &= i \frac{A_0^3}{8} [r_3 - 5r_5 A_0 \bar{A}_0 + 21r_7 A_0^2 \bar{A}_0^2] \\ \ell_5 &= i \frac{A_0^5}{24} [r_5 - 7r_7 A_0 \bar{A}_0] \\ \ell_7 &= i \frac{A_0^7}{48} r_7. \\ \ell_{\omega_0} &= \frac{sB_0}{1 - \omega_0^2} \end{aligned}$$

We first solve the anti-secularity equation (7.6.25) in the important special case

when $\mathcal{A}_5 = \mathcal{A}_7 = 0$, which is often observed for cylinders in turbulent flows. Our equation becomes

$$(7.6.29) \quad \frac{\partial a_0}{\partial \tau_2} = f(a_0) = \frac{1}{2}a_0 \left[r_1 + \frac{sD}{\omega_0^2 - 1} - \frac{3}{4}r_3 a_0^2 \right].$$

In this case, since the equation is separable, and the resulting implicit equation for $a_0(\tau_2)$ is solvable (which it is not in the case $\mathcal{A}_5, \mathcal{A}_7 \neq 0$), we can get a *complete* solution, and this gives extra insight into the higher-order polynomial cases. The solution in this case depends principally on the sign of the linear coefficient, $2f'(0) = r_1 + sD/(\omega_0^2 - 1)$. If this is negative, then it is easy to see that all solutions of (7.6.29) decay exponentially to zero (on the τ_2 -scale, for any fixed τ_3 and τ_4), and any initial conditions. If the linear coefficient is zero, the solution again decays to zero for any fixed τ_3 and τ_4 , but in this case the decay is algebraic. If the linear coefficient is positive, the solution can be written

$$(7.6.30) \quad a_0(\tau_2, \tau_3, \tau_4) = \sqrt{\frac{2f'(0)}{\frac{3}{4}r_3 - K(\tau_3, \tau_4)e^{-2f'(0)\tau_2}}}$$

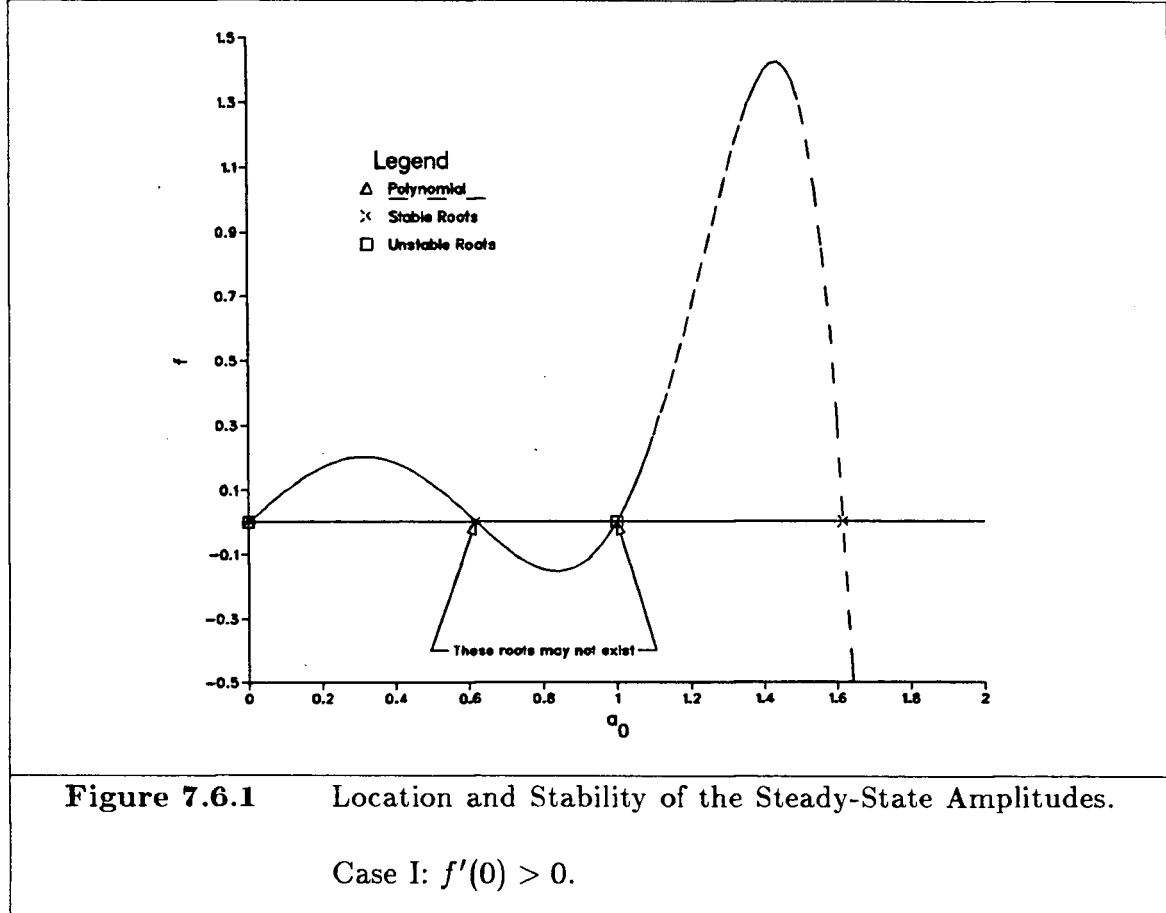
where as before K is an arbitrary constant of integration on the τ_1 -scale. We see that for all finite values of K and all fixed values of τ_3 and τ_4 that the solution tends exponentially to a nonzero steady state. The zero solution corresponds to the case of infinite K ; we should really go back to the complex form to investigate the zero solution, however, to avoid the singularity introduced in the transformation to real form. When we do this, we find, as expected, that if $2f'(0) > 0$ then the

zero solution is unstable, and likewise when it is negative the zero solution is stable. Thus in the case of $\mathcal{A}_5 = \mathcal{A}_7 = 0$, we have a complete description of the first terms of the solution to the model equations. It is important to note that all nonzero solutions tend to the single nonzero solution (an ‘orbital attractor’ in mathematical dynamics jargon), the steady state given by $\mathcal{K} = 0$ or

$$(7.6.31) \quad a_0 = \sqrt{\frac{4(r_1 + s \frac{D}{\omega_0^2 - 1})}{3r_3}}.$$

Remark In the case $D = 0$, this reduces to precisely the quasi-steady solution. Recall, though, that the solution here is valid only outside of the resonance region. On closer inspection of the solution given above, we note that for $\omega_0 \approx 1$ the value of a_0 can become arbitrarily large. However, before a_0 gets too large, we see by equations (7.6.17) and (7.6.18) that b_0 will go to zero if a_0 is too large. We simply have to use our judgement as to when the solution given above is valid, as it is outside the resonance region. One could wish for a more clear-cut division of the solution into regions, but it is usually clear from the regions of overlap of the solutions just how far each region’s solution may be pushed.

Remark Note that the steady states of the solution and the stability of these states provides a complete description of the long-time behaviour of the solutions to the model equations. We now have a complete solution of the model equations to $O(1)$, in that b_0 and a_0 are both known, in the case $\mathcal{A}_5 = \mathcal{A}_7 = 0$. We next

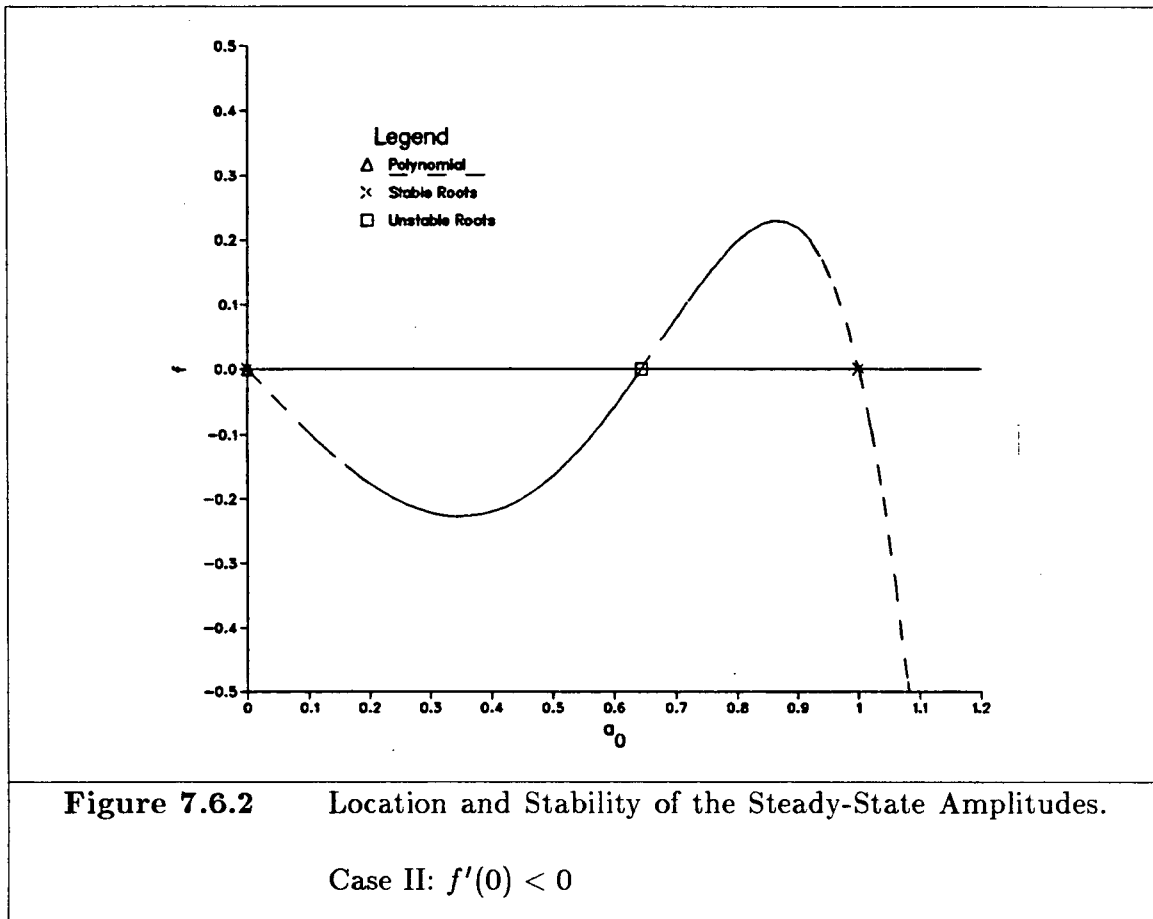


investigate the solution in the case of nonzero \mathcal{A}_5 and \mathcal{A}_7 .

Recall from equation (7.6.26) that

$$\frac{\partial a_0}{\partial \tau_2} = f(a_0) = \frac{1}{2}a_0 \left[r_1 + \frac{sD}{\omega_0^2 - 1} - \frac{3}{4}r_3 a_0^2 + \frac{5}{8}r_5 a_0^4 - \frac{35}{64}r_7 a_0^6 \right]$$

so the zeros of $f(a_0)$ are the steady-states of (7.6.25), and the stability of a steady state a_0^* is determined by the sign of $f'(a_0^*)$ from the usual linearization technique.



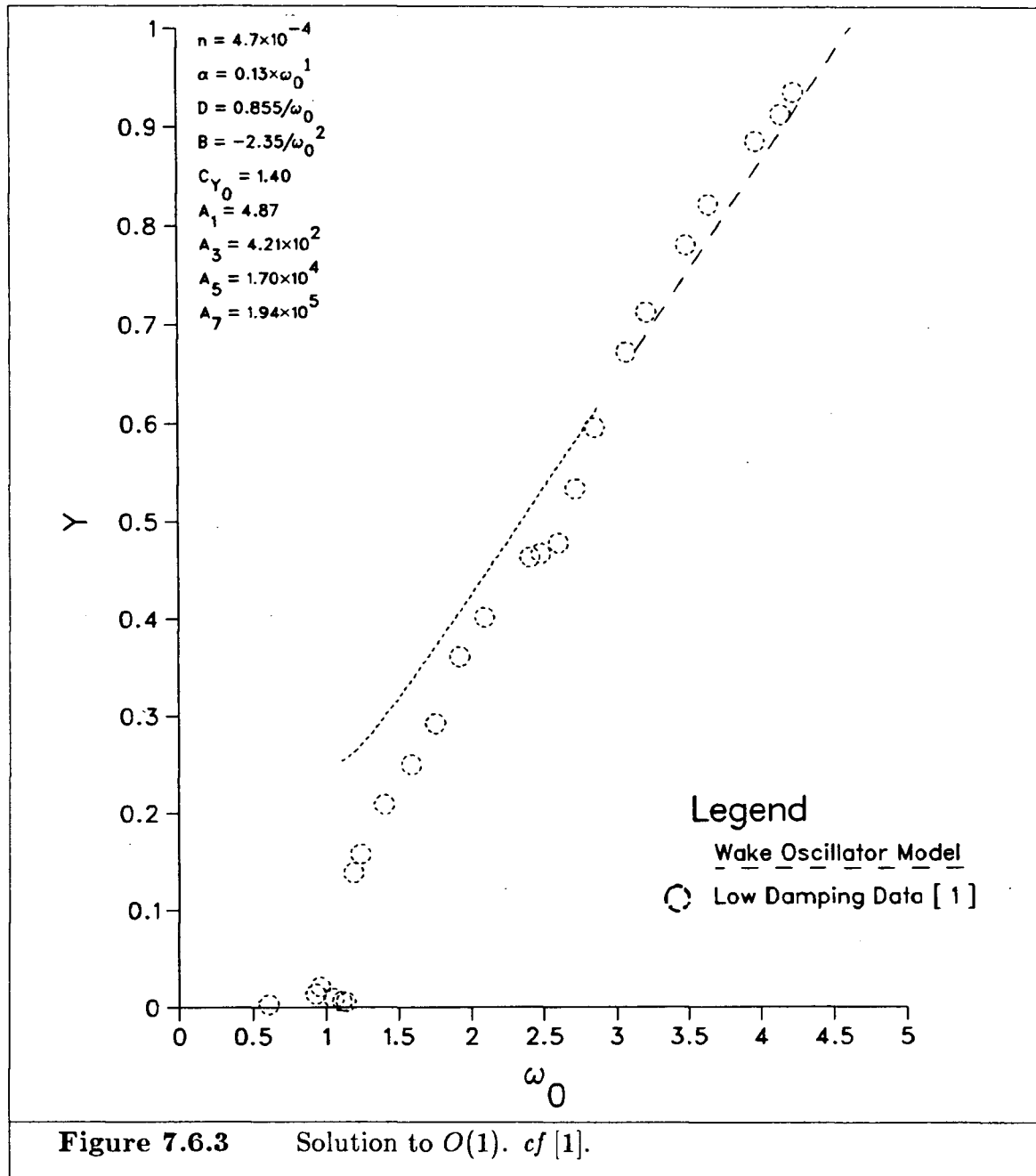
In particular, the zero solution is stable if and only if

$$(7.6.32) \quad 2f'(0) = r_1 + \frac{sD}{\omega_0^2 - 1} = \mathcal{A}_1(U - U_0) + \frac{U^2 D(\omega_0)}{\omega_0^2 - 1} < 0.$$

It is interesting to note that this, together with the *number* of real positive roots of $f(a_0)$, completely determines the stability of each real root. The possible situations are summarized in Figures 7.6.1 and 7.6.2. Figure 7.6.1 shows a graph of a typical polynomial of the type presented in equation (7.6.26), with $f'(0) > 0$. There is always a root at 0, and there is always at least one positive root with $f'(a_0^*) < 0$

as the highest-order coefficient in the polynomial is negative. There may or may not be another two roots present, depending on the values of the other coefficients. The roots with $f'(a_0^*) < 0$ are stable, and the others are unstable. Figure 7.6.2 shows the analogous situation when $f'(0) < 0$. In this case it is possible that there are no roots other than 0. This completes the solution of the equations to $O(1)$. In Figure 7.6.3 we present a sample solution of the model equations to this order, and compare this solution to data from [1]. Note that, to $O(1)$, the solution in the resonance region is zero, but that outside the resonance region, agreement with the data presented is quite good. In this low-damping low-turbulence case, the quasi-steady model predicts a nonzero amplitude starting from $\omega_0 = U_0/U_r = 0.63$. This model on the other hand predicts that nonzero amplitudes will occur only *after* the resonance region, which is what is physically observed.

Remark To this order, solving the model equations is precisely as easy as solving the galloping equation. The solution is zero in the resonance region (to first order) and the steady states outside this region are given by the roots of the cubic (in a_0^2) polynomial (7.6.32). To this order, the subharmonic and the superharmonic resonances do not enter into the solutions. These resonances play a part in the next order terms.



7.7 Nonresonance Solution to $O(\mu)$

The first $O(\mu^3)$ equation is, by REDUCE, in the case $\sigma_1 = 0$,

$$\begin{aligned}
 \frac{\partial^2 Y_3}{\partial T^2} + Y_3 = & -2 \frac{\partial^2 Y_2}{\partial T \partial \tau_1} - 2\sigma_2 \frac{\partial^2 Y_1}{\partial T^2} - 2 \frac{\partial^2 Y_1}{\partial T \partial \tau_2} \\
 & - 2\sigma_3 \frac{\partial^2 Y_0}{\partial T^2} - 2 \frac{\partial^2 Y_0}{\partial T \partial \tau_3} \\
 & + \left(r_1 - 3r_3 \left(\frac{\partial Y_0}{\partial T} \right)^2 + 5r_5 \left(\frac{\partial Y_0}{\partial T} \right)^4 - 7r_7 \left(\frac{\partial Y_0}{\partial T} \right)^6 \right) \left(\frac{\partial Y_1}{\partial T} \right) \\
 & + s \cdot C_1.
 \end{aligned} \tag{7.7.1}$$

and our anti-secularity equations are thus in the case $\omega_0 \not\approx 3$ and $\omega_0 \not\approx 1/3$ and taking $\sigma_1 = 0$

$$(7.7.2) \quad -2i \frac{\partial A_2}{\partial \tau_1} = 0$$

$$(7.7.3) \quad -2i \frac{\partial A_0}{\partial \tau_3} = 0$$

$$\begin{aligned}
 (7.7.4) \quad -2i \frac{\partial A_1}{\partial \tau_2} = & -2\sigma_3 A_0 - s\kappa_1 \\
 & + i \left(r_1 A_1 - 3r_3 [A_0^2 \bar{A}_1 + 2A_0 \bar{A}_0 A_1] \right. \\
 & \quad + 5r_5 [4A_0^3 \bar{A}_0 \bar{A}_1 + 6A_0^2 \bar{A}_0^2 A_1] \\
 & \quad \left. - 7r_7 [15A_0^4 \bar{A}_0^2 \bar{A}_1 + 20A_0^3 \bar{A}_0^3 A_1] \right).
 \end{aligned}$$

Now (7.7.2) and (7.7.3) are trivial, and we may find the steady-states of (7.7.4) in the following manner: Put $\phi_d = \phi_0 - \phi_1$; then on division by $e^{i\phi_1}$, (7.7.4) in real

form becomes

$$(7.7.5) \quad -\frac{\partial \phi_d}{\partial \tau_2} = \frac{1}{2} \sin(2\phi_d) m_1 - \frac{m_2}{a_1} \left(-D \cos \phi_d + B \sin \phi_d \right) - \sigma_3 \left(\frac{a_0}{a_1} \right) \cos \phi_d$$

and

$$(7.7.6) \quad -\frac{\partial a_1}{\partial \tau_2} = -\sigma_3 a_0 \sin \phi_d - \frac{1}{2} m_1 a_1 \cos(2\phi_d) - \frac{1}{2} a_1 m_3 - m_2 \left(-D \sin \phi_d - B \cos \phi_d \right)$$

where

$$(7.7.7) \quad m_1 = -\frac{3}{4} r_3 a_0^2 + \frac{5}{4} r_5 a_0^4 - \frac{105}{64} r_7 a_0^6$$

$$(7.7.8) \quad m_2 = s \left\{ \frac{g a_0}{2(\omega_0^2 - 1)^2} - \gamma \left[\frac{3\omega_0^2 b_0^2 a_0}{4(\omega_0^2 - 1)^2} + \frac{3(D^2 + B^2) a_0^3}{8(\omega_0^2 - 1)^4} \right] \right\}$$

$$(7.7.9) \quad m_3 = r_1 + \frac{sD}{(\omega_0^2 - 1)} - \frac{3}{2} r_3 a_0^2 + \frac{15}{8} r_5 a_0^4 - \frac{35}{16} r_7 a_0^6.$$

Now, denoting $\cos \phi_d$ by c_d , $\sin \phi_d$ as s_d , and similarly for the other angles, and noting that $m_1 - m_3 = f(a_0) = 0$ and that $m_1 + m_3 = f'(a_0)$, and putting $p_1 = \sigma_3 a_0 - m_2 D$, we get at steady state

$$(7.7.10) \quad p_1 \cdot c_d - s_d(m_2 B - m_1 a_1 c_d) = 0$$

and

$$(7.7.11) \quad p_1 \cdot s_d + c_d(m_2 B - m_1 a_1 c_d) = 0.$$

Now, multiplying (7.7.10) by c_d , (7.7.11) by s_d , and adding, we get $p_1(s_d^2 + c_d^2) = 0$. Thus $p_1 = 0$ or $\sigma_3 = m_2 D/a_0$, or the appropriate limit when $a_0 = 0$. Similarly, multiplying by $-s_d$ and c_d and adding, we get $(s_d^2 + c_d^2)(m_2 B - m_1 a_1 c_d) = 0$, so we have an equation for the product $a_1 c_d$. This is sufficient, as by our use of σ_3 we have shown that $\phi_1 = -\phi_d$ is now a free variable. Then we can choose the steady state solution as

$$\sin \phi_d = 0 \text{ by choice}$$

$$(7.7.12) \quad a_1 = \frac{m_2 B}{m_1 c_d}$$

so $Y_1 = a_1 \cos(T + \phi_d) = a_1 \cos \phi_d \cos(T)$ if we take $\phi_0 = 0$ by the freedom to choose a time origin.

Remark Note that $m_1 \equiv f'(a_0)$, and a simple stability analysis shows that a_1 is stable if and only if the corresponding a_0 is stable. This consistency gives confidence in the results. Note also that the choice of $\phi_d = 0$ or $\phi_d = \pi$ is immaterial, as the sign will cancel out in the Y_1 term.

7.8 Subharmonic Solution to $O(\mu)$: $\omega_0 = 3 + \mu\omega_3$

Equations (7.6.1) through (7.6.10) are unchanged in this case, but the anti-secularity equation for (7.6.6) is not (7.6.11) but rather, using $\omega_0 = 3 + \mu\omega_3$ and

$$\tau_1 = \mu T,$$

$$(7.8.1) \quad -2i\omega_0 \frac{\partial B_0}{\partial \tau_1} + 2\sigma_1 \omega_0^2 B_0 = -i\omega_0 g B_0 \\ + \gamma \left[3\nu^2 \bar{\nu} + 6\lambda \bar{\lambda} \nu + \lambda^3 e^{-i\omega_3 \tau_1} \right]$$

which has the new term $\gamma \lambda^3 e^{-i\omega_3 \tau_1}$, which is included because the e^{i3T} term resonates with ω_0 . This equation is autonomous if and only if one of $a_0 = 0$ (which implies that $\lambda = 0$) or

$$(7.8.2) \quad -3\sigma_1 \tau_1 - \omega_3 \tau_1 = 0.$$

So we naturally take $\sigma_1 = -\omega_3/3$, compared to 0 in the nonresonance case. This is immaterial in the case $a_0 = 0$. Then,

$$\lambda^3 e^{-i\omega_3 \tau_1} = \left[-\frac{D + iB}{\omega_0^2 - 1} A_0(\tau_2, \tau_3, \tau_4) \right]^3 e^{-i(3\sigma_1 + \omega_3)\tau_1} \\ = -\frac{E^3}{8(\omega_0^2 - 1)^3} a_0^3 e^{i(3\phi_0 + 3\theta)}$$

where

$$E e^{i\theta} = D + iB.$$

Remark We have used σ_1 to transform the nonautonomous equation (7.8.1) to an autonomous one. We could have avoided using σ_1 by looking for a solution for B_0 at the frequency $3(\sigma_1 + \omega_3/3)$ instead of a steady state solution of the resulting

autonomous equation. This approach is taken merely for convenience.

With this notation, (7.8.1) becomes in real form

$$(7.8.3) \quad \omega_0 b_0 \frac{\partial \psi_0}{\partial \tau_1} = -\sigma_1 \omega_0^2 b_0 - \gamma \frac{E^3}{8(\omega_0^2 - 1)^3} a_0^3 \cos(3\phi_0 + 3\theta - \psi_0)$$

and

$$(7.8.4) \quad \begin{aligned} \omega_0 \frac{\partial b_0}{\partial \tau_1} = & \frac{1}{2} \omega_0 g b_0 - \gamma \left[\frac{3}{8} \omega_0^3 b_0^3 + \frac{6E^2 \omega_0 a_0^2 b_0}{8(\omega_0^2 - 1)^2} \right] \\ & + \gamma \frac{E^3}{8(\omega_0^2 - 1)^3} a_0^3 \sin(3\phi_0 + 3\theta - \psi_0). \end{aligned}$$

We can get a more compact representation by putting

$$\alpha_1 = \frac{E a_0}{C_{Y_0} \omega_0 (\omega_0^2 - 1)}$$

$$\alpha_2 = -2\omega_0 \sigma_1 / g$$

$$\tau = \frac{1}{2} g \tau_1$$

$$r = b_0 / C_{Y_0}$$

$$\hat{\psi}_0 = \psi_0 - 3\theta$$

$$R_0^2 = 1 - 2\alpha_1^2 \quad (\text{possibly negative})$$

so we get instead

$$(7.8.3) \quad r \frac{\partial \hat{\psi}_0}{\partial \tau} = \alpha_2 r - \frac{1}{3} \alpha_1^3 \cos(\hat{\psi}_0)$$

$$(7.8.4) \quad \frac{\partial r}{\partial \tau} = r(R_0^2 - r^2) - \frac{1}{3} \alpha_1^3 \sin(\hat{\psi}_0)$$

Thus, at steady state, by squaring and adding appropriately we get

$$(7.8.5) \quad \alpha_2^2 r^2 + r^2 (R_0^2 - r^2)^2 = \frac{1}{9} \alpha_1^6$$

This is a cubic equation for r^2 , which allows us to find the steady states for b_0 .

Remark For a consistent asymptotic expansion, we note that g , D , and B are (at this moment unspecified) functions of ω_0 . This means that for convenience and consistency we do not replace each occurrence of ω_0 in the above equation with 3, and likewise when the time comes to evaluate B , D , and g , we use the exact value of ω_0 . This may seem unnecessary, as the computed value of b_0 is accurate only to $O(1)$, with errors $O(\mu)$, and $\omega_0 = 3 + O(\mu)$ here, but it is a valid procedure, and convenient for programming. For hand computation of a less complicated problem, it would make sense to evaluate the parameters at $\omega_0 = 3$ and use those values throughout. Here it is easier to make the parameters dependent on the wind speed, and any errors introduced will be of higher order.

We can evaluate $\xi_3 = 3\phi_0 + 3\theta - \psi_0$ at steady state once b_0 is known by using (7.8.3) and (7.8.4). This completes the solution to $O(1)$ in the subharmonic resonance case. Notice that A_0 is completely unaffected by the subharmonic resonance.

Note that what is left in the Second $O(\mu)$ equation is different than the solution

of (7.6.12), being

$$\begin{aligned}
 (7.8.6) \quad C_1 = & B_1(\tau_1, \tau_2, \tau_3)e^{i\omega_0 T} + \kappa_1 e^{iT} \\
 & + \kappa_{3\omega_0} e^{i(3\omega_0)T} + \kappa_{2\omega_0+1} e^{i(2\omega_0+1)T} \\
 & + \kappa_{2\omega_0-1} e^{i(2\omega_0-1)T} \\
 & + \text{c.c.}
 \end{aligned}$$

where

$$\begin{aligned}
 \kappa_1 &= \frac{1}{\omega_0^2 - 1} \left((iD - B)A_1 + g\lambda - 3\gamma\lambda(2\nu\bar{\nu} + \lambda\bar{\lambda}) - 3\gamma\nu\bar{\lambda}^2 e^{i\omega_0\tau_1} \right) \\
 \kappa_{3\omega_0} &= -\frac{\gamma\nu^3}{\omega_0^2 - (3\omega_0)^2} \\
 \kappa_{2\omega_0+1} &= -\frac{3\gamma\nu^2\lambda}{\omega_0^2 - (2\omega_0 + 1)^2} \\
 \kappa_{2\omega_0-1} &= -\frac{3\gamma\nu^2\bar{\lambda}}{\omega_0^2 - (2\omega_0 - 1)^2} - \frac{3\gamma\nu\lambda^2}{\omega_0^2 - (\omega_0 + 2)^2} e^{-i\omega_0\tau_1}.
 \end{aligned}$$

This should be compared with (7.6.13) to appreciate the differences. The component at frequency 1 has a new, apparently τ_1 -varying term, the terms at frequencies $\omega_0 - 2$ and 3 are absorbed, and the $\omega_0 + 2$ and $2\omega_0 - 1$ frequency terms combine.

The first $O(\mu^3)$ equation in the subharmonic case differs from (7.7.1) in that there are some terms involving σ_1 , which was zero in the nonresonance case. We

have

$$\begin{aligned}
 (7.8.7) \quad \frac{\partial^2 Y_3}{\partial T^2} + Y_3 = & -2 \frac{\partial^2 Y_2}{\partial T \partial \tau_1} - 2\sigma_1 \frac{\partial^2 Y_2}{\partial T^2} \\
 & - 2 \frac{\partial^2 Y_1}{\partial T \partial \tau_2} - 4\sigma_1 \frac{\partial^2 Y_1}{\partial T \partial \tau_1} - (2\sigma_2 + \sigma_1^2) \frac{\partial^2 Y_1}{\partial T^2} \\
 & - \frac{\partial^2 Y_1}{\partial \tau_1^2} - 2 \frac{\partial^2 Y_0}{\partial T \partial \tau_3} - 4\sigma_1 \frac{\partial^2 Y_0}{\partial T \partial \tau_1} - (4\sigma_2 + 2\sigma_1^2) \frac{\partial^2 Y_0}{\partial T \partial \tau_1} \\
 & - (2\sigma_3 + 2\sigma_1\sigma_2) \frac{\partial^2 Y_0}{\partial T^2} \\
 & - 2 \frac{\partial^2 Y_0}{\partial \tau_1 \partial \tau_2} - 2\sigma_1 \frac{\partial^2 Y_0}{\partial \tau_1^2} \\
 & + \left(r_1 - 3r_3 \left(\frac{\partial Y_0}{\partial T} \right)^2 + 5r_5 \left(\frac{\partial Y_0}{\partial T} \right)^4 - 7r_7 \left(\frac{\partial Y_0}{\partial T} \right)^6 \right) \frac{\partial Y_1}{\partial T} + s \cdot C_1
 \end{aligned}$$

The anti-secularity equation is thus more complicated, being

$$(7.8.8) \quad -2i \frac{\partial A_2}{\partial \tau_1} + 2\sigma_1 A_2 = -e^{-i\sigma_1 \tau_1} \left[\text{fn}(\tau_2, \tau_3, \tau_4) \right]$$

where

$$\begin{aligned}
 (7.8.9) \quad \text{fn}(\tau_2, \tau_3, \tau_4) = & -2i \frac{\partial A_1}{\partial \tau_2} + (2\sigma_2 - 2\sigma_1^2) A_1 \\
 & - 2i \frac{\partial A_0}{\partial \tau_3} - 2\sigma_1 \frac{\partial A_0}{\partial \tau_2} + (2\sigma_3 - 2\sigma_1\sigma_2) A_0 \\
 & + i \left(r_1 A_1 - 3r_3 [A_0^2 \bar{A}_1 + 2A_0 \bar{A}_0 A_1] \right. \\
 & \quad + 5r_5 [4A_0^3 \bar{A}_0 \bar{A}_1 + 6A_0^2 \bar{A}_0^2 A_1] \\
 & \quad \left. - 7r_7 [15A_0^4 \bar{A}_0^2 \bar{A}_1 + 20A_0^3 \bar{A}_0^3 A_1] \right) \\
 & + s \cdot \kappa_1 e^{i\sigma_1 \tau_1}
 \end{aligned}$$

To avoid secularity in (7.8.8) on the τ_1 -scale, we must have $\text{fn}(\tau_2, \tau_3, \tau_4) \equiv 0$. This gives, as before,

$$(7.8.10) \quad A_2(\tau_1, \tau_2) = A_2(\tau_2)e^{-i\sigma_1\tau_1}$$

Remark $e^{i\sigma_1\tau_1}\kappa_1$ is in fact independent of τ_1 , as long as B_0 is at a steady state.

From (7.8.6) we have

$$(7.8.11) \quad \kappa_1 = \frac{1}{\omega_0^2 - 1} \cdot \left((iD - B)A_1(\tau_2, \tau_3)e^{-i\sigma_1\tau_1} \right. \\
+ g \cdot \frac{-D - iB}{\omega_0^2 - 1} A_0(\tau_2, \tau_3, \tau_4)e^{-i\sigma_1\tau_1} \\
- 3\gamma \cdot \frac{-D - iB}{\omega_0^2 - 1} A_0(\tau_2, \tau_3, \tau_4)e^{-i\sigma_1\tau_1} [2|\nu|^2 + |\lambda|^2] \\
- 3\gamma i\omega_0 B_0(\tau_1, \tau_2, \tau_3, \tau_4) \cdot \\
\left. \left(\frac{-D - iB}{\omega_0^2 - 1} \right)^2 \frac{A_0^2}{A_0} e^{i \cdot (2\sigma_1 + \omega_3)\tau_1} \right)$$

and as $\omega_3 + 2\sigma_1 = -\sigma_1$ by (7.8.2), we see that the only dependence on τ_1 is through B_0 . Thus, if B_0 is at a steady τ_1 -state, this last term must be included in the above anti-secularity equation, to avoid τ_1 -secularity in A_1 . This inclusion will affect the stability analysis later.

When we convert (7.8.9) to real form we get, with m_1 , m_2 , and m_3 as in (7.7.7), (7.7.8), and (7.7.9) respectively, and with the real form definitions as in the nonres-

onance case (e.g. $A_1 = \frac{1}{2}a_1 e^{i\phi_1}$),

$$\begin{aligned}
 (7.8.12) \quad -a_1 \frac{\partial \phi_1}{\partial \tau_2} = & (\sigma_2 - \sigma_1^2 - s \frac{B}{2(\omega_0^2 - 1)}) a_1 \\
 & + [a_0 \frac{\partial \phi_0}{\partial \tau_3} + \sigma_1 a_0 \frac{\partial \phi_0}{\partial \tau_2} + (\sigma_3 - \sigma_2 \sigma_1) a_0] c_d \\
 & + [\frac{\partial a_0}{\partial \tau_3} + \sigma_1 \frac{\partial a_0}{\partial \tau_2}] s_d \\
 & - m_1 \cdot \frac{1}{2} a_1 \cdot s_{2d} + m_2 \cdot (-D c_d + B s_d) \\
 & + s \cdot \frac{3\gamma\omega_0 b_0 a_0^2 E^2}{8(\omega_0^2 - 1)^3} \sin(\psi_0 - 3\phi_0 - 2\theta + \phi_d)
 \end{aligned}$$

where $E e^{i\theta} \equiv D + iB$ as before, and the imaginary part becomes

$$\begin{aligned}
 (7.8.13) \quad \frac{\partial a_1}{\partial \tau_2} = & [a_0 \frac{\partial \phi_0}{\partial \tau_3} + \sigma_1 a_0 \frac{\partial \phi_0}{\partial \tau_2} + (\sigma_3 - \sigma_2 \sigma_1) a_0] s_d \\
 & - [\frac{\partial a_0}{\partial \tau_3} + \sigma_1 \frac{\partial a_0}{\partial \tau_2}] c_d \\
 & + m_1 \cdot \frac{1}{2} a_1 \cdot c_{2d} + m_2 \cdot (-B c_d - D s_d) \\
 & + m_3 \cdot \frac{1}{2} a_1 \\
 & - s \cdot \frac{3\gamma\omega_0 b_0 a_0^2 E^2}{8(\omega_0^2 - 1)^3} \cos(\psi_0 - 3\phi_0 - 2\theta + \phi_d)
 \end{aligned}$$

The solution of these equations parallels the solution of (7.7.5) and (7.7.6) precisely. We again simplify the solution by choosing σ_3 so that $\sin(\phi_d) = s_d = 0$.

Also, to make the limit cycle solution actually a steady state, we choose as in the nonresonance case

$$\sigma_2 = \sigma_1^2 + s \frac{B}{2(\omega_0^2 - 1)}$$

Thus at steady state we have

$$(7.8.14) \quad a_1 = \frac{2c_d}{m_1 + m_3} \left[m_2 B + s \cdot \frac{3\gamma\omega_0 b_0 a_0^2 E^2}{8(\omega_0^2 - 1)^3} \cos(\xi_z) \right]$$

where $\xi_z = \psi_0 - 3\phi_0 - 2\theta$ is known, as are the other quantities. Again, the choice $\phi_d = 0$ or π is immaterial, as the sign cancels out as before. Also, we have $\sigma_3 = \sigma_2\sigma_1 + (m_2 D - s \cdot \frac{3\gamma\omega_0 b_0 a_0^2 E^2}{8(\omega_0^2 - 1)^3} \sin(\xi_d))/a_0$.

Remark When we wish to use the same stability analysis as in the nonresonance case, it all goes through except for one point: the anti-secularity equation with which we do the stability analysis is only *necessarily* valid if B_0 is at a τ_1 -steady state. Given that restriction, we can say that a_1 is stable if and only if the corresponding a_0 is stable.

7.9 Superharmonic Solution to $O(\mu)$

Remark This section was included for completeness. When we calculate the superharmonic resonance for the case of oscillation in air, we find that the $O(1)$ solution a_0 is zero in this region, and the maximum amplitude of the next term is less than 10^{-5} , which is insignificant. For the case of water, for larger n , this term may be significant, however, and thus the solution is included here. The analysis of

this case is very similar to the analysis of the subharmonic case. The second $O(\mu)$ anti-secularity equation is, taking $\omega_0 = 1/3 + \mu\omega_{1/3}$,

$$(7.9.1) \quad -2i\omega_0 \frac{\partial B_0}{\partial \tau_1} + 2\sigma_1 \omega_0^2 B_0 = -i\omega_0 g B_0 + \gamma \left[3\nu^2 \bar{\nu} + 6\lambda \bar{\lambda} \nu + 3\bar{\nu}^2 \lambda e^{-i3\omega_{1/3}\tau_1} \right]$$

which leaves as the solution of the second $O(\mu)$ equation

$$(7.9.2) \quad C_1 = B_1(\tau_1, \tau_2, \tau_3) e^{i\omega_0 T} + \kappa_1 e^{i(1)T} + \kappa_{2\omega_0+1} e^{i(2\omega_0+1)T} + \kappa_{\omega_0+2} e^{i(\omega_0+2)T} + \kappa_3 e^{i(3)T} + \text{c.c.}$$

where

$$\begin{aligned} \kappa_1 &= \frac{1}{(\omega_0^2 - 1)} \left[(iD - B)A_1 + g\lambda - \gamma(\nu^3 e^{i3\omega_{1/3}\tau_1} + \lambda(6\nu\bar{\nu} + 3\lambda\bar{\lambda})) \right] \\ \kappa_{2\omega_0+1} &= \frac{-3\gamma}{\omega_0^2 - (2\omega_0 + 1)^2} \left[\nu^2 \lambda + \bar{\nu}^2 \lambda^2 e^{-i3\omega_{1/3}\tau_1} \right] \\ \kappa_{\omega_0+2} &= \frac{-3\gamma\nu\lambda^2}{\omega_0^2 - (\omega_0 + 2)^2} \\ \kappa_3 &= \frac{-\gamma\lambda^3}{\omega_0^2 - 3^2} \end{aligned}$$

Now, equation (7.9.1) is τ_1 -autonomous if and only if $\lambda e^{-i3\omega_{1/3}\tau_1}$ is independent of

τ_1 . This occurs if

$$A_0 = 0 \quad (\Rightarrow \lambda = 0)$$

or

$$(7.9.3) \quad \sigma_1 = -3\omega_{1/3}$$

Not coincidentally, this choice of σ_1 makes κ_1 and $\kappa_{2\omega_0+1}$ independent of τ_1 also.

Putting for convenience (almost as in the subharmonic case)

$$r = b_0/C_{Y_0}$$

$$\hat{\psi}_0 = \psi_0 - \theta/3$$

$$Ee^{i\theta} = D + iB$$

$$\phi_0 = 0$$

$$\alpha_1 = \frac{Ea_0}{C_{Y_0}\omega_0(\omega_0^2 - 1)}$$

$$R_0^2 = 1 - 2\alpha_1^2$$

$$\alpha_2 = -2\omega_0\sigma_1/g$$

$$\tau = \frac{1}{2}g\tau_1$$

we have as the real form of the anti-secularity equations

$$(7.9.4) \quad \begin{aligned} r \frac{\partial \hat{\psi}_0}{\partial \tau} &= \alpha_2 r + \alpha_1 r^2 \cos(3\hat{\psi}_0) \\ \frac{\partial r}{\partial \tau} &= r(R_0^2 - r^2) + \alpha_1 r^2 \sin(3\hat{\psi}_0) \end{aligned}$$

Remark The range of values of α_2 includes zero, when the wind speed is precisely $1/3$. Note also that α_1 is zero when a_0 is zero.

We investigate some special case solutions of (7.9.4), as a prelude. If $a_0 = 0$, the solution is particularly simple. In this case, $\alpha_1 = 0$ also, and thus the solution is

$$(7.9.5) \quad \begin{aligned} \psi_0 &= \alpha_2 \tau + P(\tau_2, \tau_3, \tau_4) \\ r &= (1 + K(\tau_2, \tau_3, \tau_4)e^{-2\tau})^{-1/2} \end{aligned}$$

or else the unstable solution $r = 0$. Note that this solution is not a steady solution unless $\alpha_2 = 0$. This case will need careful analysis later.

To find any steady-state solutions in the general case, we must solve the polynomial equation

$$(7.9.6) \quad r^2 \alpha_2^2 + r^2 (R_0^2 - r^2)^2 = \alpha_1^2 r^4$$

which is easily seen to have solutions

$$(7.9.7) \quad \begin{aligned} r &= 0 \\ r^2 &= R_0^2 + \frac{1}{2} \alpha_1^2 \pm \sqrt{R_0^2 \alpha_1^2 + \alpha_1^4/4 - \alpha_2^2} \end{aligned}$$

Note that unless $\alpha_1^2 > \frac{1}{2}$, $R_0^2 > 0$. We can easily see that if

$$\alpha_2^2 \leq (R_0^2 + \alpha_1^2/4) \alpha_1^2$$

then there will be three nonnegative steady states. The corresponding ψ_0 will be given by setting the right hand sides of (7.9.4) to zero. For each nonzero r , we will get 3 solutions for ψ_0 . This will give 6 steady states in all. If the above inequality for α_2 is violated, that is if the wind speed is too far from the exact superharmonic resonance, there are no steady-state solutions.

A final special case to consider is what happens exactly at the resonance, when $\sigma_1 = 0$. The above inequality is satisfied for all α_1 , and our steady states become

$$(7.9.8) \quad \begin{aligned} r &= \frac{1}{2}\alpha_1 + \sqrt{R_0^2 + \alpha_1^2/4} \\ \hat{\psi}_0 &= \frac{\pi}{6}, \frac{5\pi}{6}, \frac{3\pi}{2} \end{aligned}$$

and

$$(7.9.9) \quad \begin{aligned} r &= -\frac{1}{2}\alpha_1 + \sqrt{R_0^2 + \alpha_1^2/4} \\ \hat{\psi}_0 &= \frac{\pi}{2}, \frac{7\pi}{6}, \frac{11\pi}{6} \end{aligned}$$

and a simple stability analysis shows that the eigenvalues of the Jacobian are $-3r^2 + 2\alpha_1 \sin(3\hat{\psi}_0)r + R_0^2$ and $-3\alpha_1 \sin(3\hat{\psi}_0)$. Thus, since $\alpha_1 \leq 0$, the steady states are unstable if $\hat{\psi}_0 = \pi/6, \dots$ and can only be stable if $\hat{\psi}_0 = \pi/2, \dots$

We may now find the steady-state value of the $O(\mu)$ term for Y . The anti-secularity

equation for the first $O(\mu^3)$ is

$$(7.9.10) \quad 2i \frac{\partial A_2}{\partial \tau_1} - 2\sigma_1 A_2 = e^{-i\sigma_1 \tau_1} \text{fn}(\tau_2, \tau_3, \tau_4) + \text{term}$$

where $\text{fn}(\tau_2, \tau_3, \tau_4)$ is different, and ‘term’ may or may not be present, depending on whether B_0 is at a τ_1 -limit cycle or at a τ_1 -steady state. If B_0 is at a τ_1 -steady state, then

$$(7.9.11) \quad \begin{aligned} \text{fn}(\tau_1, \tau_2, \tau_3) = & 2(\sigma_2 - \sigma_1^2)A_1 - 2i \frac{\partial A_1}{\partial \tau_2} \\ & - s \frac{B}{(\omega_0^2 - 1)} A_1 + 2(\sigma_3 - \sigma_1 \sigma_2) A_0 \\ & + i \left(\left(r_1 + s \frac{D}{(\omega_0^2 - 1)} \right) A_1 - 3r_3 [A_0^2 \bar{A}_1 + 2A_0 \bar{A}_0 A_1] + \right. \\ & \quad + 5r_5 [4A_0^3 \bar{A}_0 A_1 + 6A_0^2 \bar{A}_0^2 A_1] \\ & \quad \left. - 7r_7 [15A_0^4 \bar{A}_0^2 A_1 + 20A_0^3 \bar{A}_0^3 A_1] \right) \\ & + s \frac{1}{(\omega_0^2 - 1)} \lambda [g - \gamma(3\lambda \bar{\lambda} + 6\nu \bar{\nu})] \\ & - s \frac{\gamma \nu^3}{(\omega_0^2 - 1)} \end{aligned}$$

If, however, A_0 is zero, then B_0 is not at a steady state but rather at a limit cycle.

In this case, the term

$$\begin{aligned} \nu^3 e^{i \cdot 3\omega_{1/3} \tau_1} &= \text{const} \cdot e^{i \cdot (3\sigma_1 \omega_0 + 3\omega_{1/3}) \tau_1} \\ &= \text{const} \cdot e^{i \cdot \sigma_1 (1 + 3\mu \omega_{1/3} - 1) \tau_1} \\ &= \text{const} \cdot e^{i \cdot 3\omega_{1/3} \sigma_1 \tau_2} \end{aligned}$$

and the only way that this can be equal to $e^{-i\sigma_1\tau_1}$ is for $\omega_{1/3} = 0$. Thus, when $\omega_{1/3} \neq 0$, the extra term goes into the τ_1 -equation for A_2 , and not into the τ_2 -equation for A_1 . In addition, the τ_2 equation for A_1 is much simplified, having as solutions functions of τ_2 which decay exponentially to zero, as long as the zero solution for A_0 is stable in the $O(1)$ sense. Also in this case, the equation for A_2 is linear and easily solved. However, if $\omega_{1/3} = 0$, then for any choice of σ_1 the ν^3 term must be included in the equation for A_1 , in which case the analysis proceeds as before, except for some more τ_2 -modulation of the phase.

Solutions: Case I, $A_0 \neq 0$ The anti-secularity equations in real form are

$$(7.9.12) \quad a_1 \frac{\partial \phi_d}{\partial \tau_2} = (\sigma_2 - \sigma_1^2 - s \frac{B}{2(\omega_0^2 - 1)}) a_1 + p_1 c_d \\ - m_1 a_1 s_d c_d + m_2 B s_d$$

$$(7.9.13) \quad \frac{\partial a_1}{\partial \tau_2} = p_1 s_d + m_1 a_1 c_d^2 - m_2 B c_d$$

where m_1 , m_2 , and m_3 are as in (7.7.7)—(7.7.9), so as before $m_1 = m_3 = f'(a_0)$ whenever $f(a_0) = 0$. Also,

$$(7.9.14) \quad m_4 = \frac{s\gamma\omega_0^2 b_0^3}{8(\omega_0^2 - 1)} \\ p_1 = (\sigma_3 - \sigma_1\sigma_2)a_0 - m_2 D - m_4 \sin(3\psi_0)$$

We choose as before $\sigma_2 = \sigma_1^2 + s \frac{B}{2(\omega_0^2 - 1)}$ so we have at steady-state

$$p_1 \cdot s_d + c_d(m_1 a_1 c_d - m_2 B) = 0$$

$$p_1 \cdot c_d - s_d(m_1 a_1 c_d - m_2 B) = 0$$

Thus, multiplying the first by $s_d = \sin(\phi_d)$ and the second by c_d and adding, we get $p_1(s_d^2 + c_d^2) = 0$, and thus $p_1 = 0$. Since in this case $a_0 \neq 0$, we use the only unknown present in p_1 to get

$$\sigma_3 = \sigma_2 \sigma_1 + \frac{1}{a_0} \left(m_2 D + m_4 \sin(3\psi_0) \right).$$

Then, similarly, $(s_d^2 + c_d^2)(m_1 a_1 c_d - m_2 B) = 0$ and thus

$$(7.9.15) \quad a_1 c_d = \frac{m_2 B}{m_1}$$

as in (7.7.12).

Remark This is precisely the same form as in the nonresonance case. However, note that b_0 and hence m_2 is determined by a different equation than in the nonresonance case, so that we may expect numerical differences.

Case II: $a_0 = 0$

In this case, B_0 is at a *limit cycle* rather than a steady-state, and this changes

the analysis. At the limit cycle, we have

$$b_0 = C_{Y_0}$$

$$\psi_0 = -\omega_0 \sigma_1 \tau_1 + \psi_0(\tau_2, \tau_3, \tau_4)$$

thus the anti-secularity equation for the first $O(\mu^3)$ equation is

$$\begin{aligned} -2i \frac{\partial A_2}{\partial \tau_1} + 2\sigma_1 A_2 + is \frac{\gamma \omega_0^3 C_{Y_0}^3}{8(\omega_0^2 - 1)} \cdot e^{i((3\omega_{1/3} - 3\omega_0 \sigma_1)\tau_1 + 3\psi_0)} \\ + e^{-i\sigma_1 \tau_1} \left(2(\sigma_2 - \sigma_1^2 - s \frac{B}{2(\omega_0^2 - 1)}) A_1 - 2i \frac{\partial A_1}{\partial \tau_2} + 2if'(0) A_1 \right) = 0 \end{aligned}$$

Note (and this is crucial) that the τ_1 frequency of the $s\gamma$ term is not equal to $-\sigma_1 = 3\omega_{1/3}$ unless $\omega_{1/3} = 0$. In fact we will see that if $\omega_{1/3} = O(\mu)$ then we are in a different subcase.

Case IIa: $\omega_{1/3} \neq O(\mu)$

We must, as before, have the coefficient of $e^{-i\sigma_1 \tau_1} = 0$. This gives

$$\frac{\partial A_1}{\partial \tau_2} = f'(0) A_1$$

which implies

$$A_1 = K(\tau_2, \tau_3, \tau_4) e^{f'(0)\tau_1}$$

which for any fixed values of τ_2 , τ_3 , and τ_4 tends to zero exponentially if and only if the zero root is stable (recall the zero root is stable precisely when $f'(0) < 0$). The

other equation, for A_2 , is linear and easy to solve. Putting $m_5 = \frac{1}{2}m_e^{i(3\psi_0(\tau_2)+9\omega_{1/3}^2\tau_2)}$ we get

$$A_2 = A_2^*(\tau_2, \tau_3, \tau_4)e^{-i\sigma_1\tau_1} + i\frac{m_5}{\sigma_1}e^{-i2\sigma_1\tau_1}$$

which is $O(1)$ unless $\sigma_1 = O(\mu)$ which occurs precisely when $\omega_{1/3} = O(\mu)$. Thus we see that the superharmonic resonance has a special effect in a nearer neighborhood of $\omega_0 = 1/3$.

Case IIb: $\omega_0 = 1/3 + \mu^2\omega_{1/3}$

Notice the change in the meaning of the symbol $\omega_{1/3}$. This should not cause confusion, as this usage will be confined to this section. Notice also that here $\sigma_1 = 0$, and so $\psi_0 = \psi_0(\tau_2, \tau_3, \tau_4)$, but as before $b_0 = C_{Y_0}$. In this case the anti-secularity equation for the first $O(\mu^3)$ equation is

$$2i\frac{\partial A_2}{\partial \tau_1} = -2i\frac{\partial A_1}{\partial \tau_2} + 2if'(0)A_1 - s\frac{\gamma\nu^3}{(\omega_0^2 - 1)}e^{i3\omega_{1/3}\tau_2}.$$

Thus to avoid secularity we must have $\frac{\partial A_2}{\partial \tau_1} \equiv 0$ and to solve the remaining equation we must know the dependence of ψ_0 on τ_2 . The second $O(\mu^2)$ equation, in this special case, is very simple:

$$\begin{aligned} & -2i\omega_0\frac{\partial B_0}{\partial \tau_2} + 2(\sigma_2 + s\frac{B}{2(\omega_0^2 - 1)})\omega_0^2 B_0 \\ & + \left(-wi\omega_0\frac{\partial B_1}{\partial \tau_1} + i\omega_0[g - 6\gamma\nu\bar{\nu}]B_1 \right. \end{aligned}$$

$$\left. - 3i\gamma\omega_0^3 B_0^2 \bar{B}_1 - is\omega_0 \frac{B}{(\omega_0^2 - 1)} B_0 \right) = 0$$

and as usual we set the brackets to zero separately, and this gives

$$\frac{\partial B_0}{\partial \tau_2} - is \frac{B}{(\omega_0^2 - 1)} \omega_0 B_0 = 0$$

so $\psi_0(\tau_2, \tau_3, \tau_4) = 2\sigma_2\omega_0\tau_2 + \psi_0(\tau_3, \tau_4)$. This means that

$$A_1 = A_1^* e^{f'(0)\tau_1} + m_6 e^{i(3\omega_{1/3}\tau_2 + 3\psi_0(\tau_2, \dots))}$$

where

$$m_6 = -is \frac{\gamma\omega_0^3 C_{Y_0}^3}{16(\omega_0^2 - 1)[-f'(0) + i(3\omega_{1/3} + 6\sigma_2\omega_0)]}$$

and we need only calculate the magnitude of this to find the amplitude. Note that the A_1^* term is immaterial, as it decays exponentially to zero.

Conclusion This completes the solution of the model equations to $O(\mu)$ in Y and $O(1)$ for C_v .

7.10 Results of the Method Of Multiple Scales

What follows are some graphs of the solutions to $O(\mu)$ of the model equations.

We give the root mean square amplitudes as a means of comparing with the data from [1]. In each graph, the amplitudes are those of the solutions to $O(\mu)$, so

$Y_0 + \mu Y_1$ and $C_0 + \mu C_1$ are each represented. The parameters used are those fixed by experiment, with reasonable values for the parameters outside the resonance region.

We have 9 graphs of the results of the multiple-scales solution. Figures 7.10.1 through 7.10.6 compare the data from the low turbulence, medium turbulence, and high turbulence level experiments of [1], alternating amplitude of oscillation in the odd figures with the amplitude of the wake oscillator in the even figures. Figure 7.10.7 is an *ad hoc* parameter fit showing the ability of the model to exhibit significant subharmonic resonance. Figures 7.10.8 and 7.10.9 show the predictions of this method of solution for the case of larger n occurring in the hydrodynamic case, cf [5].

We examine first Figures 7.10.1 to 7.10.6, the aerodynamic case. We see that the agreement is reasonable, even in the low-damping, low-turbulence case, presented in Figures 7.10.1 and 7.10.2, where the interaction of the galloping and the vortex-induced oscillation is the greatest. The model correctly predicts the onset of the nonzero amplitude of oscillation in all cases, and correctly predicts the growth of the amplitude of oscillation. A noticeable feature is the ‘overshoot’ occurring near the end of the resonance region. As the $O(\mu)$ solution in the resonance region does not depend on the quasi-steady parameters A_k or the damping β , this solution is the same for all cases with the same turbulence level. When we look at the $O(\mu^2)$

solution, hoping for more accuracy, we see that the solution begins to oscillate near $\omega_0 = 1.04$ (cf Figure 7.5.1), while the $O(\mu)$ solution appears to behave in the manner expected; that is, to grow large and meet the nonresonance solution which is becoming small at this point. This is a graphic demonstration of the power of this asymptotic method, as the one term solution can not be expected to be accurate, but turns out to be so anyway. When the two solutions, the $O(\mu)$ and the $O(\mu^2)$, agree reasonably, we can be sure that the error made by the $O(\mu)$ solution is less than the difference between the two. However, when the difference is large, as it is in the resonance region just after $\omega_0 = 1.04$, this error estimate does not help. In fact, we can reasonably expect more accuracy than is indicated, so it is likely that the $O(\mu)$ solution is as accurate as it needs to be. The fact that the two regions match up reasonably well in spite of the fact that the error is predicted to be large gives confidence in the solution at this point. Notice also a kink in the $O(\mu)$ solution at the left end of the nonresonance range, particularly in the higher-turbulence figures in Figure 7.10.3 and 7.10.5. This, too, is spurious, and is caused by the asymptotic solution trying to match the behaviour in a different range. In this case, however, it is the $O(\mu)$ solution indicating that the error made by the $O(1)$ solution may be becoming large. However, for this aerodynamic case, we see by comparison with Figure 5.3.1, the solution by the method of Van der Pol, that the errors made are in fact quite small.

In Figure 7.10.2 we see the predicted RMS excitation compared with the data taken from [1]. The agreement is reasonable, reflecting the general trend of the data, and indicating a peak near the resonance region. However, the low damping data shows a clear decreasing trend, which is not reflected in the predicted solution. This is caused by choosing C_{Y_0} as a constant from the fixed-cylinder experiments. It is interesting to note that a clear decreasing trend was observed in some cases in experiments by the authors of [1] prior to those reported in [1], but the amount of the decrease was not considered significant. In Figures 7.10.4 and 7.10.6 the accuracy is noticeably better, in spite of the fact that the corresponding solutions for the medium and high damping cases in Figures 7.10.3 and 7.10.5 are worse fits than in Figure 7.10.1. This is not surprising, because for the higher-damping cases the wake vortex system is not as important for the amplitude of oscillation as the shear-layer instability. The poor fit of the higher-damping amplitudes of oscillation is probably due to the poor fit of the cubic polynomial used to approximate the lift coefficient data. This observation is borne out by noticing that the low damping cases are well predicted for all turbulence levels, due to the better fit of the polynomial to the data.

For the functional form of the parameters used in Figures 7.10.1—7.10.6, that is, $a(\omega_0) = \alpha\omega_0$, $D(\omega_0) = D/\omega_0$, and $B(\omega_0) = B/\omega_0^2$, we get good overall quantitative agreement, but the kink associated with the subharmonic resonance is not present.

If instead we choose $a(\omega_0) = 0.50\omega_0^2$, $B(\omega_0) = -5.29 + 2.94\omega_0^2$, then in the low damping low turbulence case, we get a kink near $\omega_0 = 3$ that is very much like the one observed (Figure 7.10.7). This parameter fitting is rather *ad hoc*, but does not conflict with any of the parameter fixing done earlier, as the parameter fitting is done in the resonance region. As ω_0 gets larger, though, we expect more unrealistic behaviour, as the parameter $a(\omega_0)$ can no longer be considered small.

A more serious problem with the model in general is the location of the subharmonic resonance, observed physically in [1] to be near $\omega_0 = 2.5$, significantly different than the $\omega_0 = 3$ predicted here. This prediction is inherent in the model equations, and is not an artifact of the method of solution. One possible physical correction to this would be to have the Strouhal number shift to account for the change, so that $\omega_0 = 3 = U/U_r = 2\pi SU$ would occur in the correct wind speed region. This would require a 20% change in the Strouhal number, however, and this seems unrealistic.

Figures 7.10.8 and 7.10.9 show the effects of larger n . As our solution is in the form of an asymptotic series in powers of the square root of n , the accuracy of our results is expected to be better as $n \rightarrow 0$, and thus we expect poorer solutions for larger n . The solutions presented here are however not too bad, outside of the large spikes in the resonance region. Comparison with the numerical solution of Bouclin [5] shows quite good agreement, after the resonance region. Bouclin's results for this

set of parameters is contained in his Figure 23. Some data taken from that figure, corrected for RMS values, are plotted on Figure 7.10.8. The largest difference, of course, occurs in the resonance region. Before the resonance region, however, the difference is low in an absolute sense, but high in a relative sense, being about 50%. After the resonance region, at $\omega_0 = 1.2$, the relative difference is only 8%, while at the extreme end of the range of Bouclin's figure, $\omega_0 = 1.3$, the relative difference is down to 4%. This suggests that the multiple scales solution will become still more accurate as we move away from the resonance region.

Figure 7.10.9 shows the amplitude of excitation for the same parameters as Figure 7.10.8. Unfortunately Bouclin did not provide a numerical solution for the excitation, so we cannot compare. However, on comparing it to Figure 7.10.8 itself, we see that the amplitude of excitation is predicted to be large even after $\omega_0 = 1.2$, where the difference between Bouclin's numerical solution and the solution by the method of multiple scales is less than 8%. This gives us some confidence that the amplitude of excitation is also correctly predicted in this region. However, it is obvious that the numerical solution of the model equations is feasible for this n , which is about 20 times larger than the n used in the aerodynamic case. Thus, though the method of multiple scales gives acceptable answers even in this case, at much less computing cost, the accuracy of the numerical method makes it possibly more preferable in this case, and probably more so for still larger n . However, for

smaller n the computing cost of the numerical solution increases, while the accuracy of the solution by the method of multiple scales increases with the cost of solution remaining the same. Thus it is clear that there is *some* value of n above which it is better to use the numerical method, and below which it is preferable to use the asymptotic method. The precise determination of this value of n is of course impossible in this general context, depending as it does on the changing value of computing time versus the need for accuracy. However, with that *caveat* in mind, it is the belief of the author that the numerical method is preferable only when $n = O(0.1)$ or larger, and that for smaller n the method of multiple scales will provide cheaper results with adequate accuracy.

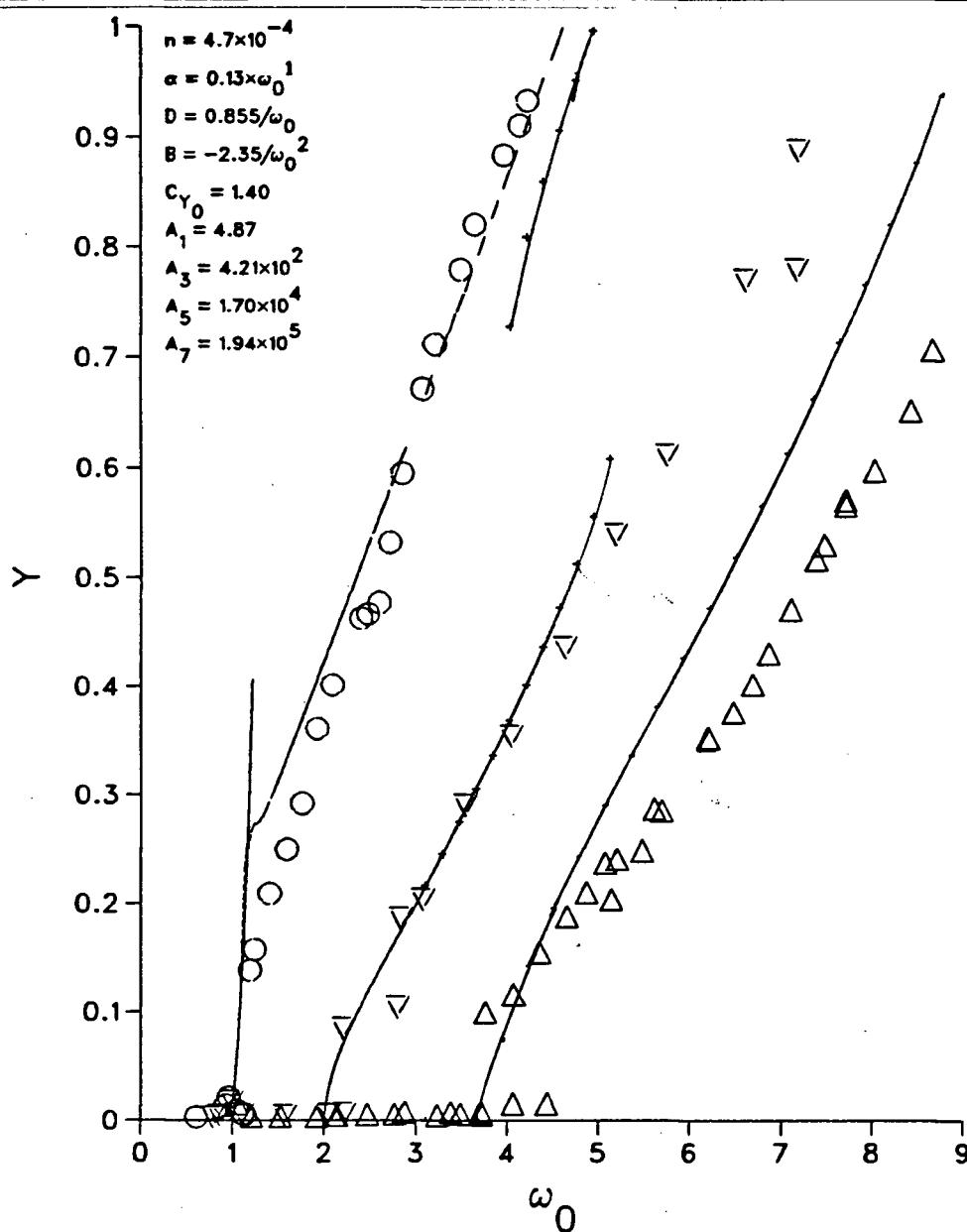
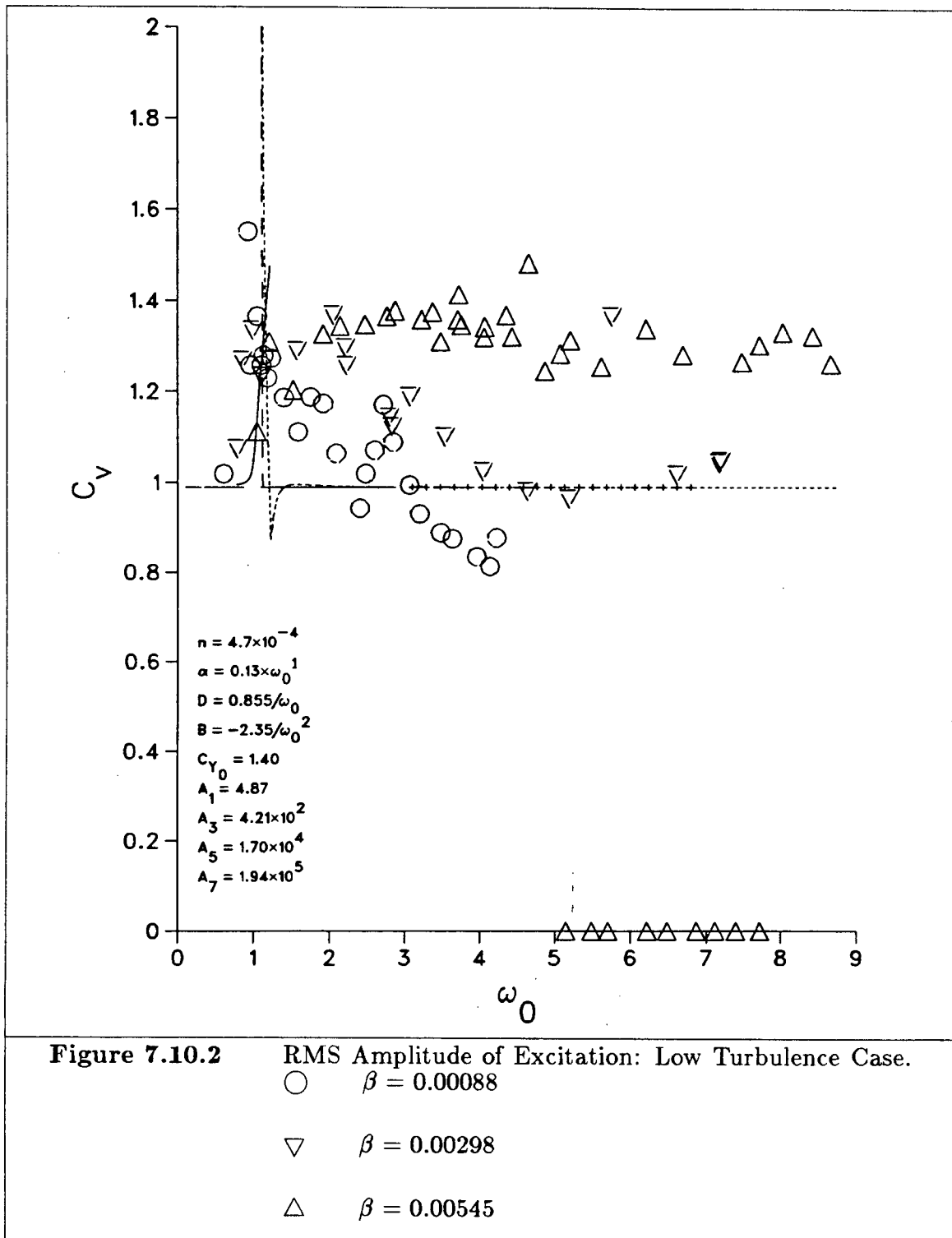


Figure 7.10.1 RMS Amplitude of Oscillation: Low Turbulence Case.

○ $\beta = 0.00088$

▽ $\beta = 0.00298$

△ $\beta = 0.00545$



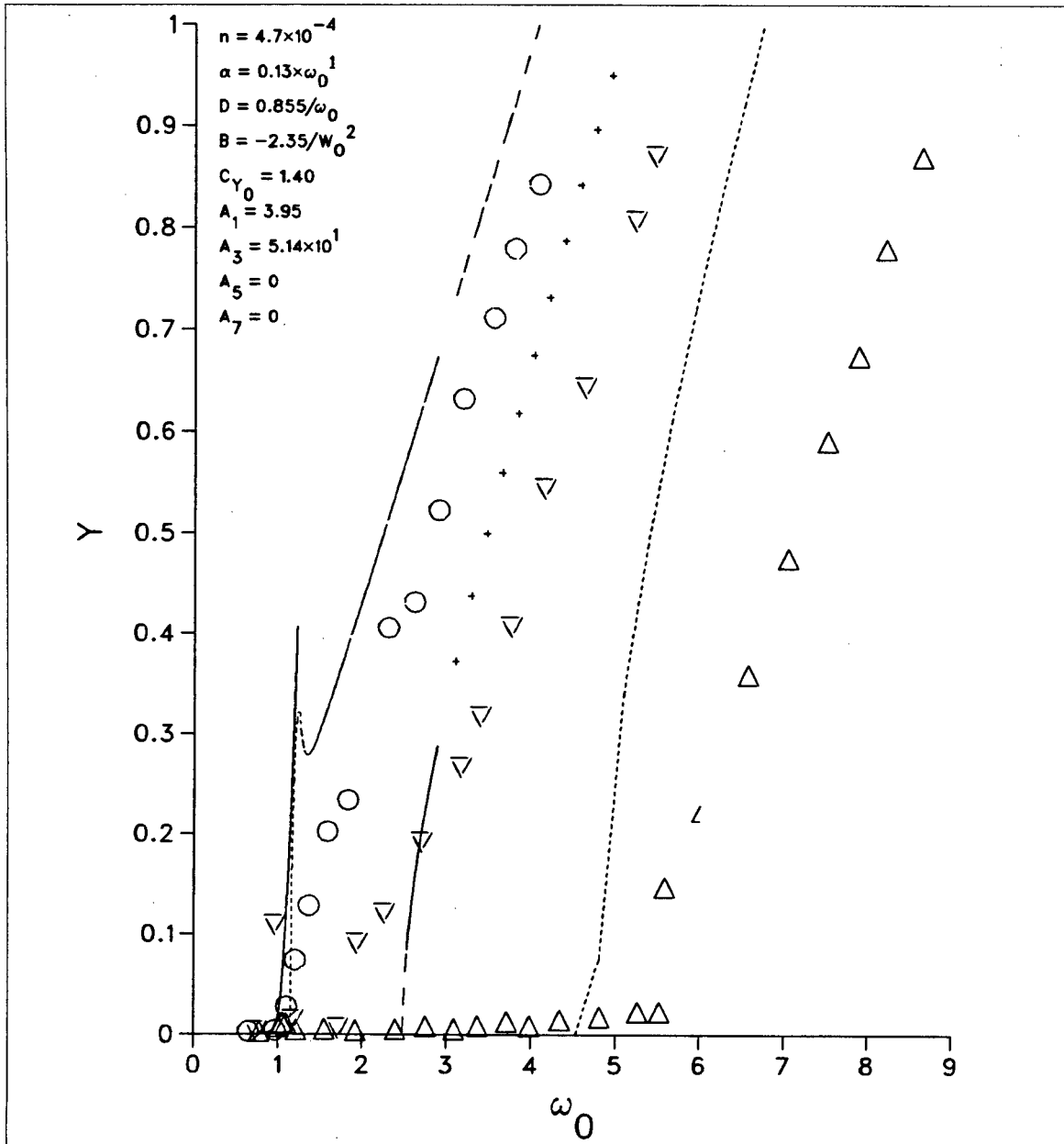
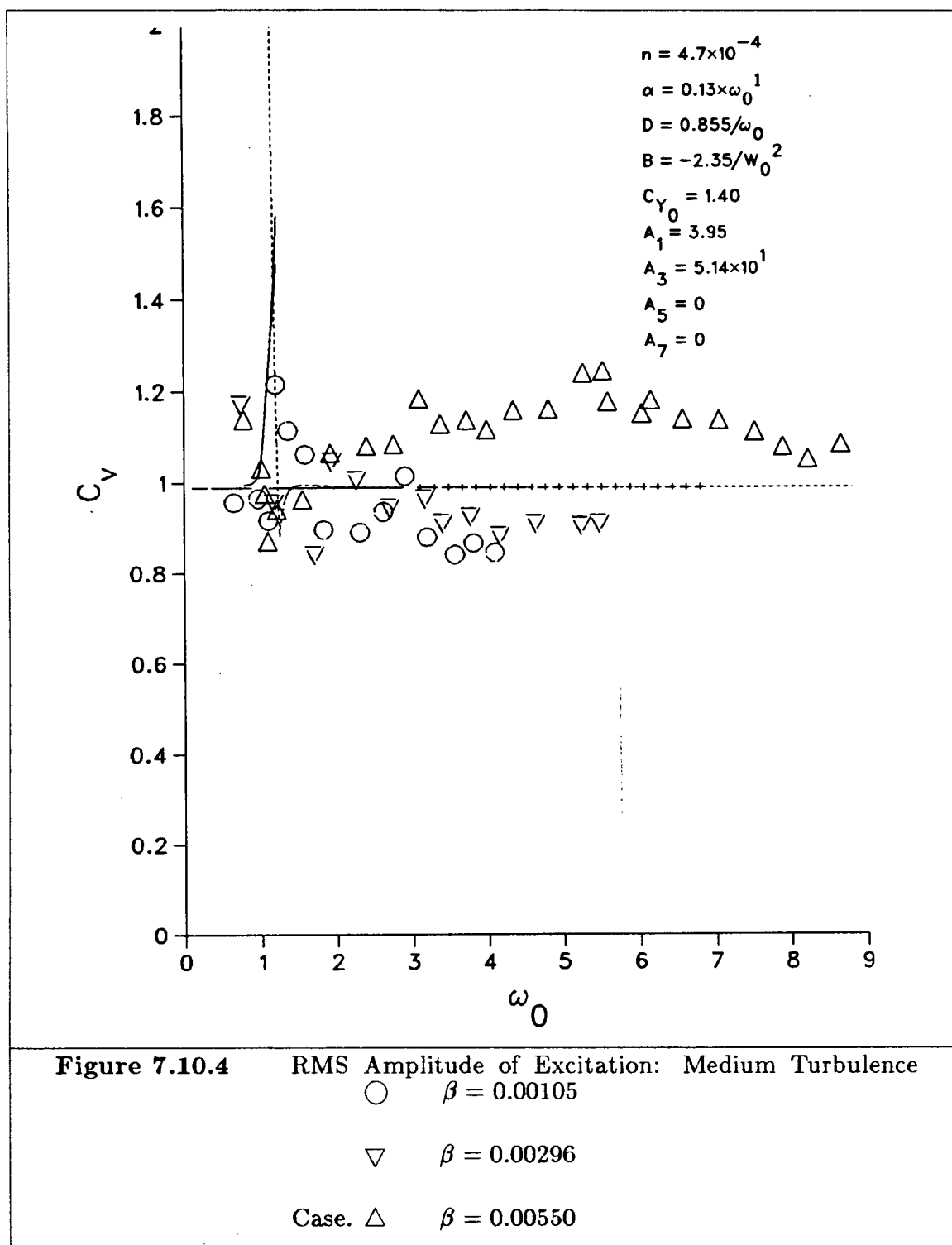


Figure 7.10.3 RMS Amplitude of Oscillation: Medium Turbulence

○ $\beta = 0.00105$

▽ $\beta = 0.00296$

△ $\beta = 0.00550$



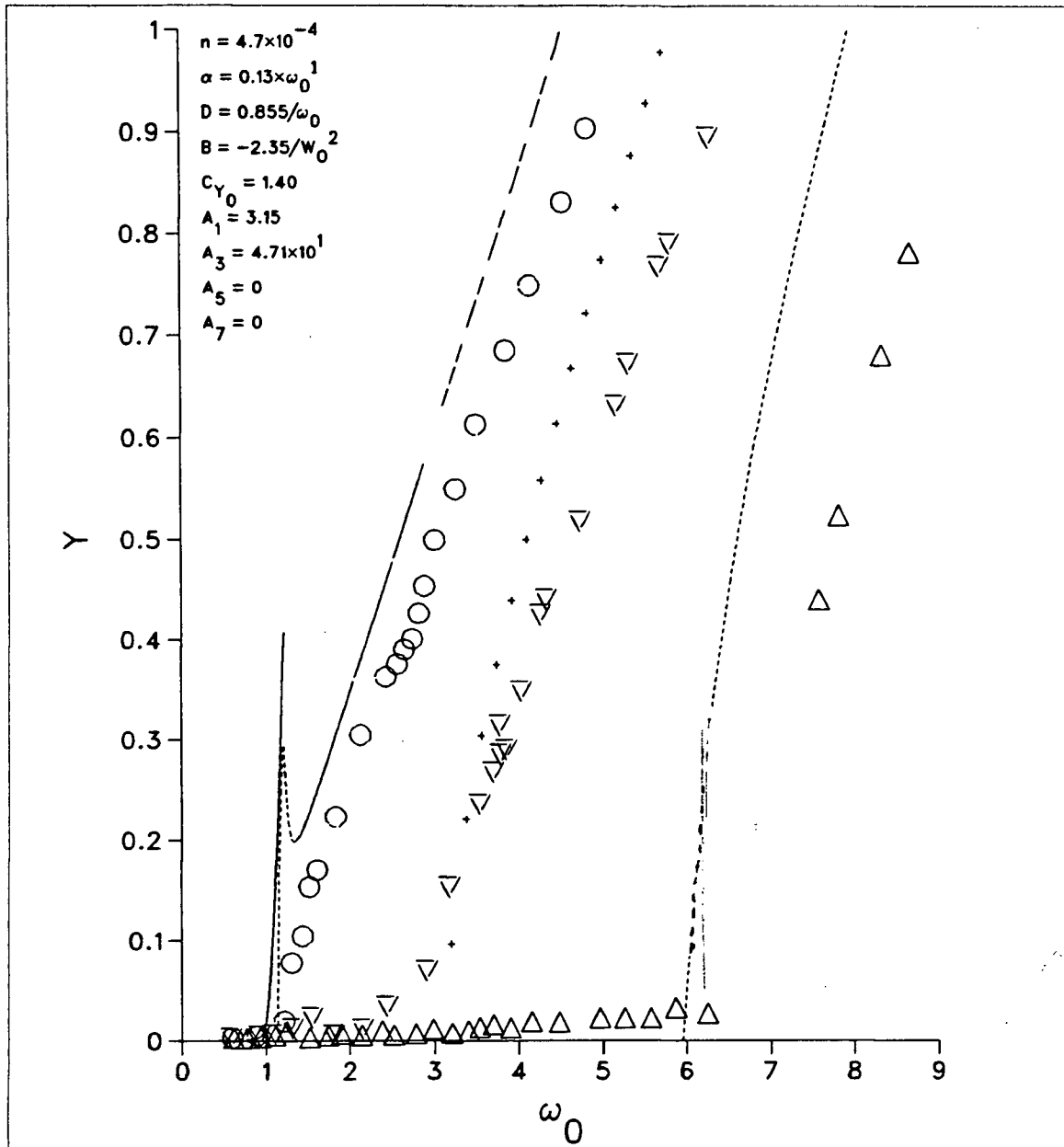


Figure 7.10.5 RMS Amplitude of Oscillation: High Turbulence Case.

○ $\beta = 0.00117$

▽ $\beta = 0.00295$

△ $\beta = 0.00550$

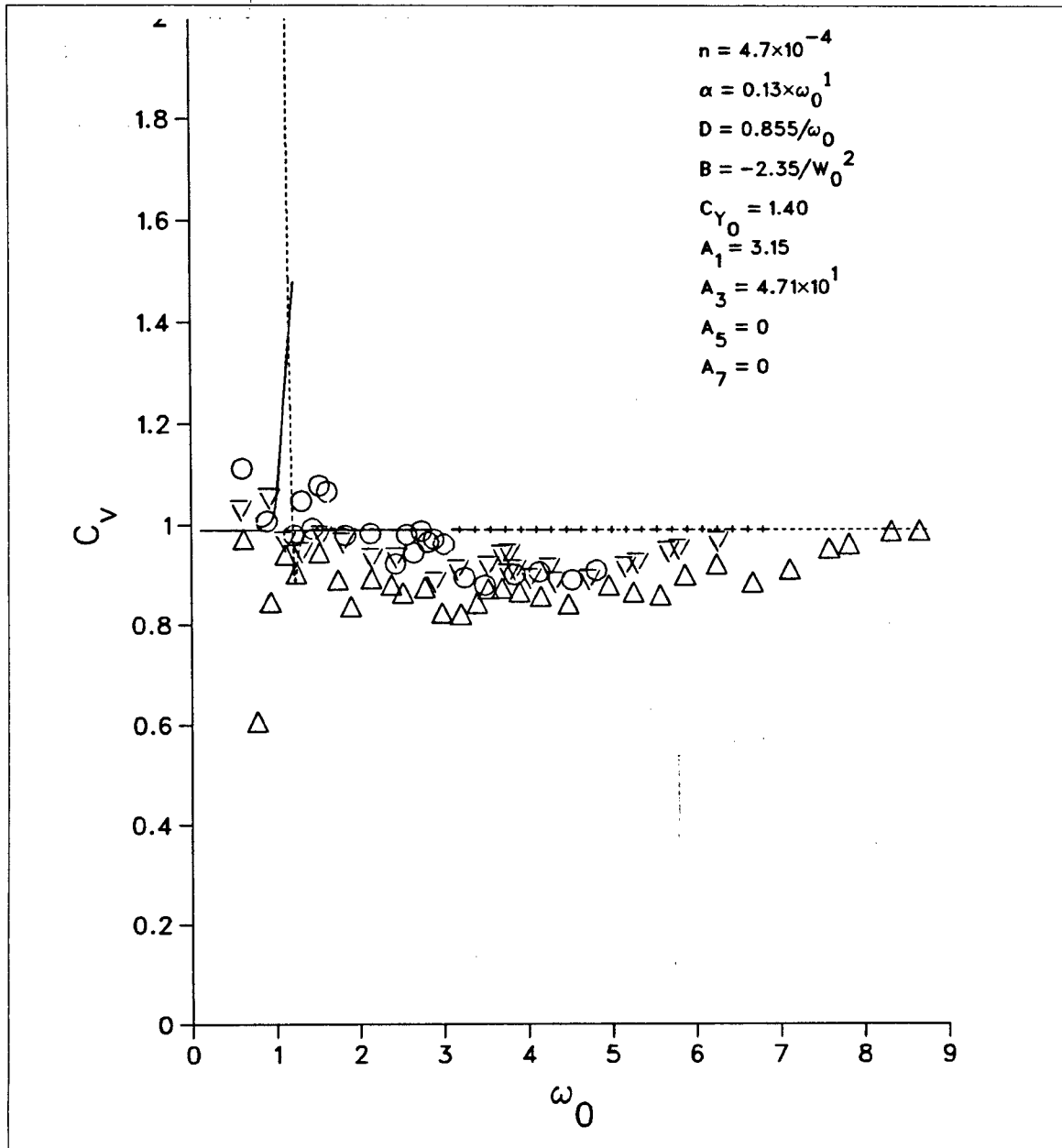
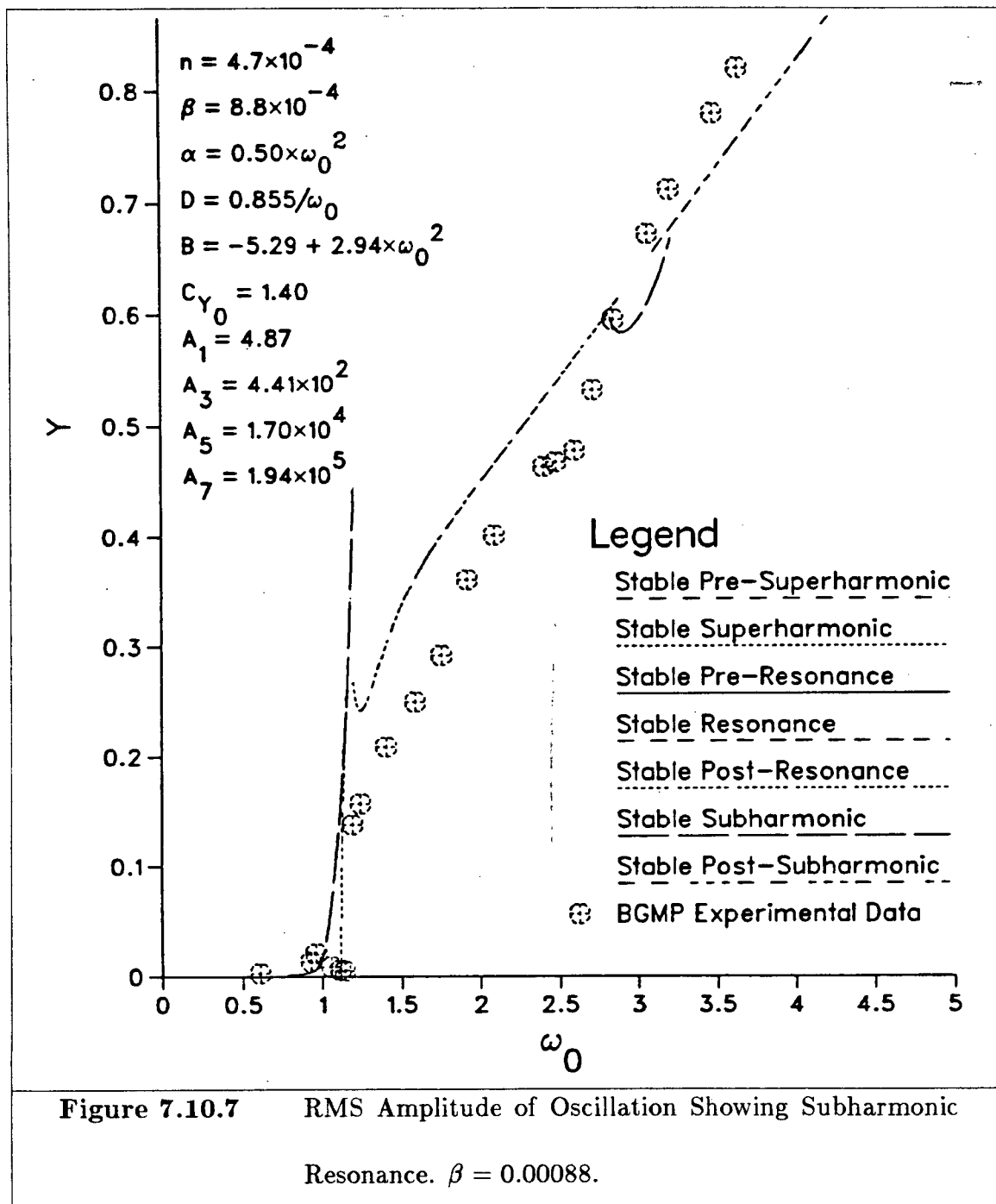


Figure 7.10.6 RMS Amplitude of Excitation: High Turbulence Case.

○ $\beta = 0.00117$

▽ $\beta = 0.00295$

△ $\beta = 0.00550$



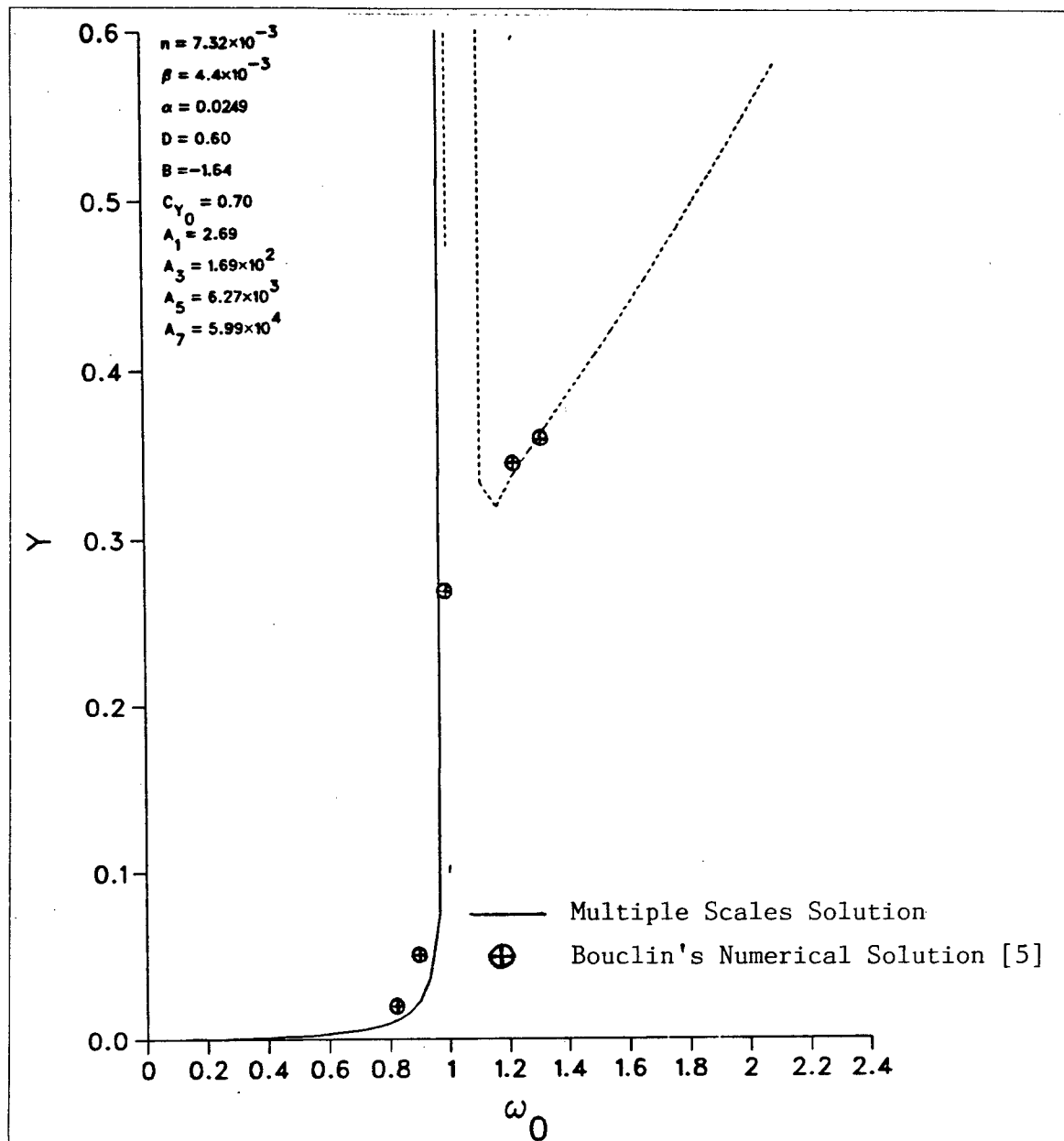
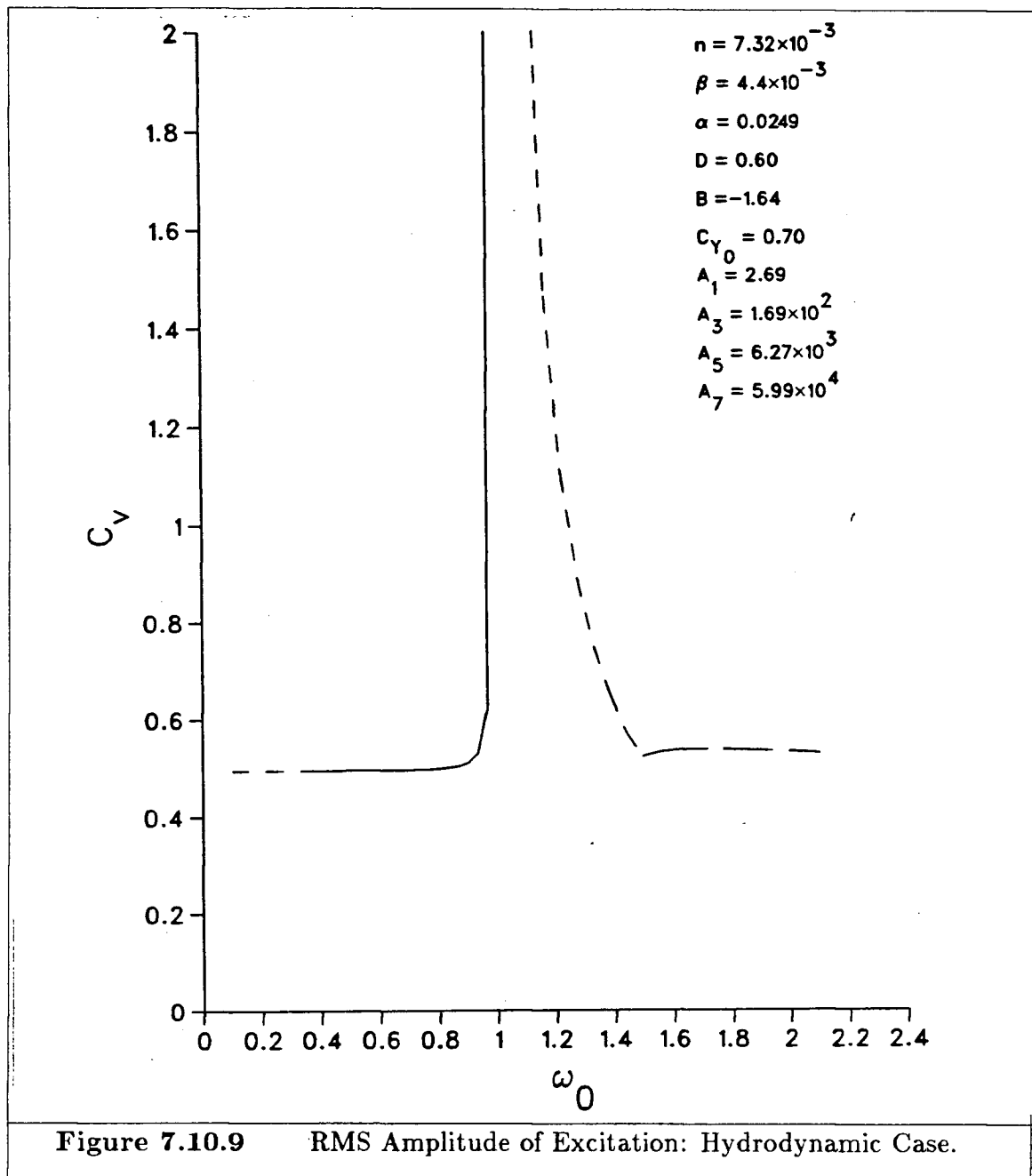


Figure 7.10.8 RMS Amplitude of Oscillation: Hydrodynamic Case.



Chapter 8

Comparison of Solutions With Each Other and With Experiment

*Not meaning to strike, but first—having
summoned us together here, in this outest
corner of the realm—to choose out, snap
in two, throw on the midden, any blades
of meaner mettle.
—E. R. Eddison*

8.1 Concordiat of Solutions

We wish to compare and contrast the results of the various methods of solution, to decide which (if any) is the best for our purposes. This will serve the purpose of error-checking as well as providing some useful details of the solutions. One of the most useful features of the solutions is the prediction of the wind speeds at which non-zero amplitudes of oscillation are initiated, henceforth denoted by U_i or $\omega_i = U_i/U_r$. We compare the results of the three methods; (I) The method of Van Der Pol, (II) Hopf Bifurcation Theory, and (III) the Method of Multiple Scales. For (I), the equations determining \bar{Y} , \bar{C}_v , and Ω , (5.1.5)—(5.1.7) are satisfied identically

when $\bar{Y} = 0$. We must instead look at the limiting case when $\bar{Y}/\bar{C}_v \rightarrow 0$. After doing the analysis, we arrive at the following polynomial equation $P_I(\omega_0)$ in the wind speed ω_0 , in the case $a(\omega_0) = \alpha\omega_0$, B and D are constant, and where $W_0 = U_0/U_r$ is the onset velocity predicted by the quasi-steady theory:

$$(8.1.1) \quad \begin{aligned} P_I(\omega_0) = & \omega_0^5 - W_0\omega_0^4 - (2 - D\eta - \alpha^2)\omega_0^3 \\ & - W_0(\alpha^2 - 2)\omega_0^2 + (1 - D\eta - \alpha B\eta)\omega_0 - W_0 = 0 \end{aligned}$$

where $\eta = U_r/\mathcal{A}_1$. The roots of this quintic equation in ω_0 are easy to find numerically, but we can investigate them analytically in the case α is small.

First, however, we look at the determining equations from the other regions.

From the Bifurcation theory, we get the location of the Hopf Bifurcation Points directly:

$$(8.1.2) \quad P_{II} = P_B(\omega_0) = \sum_{i=0}^5 c_i \omega_0^i$$

where the c_i are given in section 6.8. Closer inspection of these coefficients reveals that

$$P_{II}(\omega_0) = \alpha P_I(\omega_0) + O(n)$$

so we see that the roots of the first will, if n is small enough, be close to the roots of the second. This shows that the initiation points predicted by the method of Van Der Pol are within $O(n)$ (except of course for multiple roots, or near-multiple roots)

of those predicted by the simpler bifurcation theory, which is interesting, as the bifurcations are those from the zero steady-state, and the Van Der Pol predictions include those from the non-zero time-dependent solution with $\overline{C}_v \neq 0$. I believe that this is a result of some interaction between the two, but it is certainly not predicted by the bifurcation theory, and must be here regarded as a coincidence.

Lastly, we look at the results of the Method of Multiple Scales. We must look at two different regions here, the resonance region and the nonresonance region (considering the first order analysis only). In the resonance region, $a_0 \equiv 0$ always, so we must look at when the next order term is zero. Now, $a_1 = 0$ if and only if

$$1 + \frac{D \cos \xi}{g(b_0/a_1)} = 0$$

which occurs only if $D \cos \xi < 0$, and thus only on the $\xi = \pi$ branch of the solution. In the cases that have been presented, in Figure 7.5.1 and later figures in Chapter 7, this branch has always been the unstable branch. It is not known if there are parameter values for which this branch is stable. This equation is independent of the damping β and the quasi-steady coefficients A_k , and so any initiation points arising from this equation will be constant for all values of $W_0 = U_0/U_r$. The above equation gives

$$\omega_1 = \frac{Bg}{2D} + \frac{DU^2}{2g}$$

or

$$(8.1.3) \quad \omega_0 = 1 + \frac{B\alpha}{2D} + \frac{nDU^2}{2\alpha} + O(\mu^2)$$

In the nonresonance case, $a_0 = 0$ if and only if

$$P_{III} \equiv (\omega_0^2 - 1)(\omega_0 - W_0) + \omega_0^2 \left(\frac{U_r D}{\mathcal{A}_1} \right) = 0$$

This is a cubic equation in ω_0 , unlike $P_{II}(\omega_0)$ and $P_I(\omega_0)$, which are quintic. However, we solve the polynomial for the root near 1 in the case $\alpha \ll 1$, and we see that the roots of all three are very similar. Expanding the root near 1 of $P_{II}(\omega_0)$, we have

$$(8.1.4) \quad \omega_0 = 1 + \frac{B\alpha}{2D} + \alpha^2 \left\{ \frac{-1}{2D\eta} \left[\frac{B^2}{8D^2} (8(1 - W_0) + 6D\eta) - \frac{B^2\eta}{2D} + 1 - W_0 \right] \right\} \\ + O(\alpha^3) + O(n)$$

and of course the root near 1 of $P_I(\omega_0)$ has the same expansion to this order. We compare this to the result from the method of multiple scales. Equation (8.1.4), in the case $n = 5 \times 10^{-4}$, $B = -2.35$, $D = 0.855$, $\mathcal{A}_1 = 4.87$, and $U_0 = 0.75$, gives

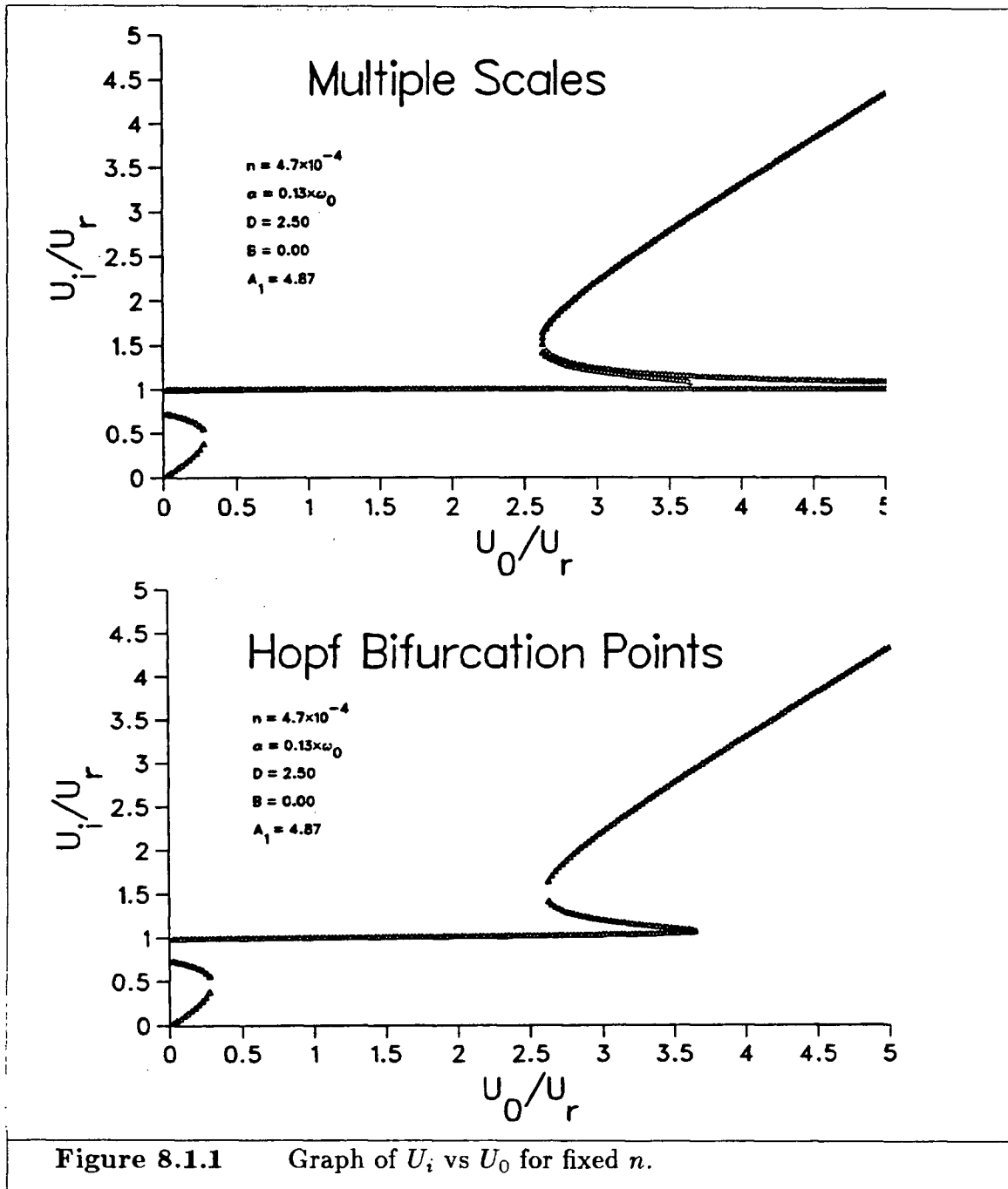
$$\omega_0 = 1 - 1.374\alpha - 8.637\alpha^2 + O(\alpha^3) + O(n)$$

and (8.1.3) gives

$$\omega_0 = 1 - 1.374\alpha + \frac{2.138 \times 10^{-4}}{\alpha} + O(n)$$

which, for $\alpha = 0.13$, is a difference of -0.146 , which is significant. If we choose $\alpha = O(\sqrt{n})$ as $n \rightarrow 0$, then equation (8.1.3) and equation (8.1.4) are not asymptotic to each other; they have a common limit, 1, as $n \rightarrow 0$, and a common dependence on α , but the detailed behaviour is different.

In Figure 8.1.1, we compare the location of the initiation points for the method of multiple scales with the location of the Hopf Bifurcation points (cf Figures 6.9.1 and 6.9.2). We see general agreement, but the initiation points predicted by the method of multiple scales seem more realistic, as they predict initiation of non-zero amplitude in the resonance region for all values of W_0 , while after $W_0 = 3.6$ the Hopf Bifurcation Points disappear. This is because of the more general nature of the initiation points calculated by the method of multiple scales. Both methods do predict the occurrence of an initiation point near $\omega_0 = W_0$ for $W_0 > 2.5$, which is in accord with experimental observations.



8.2 Behaviour in the Quasi-Steady Limit

Next, we look at the roots of the polynomials $P_I(\omega_0)$ and $P_{III}(\omega_0)$ as $U_0 \rightarrow \infty$.

In this case we assume $D(\omega_0) = D/\omega_0$, so we get from $P_I(\omega_0)$

$$\omega_0 = W_0 - \frac{D\eta}{W_0} - \frac{D\eta(D\eta + 1) - \alpha\eta(B + \alpha D)}{W_0^3} + O(W_0^{-5})$$

while from $P_{III}(\omega_0)$ we get

$$\omega_0 = W_0 - \frac{D\eta}{W_0} - \frac{D\eta(D\eta + 1)}{W_0^3} + O(W_0^{-5}) \text{ as } W_0 \rightarrow \infty$$

Of course, the quasi-steady theory predicts an initiation point of $\omega_0 = W_0 = U_0/U_r$ always, so it is good to see that this model agrees with the quasi-steady theory in the limit. It is interesting to note that if $D(\omega_0)$ is taken to be constant instead of depending inversely on ω_0 , the asymptotic results above come out as

$$\omega_0 = W_0 - D\eta + O(1/W_0) \text{ as } W_0 \rightarrow \infty$$

which is still in agreement with the quasi-steady theory, but the error is much larger, and in fact would be noticeable at moderate values of U_0 . Instead we note that for $U_0/U_r > 2$ approximately that we have good results from the quasi-steady theory. This supports the functional form D/ω_0 for $D(\omega_0)$.

8.3 Comparison of Predictions

In this section we discuss the varying predictions of the different methods of solution of the model equations, as presented in Figure 5.3.1, Figures 6.9.3—6.9.5,

and Figure 7.10.1. Each of these Figures uses the same parameter values, and should give similar results. It is easily seen that the solution by the method of Van Der Pol contains the stable solutions found by the method of multiple scales, by comparing Figure 5.3.1 with Figure 7.10.1. The agreement of the two methods is exact, as it should be, *even at the end of the resonance region*, where we expected trouble with the method of multiple scales. The extraneous branches present in Figure 5.3.1, commented on previously, are seen by comparison to the stable solutions in Figure 7.10.1 to be unstable. However, the bifurcation solutions presented in Figures 6.9.3—6.9.5 do not agree with the stable solution by multiple scales, at least for the low damping case. For the medium and high damping cases, the agreement is quite good between the methods, as far as the bifurcation solution goes. It is interesting to note that the solution by the method of Van Der Pol agrees with the bifurcation solution even in the low damping case, as the bifurcation solution shows an unstable solution arising before the resonance region, which matches exactly the initiation present in the solution by the method of Van Der Pol. The unstable branch of the solution by multiple scales is not presented here, but it has the same qualitative behaviour without matching the initiation point precisely. In fact, the difference between the initiation points predicted is -0.146 , as calculated in the previous section.

To sum up, the methods presented all have their strong points. The method of

Van Der Pol is simple and accurate whenever the solution is in fact of the assumed form; the bifurcation method is guaranteed accurate in the neighborhood of the Hopf bifurcation points; and the method of multiple scales gives an automatic stability and error analysis, gives the form of the solution as well as the numerical coefficients, and is efficiently programmed on a computer. On the disadvantage side, the method of Van Der Pol does not provide an automatic stability analysis. A stability analysis can be done, but amounts to solving a *non-autonomous* linear system of differential equations, which in general is harder than using the method of multiple scales on the original problem. Also, in the case where the assumed form of the solution is inappropriate, the method of Van Der Pol is inaccurate; further, no error estimate is available.

The bifurcation method is a local method only, and for our model predicts only unstable solutions. An error estimate is available, but is useful only near the Hopf bifurcation point, and near the zero solution.

The method of multiple scales appears to be the method of choice. It is perhaps less accurate than the method of Van Der Pol for this problem in the resonance region, because in that region the form for the solution is simple and well defined, which means that the assumptions of the method are satisfied. However, comparison with the solution by the method of Van Der Pol show that the multiple scales solution, even in the resonance region, is of adequate accuracy. Also, multiple

scales seems to be the only method to detect a subharmonic resonance. The extra complication of the solution is made up for by the wealth of information about the solution that is readily available.

Chapter 9

Conclusions

But even next morning, I woke to a discomfortable and teasing certainty that there was much forgot...

—E. R. Eddison

9.1 Conclusions

After examining the results of the various methods of solution of the model equations we arrive at the following conclusions:

1. The solutions of the model equations realistically model the combined effects of galloping and vortex-induced vibration. The solution behaves correctly in the limit as $U_0 \gg U_r$, collapsing onto the quasi-steady solution, plus a Hartlen-Currie type solution in the resonance region. In the case $U_0 \approx U_r$, the solutions match the experimental data reasonably well. In the case $U_0 < U_r$, the solution correctly exhibits a stable zero solution for $U < U_r$, and then becomes large when $U \sim U_r$. The solution exhibits a noticeable subharmonic resonance for

some values of the parameters, which seems to correspond with that observed experimentally in [1].

2. The approximate analytical solution provided by the Method of Multiple scales gives a useful solution already at the $O(1)$ level, although the $O(\mu)$ terms are necessary for the resonance region and the subharmonic resonance region. The method successfully determines the stability of the model solution in a simple fashion. To $O(\mu) = O(\sqrt{n}) = O(\alpha)$, the approximate solution predicts a superharmonic resonance near $\omega_0 = 1/3$ and a subharmonic resonance at $\omega_0 = 3$.
3. The solution by the method of Van Der Pol is less useful than the solution by the method of multiple scales, because although somewhat simpler, it does not provide enough information to be valid over a large enough range, and provides neither a stability analysis nor an error estimate.
4. The solution by the Hopf Bifurcation theory, while providing a useful ‘quick and dirty’ solution of the model equations does not provide enough information, as it predicts only unstable solutions, and these valid only in a limited range. Further, they agree with the data only by coincidence. To be useful, one would have to look at the bifurcation of solutions from the non-steady solution given by $C_v = \bar{C}_v \cos(\Omega t)$, $Y = O(n)$.
5. The functional form of the free parameters needs to be determined more completely by physical considerations for this method to be a true semi-empirical

approach, rather than fully empirical.

6. The amplitude of the solution outside the resonance region, to $O(1)$, is determined by the quasi-steady coefficients \mathcal{A}_k and the coupling coefficient D . The coupling coefficient B makes a difference in the phase difference between the displacement and the excitation only, and the coefficient $a(\omega_0)$ affects only the time taken to get to a limit cycle.
7. The size of the subharmonic resonance region depends on the coefficient $a(\omega_0)$, the coefficient B , and the coefficient D , as well as the quasi-steady coefficients. Further, the effect of the subharmonic resonance is $O(\mu)$ on the amplitude of oscillation of the body, but is $O(1)$ on the amplitude of the wake excitation term.
8. For the case of aeroelasticity, the superharmonic resonance effects are very small. The subharmonic resonance region is much more important.
9. The method of multiple scales is not as applicable to the hydrodynamic case as it is to the aerodynamic case. In the hydrodynamic case, the model equations are as valid, but in the case of large enough n , the method of multiple scales becomes less accurate and the direct numerical solution of the model equations becomes more efficient. Thus we see that there is a value of n above which numerical solution techniques are more applicable to the equations in this case. The method of multiple scales is however adequately accurate for some regions

of the solution even in the hydrodynamic case, as shown by Figures 7.10.8 and 7.10.9. Note however that the value of n for which these were plotted is in the small end of the range of values occurring in the hydrodynamic case.

10. The fact that simply adding C_{F_v} and C_v gives such good results has some implications for the physical model. It was mentioned in the first chapter that the quasi-steady model depends on the position of the time-averaged shear layers. The success of this model suggests that this concept makes sense even in the presence of a significant perturbation due to the wake vortex system.

9.2 Suggestions for Further Work

For further investigation of the model equations, it seems necessary to

1. Experimentally determine the form of the free parameters $a(\omega_0)$, $B(\omega_0)$, and $D(\omega_0)$. Several forms were tried here, with some success, but these need to be put on a firmer base. Forced vibration experiments along the line of [2,16] might provide the necessary information. Particular attention should be paid to the resonance region, but the subharmonic resonance region(s) should not be neglected.
2. Investigate the predictions of this model in a three-dimensional situation, using an analysis similar to that in Sullivan [24]. Sullivan reported some interesting interactions of galloping and vortex-induced oscillation in a three-dimensional

setting, and it would be useful to see if this model was capable of explaining this.

3. The location of the subharmonic resonance region in the solution was not exactly reproduced by the experimental data. The subharmonic resonance region appeared around the region $\omega_0 = 2.5$, and not around $\omega_0 = 3$. This may be explained by a nonconstant Strouhal number, but this is unrealistic. It would be interesting to see if a more appropriate self-starting oscillator could be found, that would model this more closely. The following suggests itself:

$$\ddot{C}_v + \omega_0^2 C_v = a(\dot{C}_v - \gamma \dot{C}_v |\dot{C}_v|^{3/2}).$$

These equations are more difficult to solve, but preliminary investigations suggest that this equation would exhibit a subharmonic resonance (i.e. terms of frequency near 3) when ω_0 was near 2.5.

4. The presence of large amplitude 'spikes' in the resonance region is undesirable. It is possible that different time scales would give a better result in this region. In particular, the time scales T , τ_1 , τ_2 , and τ_3 , where as before $\tau_i = \mu^i T$, but where now $\mu^3 = n$ instead of $\mu^2 = n$. This makes for a little more work, but in the resonance region Y_0 is still 0, but with μ being larger there may be smaller problems with the transition zone.

In addition, several interesting theoretical questions were brought up in the course of

this study. It would be interesting to investigate the connection between the steady-state Hopf Bifurcation points and the nearby non-steady bifurcation points, in order to explain the observed coincidences of predicted non-zero amplitudes of oscillation with the experimentally observed oscillation. If successful, such an analysis would have the advantage of being much more general than the current analysis using the method of multiple scales, inasmuch as more general nonlinearities would be included automatically.

The use of the method of multiple scales presupposes that the actual solutions of the model equations are bounded. No proof of the boundedness of the solution in the present case was attempted, as it is irrelevant for the practical case under consideration; a simple redefinition of our model to be only the *bounded* solutions of the model equations is sufficient to justify the analysis. However, it would be intellectually satisfying to have such a proof; or, considering the large amplitudes predicted near the end of the resonance region by the method of multiple scales, a proof that under some circumstances that the solutions to the model equations were *not* bounded.

Lastly, recent interest in this type of model has been expressed for cylinders of different cross section. It might be expected that this model will be directly applicable to a 'D'-section cylinder and to cylinders of rectangular cross section, merely by adjusting the quasi-steady parameters A_k , as the quasi-steady theory has

already been worked out for these (for references see [18]). However, the effect of the geometry on the other parameters $a(\omega_0)$, B , D , *etcetera* needs to be investigated and may throw some light on the physical significance of these parameters.

Bibliography

- [1] P. W. Bearman, I. S. Gartshore, D. J. Maull, and G. V. Parkinson, "Experiments on Flow-Induced Vibration of a Square-Section Cylinder", *Journal of Fluids and Structures* **1**, (1987) pp 19–34.
- [2] P. W. Bearman and E. D. Obasaju, "An experimental study of pressure fluctuations on fixed and oscillating square-section cylinders", *J. Fluid Mech.* (1982) vol. 119, pp 297–321.
- [3] C. M. Bender and S. A. Orzag, *Advanced Mathematical Methods for Scientists and Engineers*, McGraw-Hill (1978) QA371.B43
- [4] R. D. Blevins, *Flow Induced Vibration*, Van Nostrand (1977) TA355.B52
- [5] D. N. Bouclin, *Hydroelastic Oscillations of Square Cylinders*, M.ASc. Thesis, University of British Columbia (1977).
- [6] S-N. Chow and J. K. Hale, *Methods of Bifurcation Theory*, Springer-Verlag (1982) QA372.C544.
- [7] E. R. Eddison, *The Zimiamvian Trilogy*, Ballantine Books (1968).
- [8] C. C. Feng, *The Measurement of Vortex Induced Effects in Flow Past Stationary and Oscillating Circular and D-section Cylinders*, M.ASc. Thesis, University of British Columbia (1968).
- [9] J. K. Hale, *Ordinary Differential Equations*, Wiley-Interscience, **21** (1980), QA372.H184.
- [10] R. T. Hartlen and I. G. Currie, "Lift Oscillator Model of Vortex-Induced Vibration", *J. Eng. Mech. Div. Proc. Amer. Soc. of Civ. Eng.*, Oct 1970 p 577.
- [11] A. C. Hearn (Ed.), *REDUCE User's Manual*, Rand Publication CP78 (1984).

- [12] G. Iooss and D. P. Joseph, *Elementary Stability and Bifurcation Theory*, Springer-Verlag (1980) QA372.I68.
- [13] J. Kevorkian and J. D. Cole, *Perturbation Methods in Applied Mathematics*, Springer-Verlag (1981) QA1.A647.
- [14] N. Minorsky, *Nonlinear Oscillations*, Van Nostrand (1962).
- [15] A. H. Nayfeh and D. T. Mook, *Nonlinear Oscillations*, Wiley-Interscience, (1981) QA402.N34.
- [16] E. D. Obasaju, "Forced-Vibration Study of the Aeroelastic Instability of a Square-Section Cylinder Near Vortex Resonance", *J. Wind Engineering and Industrial Aerodynamics*, **12** No. 3 Sept 1983 pp 313-327.
- [17] G. V. Parkinson, "Aeroelastic Galloping in One Degree of Freedom", *Symposium on Wind Effects on Buildings and Structures*, paper 23 (1965).
- [18] G. V. Parkinson, "Mathematical Models of Flow-Induced Vibrations of Bluff Bodies", *Flow-Induced Structural Vibrations*, Proc. IUTAM-IAHR Symposium, Karlsruhe, Springer-Verlag (1974).
- [19] G. V. Parkinson, "Hydroelastic Phenomena of Bodies of Bluff Section in Steady Flow", *Separated Flow around Marine Structures*, Proc. Int. Symposium, Trondheim, (1985).
- [20] G. V. Parkinson and J. D. Smith, "The Square Prism as an Aeroelastic Non-Linear Oscillator", *Quarterly Journal of Mechanics and Applied Mathematics*, **XVIII** part 2, Clarendon 1964.
- [21] A. B. Poore and A. R. Al-Rawi, "Some Applicable Hopf Bifurcation Formulas and an Application in Wind Engineering", *Bifurcation Theory and Applications in Scientific Disciplines*, Annals of the New York Academy of Sciences, vol 316 (1979) pp 590-604.
- [22] A. B. Poore and A. R. Al-Rawi, "The Dynamical behaviour of the Hartlen-Currie Wake Oscillator Model", *Proc. 5th Int. Conf. Wind Eng.*, J.E. Cermak, ed. Pergamon (1979) pp 1073-1083.

- [23] J. J. Stoker, *Nonlinear Vibrations in Mechanical and Electrical Systems*, Interscience (1950) QA871.S778.
- [24] P. P. Sullivan, *Aeroelastic Galloping of Tall Structures in Simulated Winds*, M.ASc. Thesis, University of British Columbia (1977).
- [25] D. H. Turnbull and I. G. Currie, "Flow-Induced Oscillation of Cylinders in the Streamwise Direction", *Symposium on Flow-Induced Vibration 1*, ASME (1984), pp 73–84.
- [26] M. A. Wawzonek, *Aeroelastic Behavior of Square Section Prisms in Uniform Flow*, M.ASc. Thesis, University of British Columbia (1979).
- [27] K. N. Wood, *Coupled-Oscillator Models for Vortex-Induced Oscillation of a Circular Cylinder*, M.ASc. Thesis, University of British Columbia (1976).